



YAŞAR UNIVERSITY
GRADUATE SCHOOL OF NATURAL AND APPLIED SCIENCES

MASTER THESIS

ANTENNA DESIGN FOR 4G MOBILE PHONES

SERDAR OKUYUCU

THESIS ADVISOR: ASSOC. PROF. DR MUSTAFA SEÇMEN

ELECTRICAL AND ELECTRONICS ENGINEERING

PRESENTATION DATE: 08.01.2018

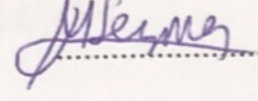
BORNOVA / İZMİR
JANUARY 2018

We certify that, as the jury, we have read this thesis and that in our opinion it is fully adequate, in scope and in quality, as a thesis for the degree of Master of Science.

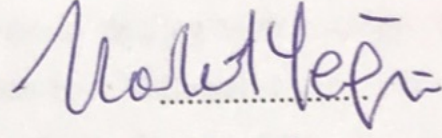
Jury Members:

Signature:

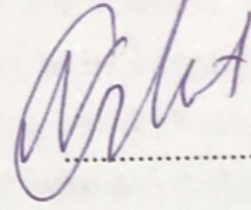
Assoc. Prof. Dr. Mustafa SEÇMEN
Yaşar University



Prof. Dr. Korkut YEĞİN
Ege University



Assist. Prof Dr. Nalan ÖZKURT
Yaşar University



Prof. Dr. Cüneyt GÜZELİŞ
Director of the Graduate School

ABSTRACT

ANTENNA DESIGN FOR 4G MOBILE PHONES

Okuyucu, Serdar

MSc, Electrical and Electronics Engineering

Advisor: Assoc. Prof. Dr. Mustafa SEÇMEN

January 2018

The progress shown in mobile phone technology in dealing with multiple band transmission and high data transmission rates has been followed by an increased demand in favor of rich content mobile services and new functionalities. To provide these services, multi-band and wide-band antennas have to be integrated into the compact structure of modern mobile phones. In this thesis, a multi-band, frequency reconfigurable main antenna and a receive diversity antenna is introduced as the cellular network antennas of a mobile phone terminal. The simulation of Specific Absorption Rate (SAR) for the main antenna operating at the GSM frequencies of 900 MHz and 1800 MHz is performed with standard Specific Anthropomorphic Mannequin (SAM) and anatomically correct head models. Additionally, a Global Positioning Service (GPS) antenna is introduced along with two WIFI antennas operating at respective frequencies of 2.4 GHz and 5.2 GHz.

The main antenna is a Planar Inverted F Antenna (PIFA) mounted at bottom of the mobile phone and grounded by a variable reactance for operation in 790-960 MHz and 1710-2690 MHz bands covering GSM, DCS, PCS and UMTS standards. The receive diversity antenna on the other hand is a monopole antenna designed to operate in the 1710-2690 MHz band. Use of laser direct structuring (LDS) structure in both antennas are proposed for fine-tuning of their response. Simulated and measured frequency responses of reflection coefficients and radiation patterns of the two antennas are presented.

As with the main and diversity antenna, part of the outer metallic structure of the mobile phone is used as the GPS and WIFI antennas operating at the respective frequencies of 1.575 GHz and 2.4GHz. The fine tuning of the resonance frequency of

the antennas are made by use of LDS stub patterns on the plastic back cover of the phone and matching circuits. The WIFI antenna operating at the frequency of 5.2 GHz on the other hand is designed as a PIFA constructed solely by an LDS pattern on the plastic back cover of the phone without the use of a matching circuit. The simulated and measured frequency responses of reflection coefficients and radiation patterns of these antennas are presented.

Following a thorough review of parametric dependence of SAR from mobile handsets, SAR analysis of the main antenna is performed when operated next to standardized and anatomically correct head models. The effect of the presence of a homogeneous hand model on antenna performance and SAR distribution is also investigated. In overall, relatively low peak spatial SAR values were obtained at higher frequency of operation due to a reduced peak output power available from the antenna at this frequency. The most influential parameter on SAR was found as the position of the antenna element which produced SAR values even higher than standardized maximum limits when placed near the pinna, at the upper part of the phone. Additionally, use of homogeneous head and hand models next to the mobile handset resulted in a down-shift in the frequency of resonance of the antenna.

Key Words: Cellular antennas, SAR, GPS antenna, WIFI antenna, LDS, 4G, LTE

ÖZ

4G CEP TELEFONLARI İÇİN ANTEN TASARIMI

Okuyucu, Serdar

Yüksek Lisans Tezi, Elektrik-Elektronik Mühendisliği

Danışman: Doç. Dr. Mustafa SEÇMEN

Ocak 2018

Cep telefonu teknolojisinin çoklu bant ve yüksek hızlı veri transmisyonunda katedilen gelişmeler, zengin içerikli mobil servislere ve yeni işlevselliklere olan artan talebi de beraberinde getirmiştir. Bu servislerin kullanıcılara sorunsuz bir biçimde sağlanması için, çoklu-bant ve geniş-bant karakteristiğine sahip antenlerin kompakt yapılı modern cep telefonlarının yapısına entegre edilmesi gerekmektedir. Bu tezde, çoklu-bant, rezonans frekansı kontrol edilebilen bir ana anten ve alıcı diversity anteni hücresele ağ antenleri olarak tanıtılmıştır. 900 MHz ve 1800 MHz GSM frekanslarında çalışan ana anten elemanına ait özgül soğurma oranı, standart SAM ve anatomik olarak doğru olan kafa modelleri için simüle edilmiştir. Bu iki antene ek olarak, bir GPS anteni ile birlikte, 2.4 GHz ve 5.2 GHz frekanslarında çalışmak üzere tasarlanan iki ayrı WIFI anteni tanıtılmıştır.

Ana anten, cep telefonunun alt kısmına konumlandırılmış bir PIFA anten elemanı olup, anten topraklaması değişken reaktans elemanları üzerinden yapılarak GSM, DCS, PCS, ve UMTS standartlarını kapsayan 790-960 MHz ve 1710-2690 MHz bantlarında çalışması sağlanmıştır. Diğer taraftan, diversity anten elemanı, 1710-2690 MHz bandında çalışmak üzere bir monopole anteni olarak tasarlanmıştır. Her iki antenin çalışma frekansına ayarlanmasında LDS teknolojisinin kullanılması önerilmiştir. Her iki antene ait çalışma frekansında simüle edilmiş ve ölçülmüş geri yansıma kaybı ve radyasyon paternleri verilmiştir.

Ana anten ve diversity anten elemanlarında olduğu gibi, telefonun dış yapısını oluşturan metalik yapının bir kısmı, 1.575 GHz bandında çalışan GPS ve 2.4 GHz bandında çalışan WIFI antenleri olarak kullanılmıştır. Antenlerin ilgili çalışma bantlarına ayarlanması, telefonun arka tarafında bulunan plastik kapak üzerine

entegre edilen LDS örnekleri ve uyumlama devreleri ile gerçekleştirilmiştir. Diğer taraftan, 5.2 Ghz bandında çalışan WIFI anteni, telefonun plastik arka kapağı üzerine inşa edilen bir PIFA elemanı ile herhangi bir uyumlandırma devresi kullanılmadan oluşturulmuştur. Bu antenlere ait simüle edilmiş ve ölçülmüş geri yansıma kayıpları ve radyasyon patternleri verilmiştir.

Cep telefonlarına ait özgül soğurma oranlarının (SAR) parametrik bağımlılığının ayrıntılı bir incelenmesini takiben, standart kafa ve anatomik olarak doğru olan kafa modelleri yanında çalışan ana anten elemanının SAR karakteristiği simüle edilmiştir. Buna ek olarak, homojen bir el modelinin varlığının, anten performansı ve SAR dağılımı üzerindeki etkisi incelenmiştir. Sonuç olarak, yüksek frekans çalışma bandında anten çıkış gücünün düşük olmasından dolayı, düşük banttakine kıyasla daha düşük SAR değerleri elde edilmiştir. Ana anten elemanının telefon üzerindeki konumu, SAR dağılımı üzerindeki en etkili parametre olarak saptanmış olup, ana antenin telefonun üst kısmında konumlandırıldığı bazı durumlarda, standartlarca belirlenen azami SAR limit değerlerini aştığı saptanmıştır. Ayrıca telefon üzerine yerleştirilen bir homojen el modelinin de anten rezonans frekansında aşağı yönlü bir kaymaya sebep olduğu saptanmıştır.

Anahtar Kelimeler: Hücresel antenler, SAR, GPS anteni, WIFI anteni, LDS, 4G, LTE

ACKNOWLEDGEMENTS

I would like to express my sincere gratitude to my advisor Dr. Mustafa SEÇMEN for his support, patience, motivation, and knowledge he provided in every phase of this study. His guidance helped me in research, experimental practice and writing of this thesis.

Besides my advisor, I would like to thank Prof. Korkut YEĞİN for his valuable ideas and efforts in planning of activities performed within the scope of this study and providing collaboration with partners from industry.

My sincere thanks go to Ceyhan TÜRKMEN for his valuable contributions in the 3D modeling phase of simulations and his support as a friend and colleague within the two years we have worked with.

My special thanks go to Bilgi ÖZKAN for his delicate work in setting up measurement setups of the antennas.

Serdar Okuyucu
İzmir, 2018

TEXT OF OATH

I declare and honestly confirm that my study, titled “ANTENNA DESIGN FOR 4G MOBILE PHONES” and presented as a Master’s Thesis, has been written without applying to any assistance inconsistent with scientific ethics and traditions. I declare, to the best of my knowledge and belief, that all content and ideas drawn directly or indirectly from external sources are indicated in the text and listed in the list of references.

Serdar Okuyucu
Signature

.....

December 22, 2017

TABLE OF CONTENTS

ABSTRACT	v
ÖZ	vii
ACKNOWLEDGEMENTS	ix
TEXT OF OATH	xi
TABLE OF CONTENTS	xiii
LIST OF FIGURES	xvii
LIST OF TABLES	xxi
SYMBOLS AND ABBREVIATIONS	xxiii
CHAPTER 1 INTRODUCTION	1
1.1. Evolution of Cellular Communication Systems	1
1.1.1. First Generation (1G) Systems	1
1.1.2. Second Generation (2G) Systems	2
1.1.3. Third Generation (3G) Systems	3
1.1.4. Fourth Generation (4G/4.5G) Systems	5
1.2. Evolution of Mobile Phone Antennas	9
1.2.1. External Antennas	11
1.2.2. Internal Antennas	15
1.2.3. Antennas in Recent Mobile Phones	25
1.3. Multiple-Input Multiple-Output (MIMO) Antennas	27
1.4. Aim of Research.....	28
1.5. Outline of Thesis	28
CHAPTER 2 MOBILE PHONE ANTENNA DESIGN OVERVIEW	30
2.1. Definitions and Concepts	31
2.1.1. Reflection Coefficient and Return Loss	31
2.1.2. Voltage Standing Wave Ratio (VSWR).....	32
2.1.3. Efficiency	33
2.2. Physical Limits of Antenna Design.....	34
2.3. Antenna Matching	35

2.3.1. Smith Chart.....	35
2.3.2. Single-Band Matching.....	37
2.3.3. Dual-Band Matching	39
2.3.4. Reconfigurable Matching	40
2.4. Antenna Manufacturing Technology	43
2.4.1. Metal Stamping.....	43
2.4.2. Molded Interconnected Device (MID)	44
2.5. Antenna Measurement	45
2.5.1. Passive Antenna Measurement on a Vector Network Analyzer	45
2.5.2. Measurement Setup and Location of Testing Cable	47
2.6. Aspects of Antenna Integration into Mobile Terminal	50
2.6.1. Impact of Ground Plane.....	50
2.6.2. The Effect of Acoustic Components.....	52
2.6.3. The Effect of Camera.....	53
2.6.4. The Effect of Battery	53
2.6.5. The Effect of Display.....	53
CHAPTER 3 DESIGN AND EVALUATION OF CELLULAR ANTENNAS	55
3.1. Main Antenna	55
3.2. Diversity Antenna.....	63
CHAPTER 4 DESIGN AND EVALUATION OF GPS AND WLAN ANTENNAS	69
4.1. GPS Antenna.....	69
4.2. 2.4 GHz Wi-Fi Antenna.....	74
4.3. 5.2 GHz Wi-Fi Antenna.....	78
CHAPTER 5 SAR ANALYSIS	81
5.1. Main antenna as the source of radiation	84
5.2. Description of Head and Hand Models.....	85
5.2.1. SAM Head and Homogeneous Hand Model	86
5.2.2. Heterogeneous Anatomical Head Model.....	87
5.2.3. Test Positions.....	87
5.2.4. Simulation Settings.....	88
5.3. SAR Results.....	89

5.4. Antenna Characteristics in the Presence of Hand and Head Models	91
CHAPTER 6 CONCLUSION	93
REFERENCES	95
APPENDIX	99



LIST OF FIGURES

Figure 1.1. Evolution of Mobile Communication Standards	6
Figure 1.2. Architecture of 4G Cellular Network	8
Figure 1.3. LTE Evolution	9
Figure 1.4. Transformation of monopole into a helix	11
Figure 1.5. Monopole and Helix antennas designed to cover 824-894 MHz.....	12
Figure 1.6. Single and multi-branch multiband stubby antennas.....	13
Figure 1.7. Simulated return loss of helix antenna with and without a plastic cover	13
Figure 1.8. Structure of a Retractable Antenna.....	14
Figure 1.9. Mobile phones with external antennas	15
Figure 1.10. Meander line stubby implementation of helix antennas and practical use	15
Figure 1.11. Impact of separation G in an L-shaped monopole antenna	16
Figure 1.12. Terminal characteristics of an L-shaped monopole antenna with matching circuit	17
Figure 1.13. Impact of separation G in an Inverted-F Antenna	17
Figure 1.14. PIFA antenna and its resonance frequency for varying widths	18
Figure 1.15. PIFA antenna and resonance frequency over varying heights.....	19
Figure 1.16. Dual band PIFA antenna with paths shown for high and low bands	19
Figure 1.17. Effect of design parameters C, D, and F on a dual band PIFA.....	20
Figure 1.18. Alternative matching methods in a PIFA	20
Figure 1.19. Current distribution on a dual band PIFA.....	21
Figure 1.20. PIFA as the 3G GSM antenna in commercial mobile phones	21
Figure 1.21. PIFA as the 3G GSM antenna in commercial mobile phones	22
Figure 1.22. PIFAs with parasitic elements in commercial mobile phones.....	22
Figure 1.23. A sample internal folded monopole antenna	23
Figure 1.24. Frequency tuning of monopole antenna by branch length.....	24
Figure 1.25. Various practical implementations of folded monopole antennas.....	24

Figure 1.26. Planar monopole antennas in commercial mobile phones	25
Figure 1.27. A multiband IFA implemented in a Hongmi 2A mobile phone as the main antenna.....	25
Figure 1.28. Matching circuit of antenna built onto the PCB by SMD components.....	26
Figure 1.29. A single dual band antenna used for GPS and WLAN services.....	26
Figure 2.1. Definition of antenna bandwidth under a certain return loss criterion.....	32
Figure 2.2. Minimal sphere enclosing an antenna	34
Figure 2.3. Constant $ \Gamma $, r_L , and x_L curves.....	36
Figure 2.4. The Smith Chart	36
Figure 2.5. The ZY Smith Chart.....	38
Figure 2.6. Respective ZY chart directions for 4 possible connections of lumped reactive matching elements	38
Figure 2.7. Four possible matching circuit options for a single load impedance	39
Figure 2.8. Dual band matching with four elements.....	40
Figure 2.9. Reconfigurable Matching Circuit in four bands.....	41
Figure 2.10. Impedance curves for each matching circuit in four bands	42
Figure 2.11. Simplified reconfigurable switching by reuse of matching components	42
Figure 2.12. Return loss for matching circuit with reused components	43
Figure 2.13. Antennas printed by metal stamping on plastic carrier	43
Figure 2.14. Three-dimensional structuring on carrier plastic by LDS	45
Figure 2.15. Sample vector network analyzer with its simplified schematics.....	46
Figure 2.16. Antenna testing setup on a vector network analyzer	47
Figure 2.17. Sample test configuration of a PIFA antenna.....	48
Figure 2.18. Sample switch connector and its operation	49
Figure 2.19. Switch connector operated in opposite direction by rotation	49
Figure 2.20. Current distribution of a PIFA over a finite ground plane	50
Figure 2.21. Radiation pattern of PIFA at 900MHz and 1800 MHz	51
Figure 2.22. Mobile phones with a lossy ground plane.....	52

Figure 2.23. Spurious emission from a mobile phone camera.....	53
Figure 2.24. Spurious emission from a LCD display.....	54
Figure 3.1. 3D structure modeling of main antenna and mobile phone.....	56
Figure 3.2. Metallic bottom case as the main antenna.....	56
Figure 3.3. Return loss of antenna (poly-carbon fill included in simulation).....	57
Figure 3.4. Return loss of antenna (poly-carbon fill excluded from simulation).....	57
Figure 3.5. Tuner Switch Configuration.....	58
Figure 3.6. Upper band coverage by capacitive loading at grounding terminal.....	59
Figure 3.7. Return loss for a number of inductive loads at the grounding terminal.....	59
Figure 3.8. Physical implementation and measured return loss of Main antenna.....	60
Figure 3.9. Simulated return loss of main antenna with 18nH connected at its grounding terminal.....	60
Figure 3.10. Main antenna with stub element built on plastic back cover.....	61
Figure 3.11. Lower band coverage by use of stub element and inductive loading.....	61
Figure 3.12. Upper band coverage by capacitive loading in two configurations.....	62
Figure 3.13. Far-field gain radiation patterns of main antenna.....	63
Figure 3.14. Metallic bottom case as the diversity antenna.....	64
Figure 3.15. Return loss (dB) of diversity antenna with and without the stub element.....	65
Figure 3.16. Physical setup for measurement of Return loss (dB) of diversity antenna.....	66
Figure 3.17. Measured Return loss (dB) of diversity antenna.....	66
Figure 3.18. Far-field gain radiation patterns of diversity antenna.....	67
Figure 4.1. Geometry of GPS Antenna.....	70
Figure 4.2. Return loss of GPS Antenna without a matching circuit.....	70
Figure 4.3. Matching circuit of the GPS antenna.....	71
Figure 4.4. Return loss of GPS antenna with matching circuit.....	71
Figure 4.5. Physical implementation and measured return loss of GPS antenna.....	72
Figure 4.6. Simulated and measured return losses for the GPS.....	72
Figure 4.7. Measured return loss of GPS antenna for different cable positions.....	73

Figure 4.8. Measured return loss of GPS antenna by use of switch connectors	73
Figure 4.9. Simulated and measured (with switch connector) return losses for GPS antenna	74
Figure 4.10. Geometry of 2.4 GHz WIFI Antenna.....	75
Figure 4.11. Return loss of 2.4 GHz WIFI antenna without a matching circuit.....	75
Figure 4.12. Matching circuit of the 2.4 GHz WIFI antenna.....	76
Figure 4.13. Simulated return loss of 2.4 GHz WIFI antenna with matching circuit.....	76
Figure 4.14. Measured return loss of Wi-Fi 2.4 GHz antenna by use of switch connectors .	77
Figure 4.15. Simulated far-field gain of the 2.4 GHz WIFI antenna	77
Figure 4.16. Geometry of 5.2 GHz WIFI Antenna.....	78
Figure 4.17. Simulated return loss of 5.2 GHz WIFI antenna	79
Figure 4.18. Measurement setup of 5.2 GHz WIFI antenna.....	79
Figure 4.19. Simulated and measured return losses of 5.2 GHz WIFI antenna.....	80
Figure 4.20. Simulated far-field gain of the 5.2 GHz WIFI antenna	80
Figure 5.1. Main antenna as the source of electromagnetic radiation	85
Figure 5.2. Simulated return loss of the main antenna	85
Figure 5.3. Head and hand models	86
Figure 5.4. Positioning of the phone in cheek and tilt positions.....	88
Figure 5.5. SAR distributions in all configurations considered.....	90
Figure 5.6. $ S_{11} $ (dB) from using SAM in four configurations.....	91
Figure 5.7. $ S_{11} $ (dB) from using HUGO head in four configurations	91
Figure 5.8. $ S_{11} $ (dB) from using SAM with homogeneous hand in four configurations....	91
Figure 5.9. Gain and radiation efficiency of the antenna in use positions.....	92

LIST OF TABLES

Table 1.1. Operational Parameters of 1G Cellular Standards	2
Table 1.2. Operational Parameters of 1G Cellular Standards	3
Table 5.1. Operational Parameters of 1G Cellular Standards	87



SYMBOLS AND ABBREVIATIONS

ABBREVIATIONS:

FSK	Frequency Shift Keying
FDMA	Frequency Division Multiple Access
AMPS	Advanced Mobile Phone Service
TDMA	Time-Division Multiple Access
CDMA	Code Division Multiple Access
FDD	Frequency Division Duplexing
GSM	Global System for Mobile Communication
ITU	International Telecommunication Union
UMTS	Universal Mobile Telecommunication System
WLAN	Wireless Local Area Network
MIMO	Multiple-Input Multiple-Output
LTE	Long Term Evolution
WiMAX	Mobile Worldwide Interoperability for Microwave Access
IFA	Inverted F Antenna
PIFA	Planar Inverted F Antenna
LDS	Laser Direct Structuring
SAR	Specific Absorption Rate
VSWR	Voltage Standing Wave Ratio
PCB	Printed Circuit Board

SYMBOLS:

Q Quality factor

CHAPTER 1

INTRODUCTION

1.1. Evolution of Cellular Communication Systems

Mobile communication systems have undergone substantial technological progress and growth since the launch of first mobile communication system around 1980s. In every step of the progress, user demand has been one of the most influential driving forces forcing institutions and companies to come up with technological innovations as to serve the ever-increasing number of users with rich content mobile services and new functionalities with high data rates at multiple bands of operation. In parallel to the introduction of new technologies to the field, several Cellular Wireless Generations have been identified along with their standards, capacity, and techniques of operation.

1.1.1. First Generation (1G) Systems

The first-generation wireless mobile communication system was an analog system introduced in early 1980s, where analog systems were based on switching circuit technology, offering voice communication only (Agrawal, 2015). In this system, the speech signal is processed by use of analog frequency modulation technique of Frequency Shift Keying (FSK) and the allocated spectrum is utilized by Frequency Division Multiple Access (FDMA). Advanced Mobile Phone Service (AMPS), Total Access Communication System (TACS), Nordic Mobile Telephone (NMT), Nippon Telephone and Telegraph (NTT) and C450 are some of the popular standards developed around the world in which two separate frequency channels are used, one for base-to-mobile and the other for mobile-to-base in a full duplex transmission. Operational parameters of these first-generation cellular standards are given in Table 1.1.

Table 1.1. Operational Parameters of 1G Cellular Standards

Parameters	AMPS	C450	NMT 450	NTT	TACS
Tx Frequency (MHz)					
Mobile	824–849	450–455.74	453–457.5	925–940	890–915
Base Station	869–894	460–465.74	463–467.5	870–885	935–960
Channel bandwidth (kHz)	30	20	25	25	25
Spacing between forward and reverse channels (MHz)	45	10	10	55	45
Speech signal FM deviation	±12	±5	±5	±5	±9.5
Control signal data rate (kbps)	10	5.28	1.2	0.3	8
Handoff decision is based on	Power received at base	Round-trip delay	Power received at base	Power received at base	Power received at base

In the AMPS system, 824-825 MHz and 869-894 MHz bands were used for uplink and downlink transmission respectively. The available spectrum is divided into channels with 30-kHz bandwidth. Out of the 832 duplex channels in the spectrum, 42 of them are used as control channels used for downlink and uplink transmission, which are referred to as forward control channels (FCC) and reverse control channels (RCC) respectively. The remaining 790 channels are similarly divided into forward voice channels (FVC) and reverse voice channels (RVC). In a two-way communication between the base station and the mobile terminal, a pair of channels separated by 45-MHz is selected which enables the use of unexpected but highly selective duplexers. (Godara, 2001)

1.1.2. Second Generation (2G) Systems

The second-generation wireless mobile communication system is developed in late 1980s as an improvement over 1G communication system. These systems are designed to use digital transmission and multiple access themes of Time-Division Multiple Access (TDMA) and Code Division Multiple Access (CDMA) in offering the end users with additional services such as short message services (SMS), picture messages, and multimedia message services (MMS). Some of these standard systems are North American dual-mode cellular system (IS-54), European GSM, North American IS-95 system, and Japanese Personal Digital Cellular (PDC) system with their operational properties given in Table 1.2.

Table 1.2. Operational Parameters of Some 2G Cellular Standards

TABLE 1.2 Parameters of Some Second-Generation Cellular Standards

Parameters	IS-54	GSM	IS-95	PDC
TX frequencies (MHz)				
Mobile	824–849	890–915	824–849	940–956 and 1429–1453
Base station	869–894	935–960	869–894	810–826 and 1477–1501
Channel bandwidth (kHz)	30 kHz	200 kHz	1250 kHz	25 kHz
Spacing between forward and reverse channels (MHz)	45	45	45	30/48
Modulation	$\pi/4$ DQPSK	GMSK	BPSK/QPSK	$\pi/4$ DQPSK
Frame duration (ms)	40	4.615	20	20

Among these systems, IS-54, GSM, and PDS use TDMA while, IS-95 uses CDMA along with Frequency Division Duplexing (FDD).

In TDMA, in order to allow several users to use the same frequency channel, the channel is divided into a series of time segments (slot), where each user transmits one after the other in a rapid succession. In this way, by keeping the time segments small at a high slicing frequency, a continuous communication is perceived by the end user. When compared with the AMPS standard of the 1G system, up to six channels are able to be sent in the same bandwidth where AMPS uses one channel.

In CDMA, the same frequency channel can be used to transmit data from multiple users. In doing so, unlike TMDA, the user has access to the channel bandwidth over the entire duration of transmission and the CDMA codes are used for distinguishing data from multiple users. One of the significant improvements with this technology was on network capacity with a factor of two when compared with TDMA and GSM.

The mostly widely used 2G system is the Global System for Mobile Communication (GSM) which was the first standard to support international roaming. In this system, two frequency bands are used with 900 MHz as the primary and 1800 MHz as the secondary band. The primary band is divided into two sub-bands of 25 MHz, one for uplink (lower band) and one for downlink (upper band), with a separation 20 MHz between them. Additionally, carrier frequencies are separated by 200 kHz, providing a total of 124 frequency channels over the 25 MHz band.

1.1.3. Third Generation (3G) Systems

Following the development of the 2.5G standard which stood as a retrofit of 2G standard for increased data rates to support a wider range of internet applications,

third generation mobile phone standards have been defined based on International Telecommunication Union (ITU) family of standards under the International Mobile Telecommunications-2000 (IMT-2000). By the achievement of better network capacity through improved spectral efficiency in 3G networks, the users are provided with a wide range of advanced services such as wide-area wireless voice telephony, video calls, and broadband wireless data in a mobile environment.

There have been many different radio access technologies defined within ITU such as the Universal Mobile Telecommunication System (UMTS) defined by the 3rd Generation Partnership Project (3GPP) group. After several trials of establishing a single 3G standard, a family of five 3G standards has been approved by the ITU which are part of the IMT-2000 framework. These Standards are

- W-CDMA (UMTS)
- CDMA2000
- TD-SCDMA

In WCDMA, direct sequence code division multiple access (DS-SS) is employed in spreading the user information over a wide bandwidth where the user data is multiplied by the spreading code. In this scheme, 5-MHz carrier spacing is employed together with a chip rate of 3.84 Mcps for the spreading sequence. The carrier spacing may vary between approximately 4.4 and 5 MHz from one operator to the other which is decided based on the spectrum arrangement of the particular operator. In a CDMA scheme, all the users have access to the whole channel at a given time and each user is separated by use of specific spreading codes. In WCDMA, time duration of 10 ms is allocated for each user over which the data rate of a particular user is kept constant. Even though the data rate is constant for a particular user it might change among users. According to the rate of use of users at a given time, the radio capacity allocation is organized by the radio resource management system in order to ensure a sufficient quality of service (QoS) and achieve optimum throughput for data services. FDD and TDD are supported by WCDMA as basic modes of operation. In FDD mode of operation, two 5-MHz frequency bands are used with duplex spacing between them for the uplink and downlink transmission. In TDD mode, a single 5 MHz carrier is shared in time between uplink and downlink.

CDMA2000 is the natural evolution of IS-95 standard, which includes additional functionality in increasing data rate capability and spectral efficiency. CDMA2000 1xRTT, CDMA2000 1xEV and CDMA2000 EV-DV are among the main standards of CDMA2000.

TD-SCDMA is 3G mobile communication standard that is based on spread spectrum technology. TDD scheme is employed in this standard in contrast to the FDD technology used by W-CDMA. By the dynamic adjustment of the number of downlink and uplink time slots used, the system is able to accommodate data traffic requirements more easily than the FDD counterpart. Use of the same carrier frequency is another aspect of the system that is helpful to the application of beamforming techniques since the base station can deduce the downlink channel from uplink estimates as the channel condition is the same in both directions. In addition to the CDMA used in WCDMA, TD-SCDMA uses TDMA which reduces the number of users in each time slot, which eventually reduces the complexity of beamforming schemes. By employing continuous timing adjustments, the uplink signals are synchronized at the base station receiver. This is represented by the “S” in TD-SCDMA. The synchronization reduces the interference between the users occupying the same slot by improving the orthogonality of different codes used for each user. This process increases system capacity at the cost of hardware complexity for achieving synchronization in uplink.

In general, 3G mobile communication networks are able provide data transfer speeds of up to 3Mbps. The available bandwidth and location information available to 3G handsets give rise to a number of applications that were not previously available to mobile phone users. Some of these applications include Mobile TV (redirection of a TV channels to the user’s phone), Video on demand (downloading a movie from the service provider), Video-conferencing (subscribers can see and talk to each other), Tele-medicine (Monitoring the health of an isolated subscriber providing advice), and Location based services (fetching localized traffic and weather conditions, finding businesses and friends nearby).

1.1.4. Fourth Generation (4G/4.5G) Systems

The 4G mobile communication system is introduced as an extension on 3G mobile communication systems for solving the problems faced in providing the user with a

variety of services ranging from high quality voice to HD video transmission over wireless channels at high data rates. When compared with 3G systems, it is broad in scope such that it includes several types of broadband wireless access communication systems together with cellular telephone systems. Within the frame of accessing a wide range of information over a seamless network, the 4G infrastructure comprises various networks using internet protocols (IP) as to give the users the control of what environment and application to use. By the application adaptability and highly dynamic nature of 4G service, connection to the network can take various forms, where the dominant methods of access are mobile telephone and laptops. In this way, the fourth generation will cover broadband operator-driven and public, private networks. By using IP as the integrating mechanism, the integration of satellite broadband, high altitude platform, cellular, wireless local loop (WLL), fixed wireless access (FWA), wireless local area network (WLAN) and personal area network (PAN) are implemented.

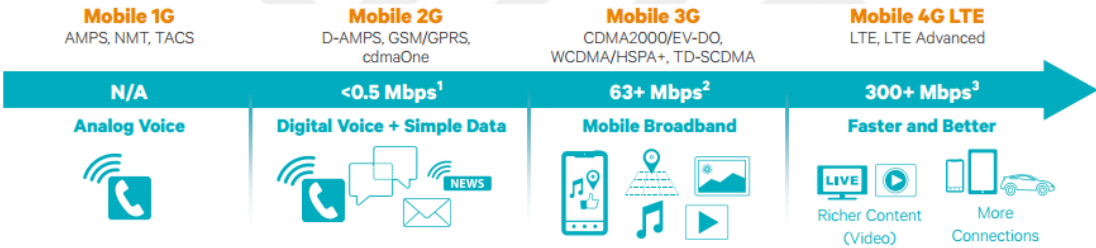


Figure 1.1. Evolution of Mobile Communication Standards

In order to be able to accommodate the intended services such as video chat, MMs, mobile TV, digital video broadcasting, etc., the following qualitative performance parameters have been identified by the 4G working group.

- Spectral efficiency
- Network capacity (Accommodating more simultaneous users in each cell)
- Data rate (100 Mbps for users moving at a high-speed relative to the base station and 1Gbps for those users who are in a relatively fixed position)
- Hand-off (smoothness across heterogeneous networks)
- Global roaming and seamless connectivity across multiple networks

In performing these objectives, the aspects of low cost, wide area coverage, and broadband wireless access must also be taken into account in the implementation of the system.

In providing data transfer at very high rates despite the extensive multi-path radio propagation, Orthogonal Frequency Division Multiple Access (OFDMA), multi-carrier transmission and Frequency Domain Equalization (FDE) schemes are used in place of the spread spectrum radio technology used in 3G systems. In OFDM, a high number of closely spaced orthogonal subcarriers are used in multicarrier modulation method. The data that is to be transmitted is divided into multiple data streams or channels which in turn are carried by a sub-carrier. Additionally, peak rate is increased by use of antenna arrays for multiple-input multiple-output (MIMO) communications. As the name implies, MIMO is the use of multiple antennas at the transmitter and receiver with the purpose of improving communication performance. It enables increase in data throughput and link range without requiring additional bandwidth or transmitting power.

Even though there are some significant changes, the architecture of a 4G communication network is similar to that of a 3G communication system. The main difference between the two is the removal of the redundant circuit-switching capability in 4G systems. Without the mobile switching center (MSC), the voice transfer is treated as packet data at the base station. Following the maintenance of backward compatibility by segmentation of voice data into packages, the packages are routed through the IP backbone where voice over IP (VOIP) technology is employed. The integration of wireless local area networks (WLAN) into the mobile network is another major advancement in the 4G technology. Similarly, for the purpose of interconnecting WLANs to the 4G IP backbone via routers with built-in wireless access, new air interface standards have been developed. In this way, there is no need for the use of a control module at any wired infrastructure. The overall architecture of a 4G cellular network is shown in Figure 1.2.

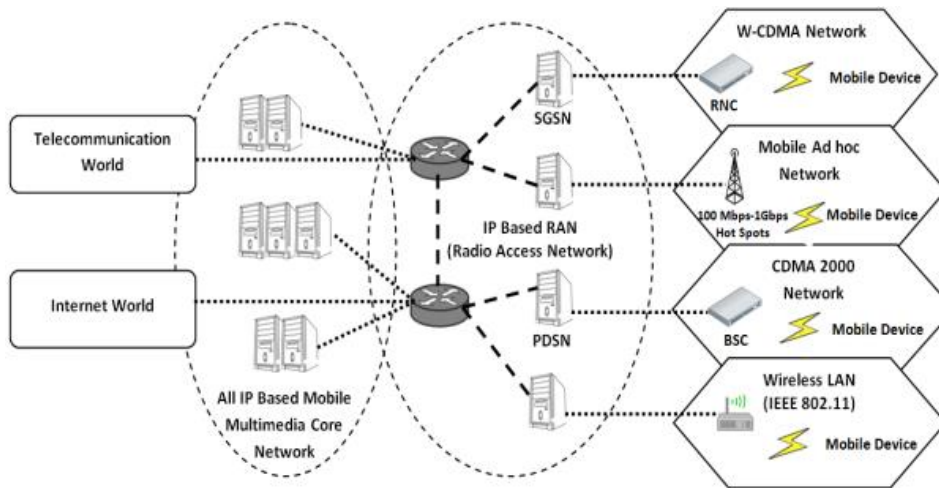


Figure 1.2. Architecture of 4G Cellular Network (Singh,2016)

Based on the standards defined by ITU-R, an IMT-Advanced cellular system must satisfy the following requirement:

- Structure based on an all IP packet switched network
- Peak data rate of 100 Mbits/s for high users moving at a high-speed relative to the base station, and up to 1Gbit/s for low mobility or static wireless access.
- Dynamic utilization of network resources for supporting a higher number of users per cell.
- Scalable channel bandwidth in the range from 5MHz to 20 MHz, or optionally up to 40 MHz.
- Peak link spectral efficiencies of 15 bits/s/Hz and 6.75 bits/s/Hz for downlink and uplink respectively.
- Seamless handovers across heterogeneous networks
- High quality of service for multimedia support of the next generation

In the path followed to achieve 4G speeds, Long Term Evolution (LTE) has been developed by the Third Generation Partnership Project (3GPP) as a wireless broadband technology, which made fast mobile internet connections possible. The structure of a LTE network can be divided into two parts as radio access network and core network. The radio access network is the medium used for the connection of mobile phones to the base station antennas of the mobile operator. This network is also called Evolved Universal Mobile Telecommunications System Terrestrial Radio

Access Network (EUTRAN). The EUTRAN is formed by three nodes, namely, LTE mobile terminal, radio interface, and eNodeB. On the other hand, the core network of LTE is the brain of the system connecting mobile devices to the network and mobile networks to the fixed telephony network and internet. The core network of LTE is composed of five nodes namely, mobility management entity (MME), Serving Gateway (S-GW), Packet Data Network Gateway (D-GW), Home Subscriber Server (HSS), and Policy and Charging Rules Function (PCRF).

As approved by the ITU in October 2010 before the WiMAX Release 2 (IEEE 802.16m-2011), LTE-advanced is one of the milestones in the evolution of LTE.



Figure 1.3. LTE Evolution

LTE advanced is the enhancement of LTE technology in terms of carrier aggregation for leveraging more spectrum and increased data rates, advanced antenna techniques for increased spectral efficiency, and increasing capacity per coverage area.

In carrier aggregation, multiple carriers are combined at the device as to provide higher data rates to the user. The higher data rates obtained in this way can be traded off to increase capacity for applications such as browsing and social media apps. In the first step, the aggregation of two 10 MHz carriers was supported which enabled a 150 Mbps peak data rate. This in turn doubles the user data rates independent of the user being located close to the cell center or at the edge.

LTE evolution of LTE advanced continues in terms of evolutionary system components and revolutionary approaches in operation that can transform industries not touched by the LTE. Due to the robust and versatile nature of the LTE advanced technology, it is able to be morphed to suit the needs of specific areas and is projected to extend its influence to new horizons beyond mobile broadband.

1.2. Evolution of Mobile Phone Antennas

The fast-paced evolution of mobile communication systems gave rise to an explosive growth in the user demand for information services to smart personal handheld

devices. Since the common network technologies of GSM, UMTS (3G), and LTE use different frequency bands, the antenna of a particular handset terminal must be designed accordingly as to support transmit and receive of signals at the respective frequency of operation employed in any of these services. Additionally, since countries around the world use different frequencies for each service, the number of bands that is to be covered by the antenna of commercial mobile phone shipping worldwide is increased. In addition to the deployment of mobile phone systems, various wireless mobile systems (WMS) have been incorporated into the modern smart phone terminals. When compared with the nationwide service of mobile phone systems, WMS service is provided to areas at very short to intermediate distances. Some of the short-range systems include Bluetooth, near field communication (NFC), and UWB. Typical middle to long range systems are wireless local area network (WLAN), wireless metropolitan area network (WMAN), and mobile worldwide interoperability for microwave access (WiMAX). As a vital part of the system in using these services, various antenna systems have been developed in parallel to the deployment of these systems.

The efforts made in the development of the antennas of current mobile phones can be categorized under two major trends. One of these trends is the development of antennas for wireless terminals requiring small, built-in, and multiband operation. The second trend is the development of antennas for wireless mobile services that require specific performance characteristics depending on the complexity of the system, its service area, and spectral and temporal properties of the data that is to be transmitted.

The compact built-in multiband antennas of recent mobile phones are designed to cover the frequency bands of various systems such as GSM (800-, 900-, 1800-, and 1900-MHz bands), UMTS (1.8-, 1.9-, 2.1-, and 2.5-GHz bands), and GPS L1 (1.575-GHz band). In addition, small antennas are incorporated into the structure of the phone for many wireless mobile systems due to the operation of these systems for shorter ranges.

In the following subsections, the introduction of mobile phone antenna structure of frequent use for various mobile phone terminals is presented.

1.2.1. External Antennas

External antennas were the first type of antennas employed in early days of mobile communication. It made its first appearance in a commercial mobile phone with Motorola DynaTAC 8000X, in 1983. In the following 15 years of external antennas in the mobile phone antenna market before being replaced by internal antennas, various types of single band, multiband and wideband configurations have been incorporated into the structure of mobile phones. External antennas are mainly categorized as stubby and whip-stubby antennas.

A stubby antenna in most of early mobile phones is a spring coil made of copper wire or copper-coated steel wire that extrudes from the phone. The spring coil has a round cross section in the shape of a column. This is why it is called as stubby.

The development of stubby helix antennas can be explained by starting from the most basic form of a dipole antenna. Despite being widely used in the wireless communication industry, they are cumbersome to be used in mobile phones due to size restrictions. As a quantitative example to this, a length of 18.2 cm is required for a dipole antenna to make it resonate at 824 MHz.

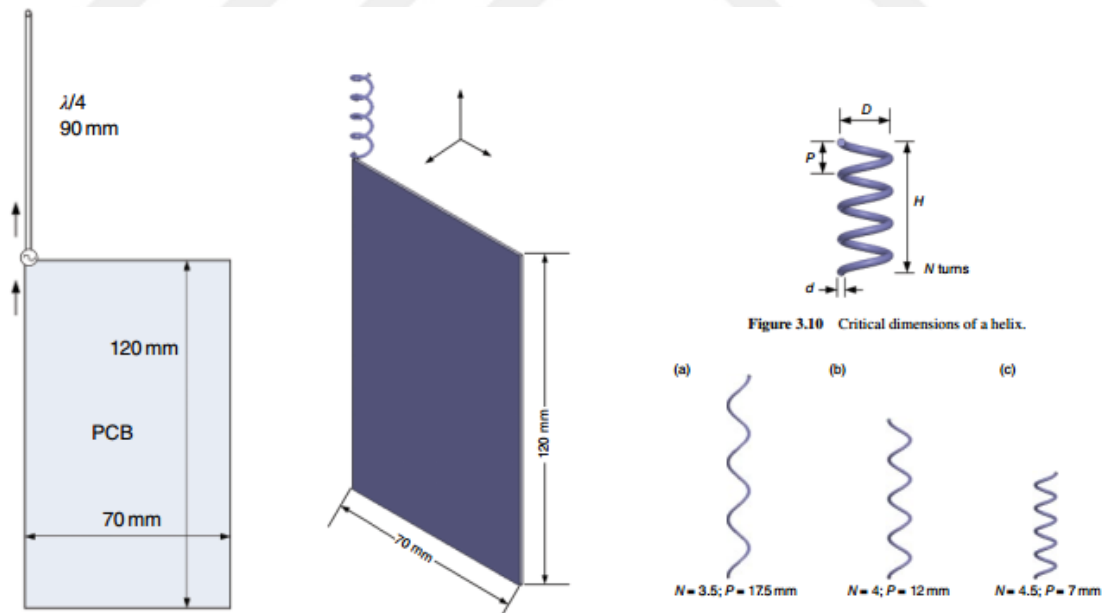


Figure 1.4. Transformation of monopole into a helix

The implementation of a dipole antenna into a mobile terminal is as shown in Figure 1.4 where the bottom arm of the dipole is expanded to represent the PCB board of the mobile phone. From the point of view of system engineering, the antenna is now

regarded as a monopole antenna. In this configuration, the monopole antenna has the length of a quarter of a wavelength instead of the half a wavelength of the initial dipole antenna. Even though the size of the antenna is reduced in half, it is still quite long to be used as a fixed antenna on a mobile phone. In order to reduce the height of the antenna, the upper arm of the dipole is coiled to make a helix as shown in Figure 1.4. The helix structure is defined by the pitch P , diameter of helix D , and diameter of the metal wire d , and the total number of turns N . By adjusting these three parameters, a helix antenna with required total wire length L_{tot} and height H can be designed by use of the following equations.

$$L_{tot} = N \times \sqrt{(\pi \times D)^2 + (P)^2} \quad , \quad H = N \times P \quad (1)$$

An example of a helix antenna that is designed to resonate in the band of 824-894 MHz is shown in Figure 1.5.

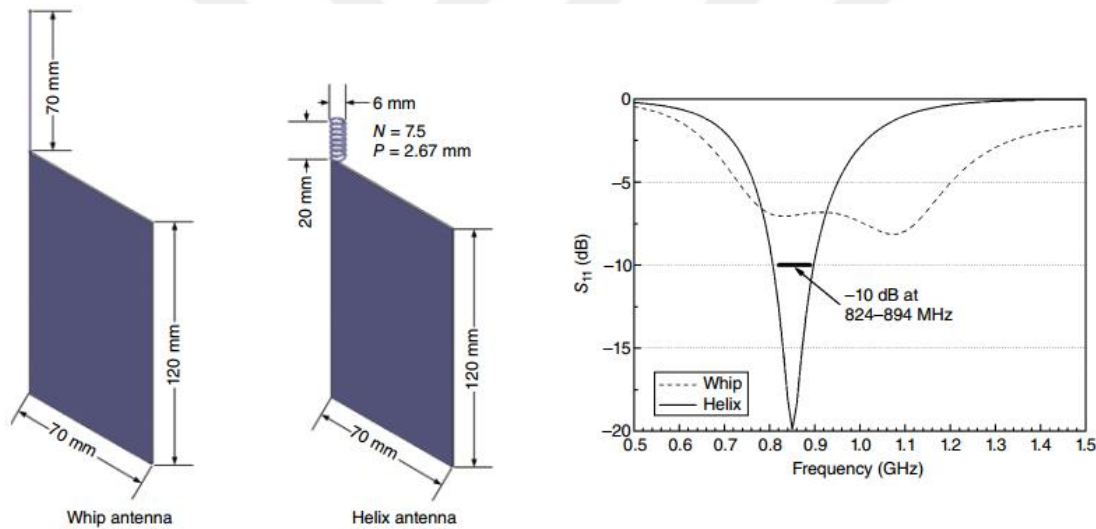


Figure 1.5. Monopole and Helix antennas designed to cover 824-894 MHz

By following the same set of design procedures used in the design of a single band Helix antenna, various configurations can be obtained as to design multiband Helix antennas as shown in Figure 1.6.

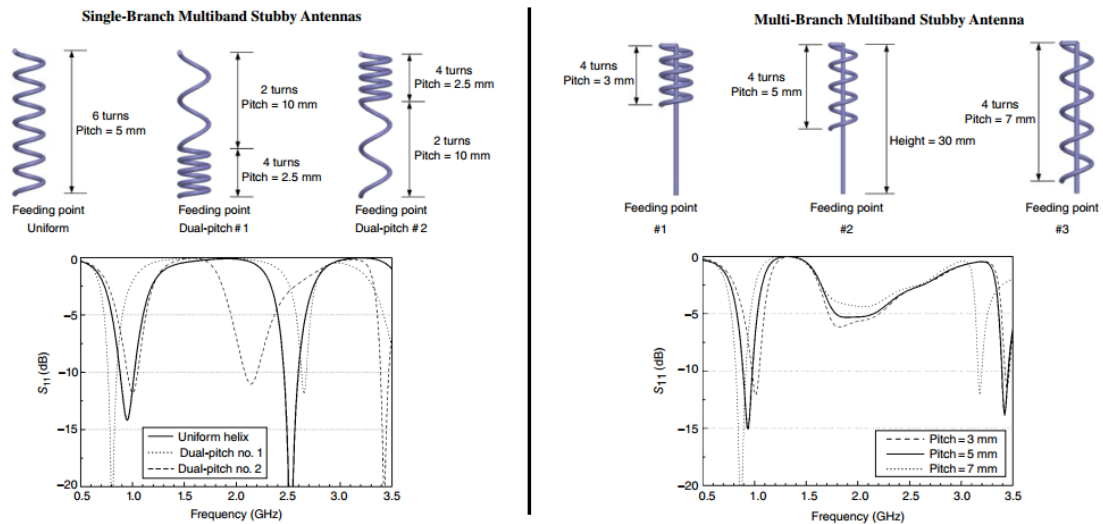


Figure 1.6. Single and multi-branch multiband stubby antennas

In a practical deployment of the antenna to the structure of the mobile phones, the helix antennas are covered by plastic covers or supports in order to ensure mechanical robustness. The plastic cover materials generally have a dielectric constant around 2.6-4.5 and impose dielectric loading on the antenna causing a downshift in the resonance frequency of the antenna. By taking this effect into account, the downshift in resonance frequency can be compensated by decreasing the length of the antenna. The effect of dielectric loading by the plastic cover on the return loss of the antenna is shown in Figure 1.7.

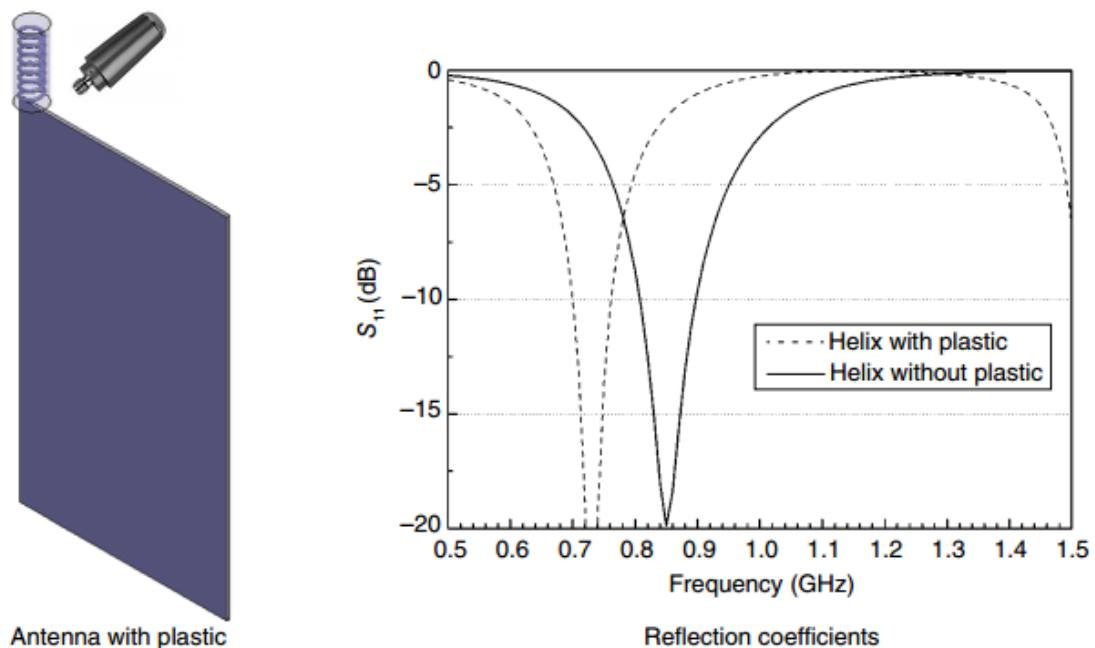


Figure 1.7. Simulated return loss of helix antenna with and without a plastic cover

A second significant issue related to the plastic cover is the loss that may degrade the efficiency of the antenna based on the loss properties of the plastic material used as the cover.

Whip-Stubby (Retractable) Antennas are another type of external mobile phone antennas that has the widest bandwidth and greatest performance when compared with its alternatives. As the name implies, the structure of a whip-stubby antenna is the combination of whip and stubby antennas. When the antenna is extended, since the whip is much longer than the stubby antenna, the characteristics of the antenna are dominated by the whip structure. When the antenna is brought back into the shorter position (closed whip), the operation is dominated by the stubby part of the antenna. In many structures as shown in Figure 1.8, the two radiators of the antenna are electrically independent which makes the design of the antenna much easier. When compared with stubby antennas, the tuning parameters of the antenna are restricted to the whip length and diameter for the lower band of operation. A single matching circuit is designed and used for the retracted position (stubby antenna) and extended position (whip antenna).

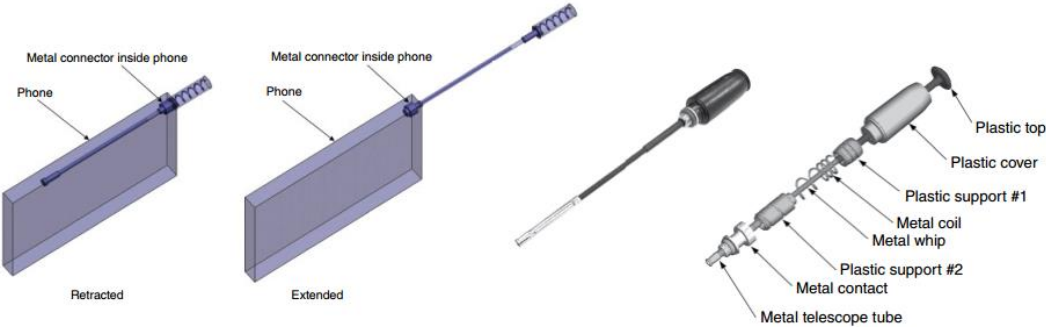


Figure 1.8. Structure of a Retractable Antenna

Some examples of the mobile phones incorporating stubby and retractable antennas are shown in Figure 1.9.



Figure 1.9. Mobile phones with external antennas (a) Nokia 6150 (Stubby Antenna), (b) Telstra explorer 165 (Retractable Antenna), (c) Motorola V180 (Stubby Antenna)

Following the technological advancements shown in the flex technology, stubby antennas with irregular cross sections could be implemented practically. In these structures, the radiator elements (wires) of helix antennas are replaced by flex and meander lines are introduced in place of the coil structure. Meander line implementations of previously shown retractable antennas are shown in Figure 1.10.

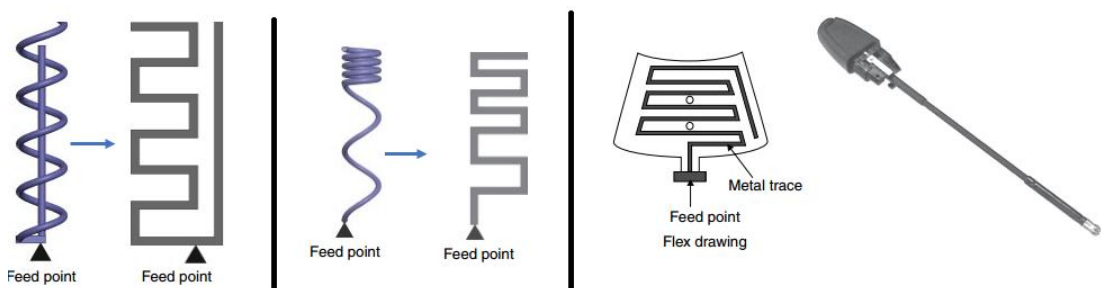


Figure 1.10. Meander line stubby implementation of helix antennas and practical use

When compared with the coiled wire structure of former antennas, flex provides much more freedom on the trace layout such that it is easier to incorporate multiple branches into the structure of the antenna.

1.2.2. Internal Antennas

Due to the aesthetical reasons and competition in the market for building robust wireless handset terminals, the internal mobile phone antennas have emerged and gained extensive popularity in the few years at the end of the twentieth century.

Considering the structure of a candy-bar mobile phone with a single printed circuit board and no moving parts, in the case of being dropped on the ground or being exposed to extreme pressure, the covers endure most of the force in preserving the compact structure of the phone. Due to the robustness and compact structure of mobile phones with internal antennas, the mobile phone market has been dominated by candy-bar type mobile phone antennas with internal antennas since the first marketing of the phone with an internal antenna by Nokia. In the following parts of this subsection, various types of internal antennas of frequent use in history of mobile phones is introduced.

• **Inverted F Antenna**

Similar to the stubby antennas introduced in the previous section, the origin of inverted F antennas is the result of an effort to decrease the size of a monopole antenna by bending the monopole arm into an L-shape. In doing so, the total length of the dipole arm is kept constant and bent into an L-shape at a distance of G from the from the ground plane of the handset. The separation G between the dipole arm and the ground plane is a critical design parameter which determines the impedance of the antenna. As the impedance of a straight dipole arm is around 100Ω , the real part of the antenna’s impedance can be tuned to match that of the feed line by bending the arm towards the ground plane.

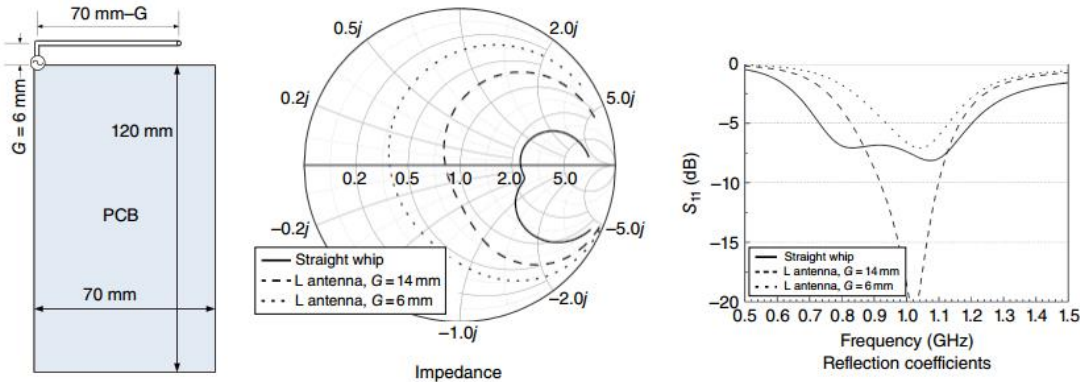


Figure 1.11. Impact of separation G in an L-shaped monopole antenna

However, for separation distances of dipole arm and ground plane that are smaller than 14mm, the matching starts to degrade calling for use of external matching circuits as shown in Figure 1.12 (Zhang, 2017).

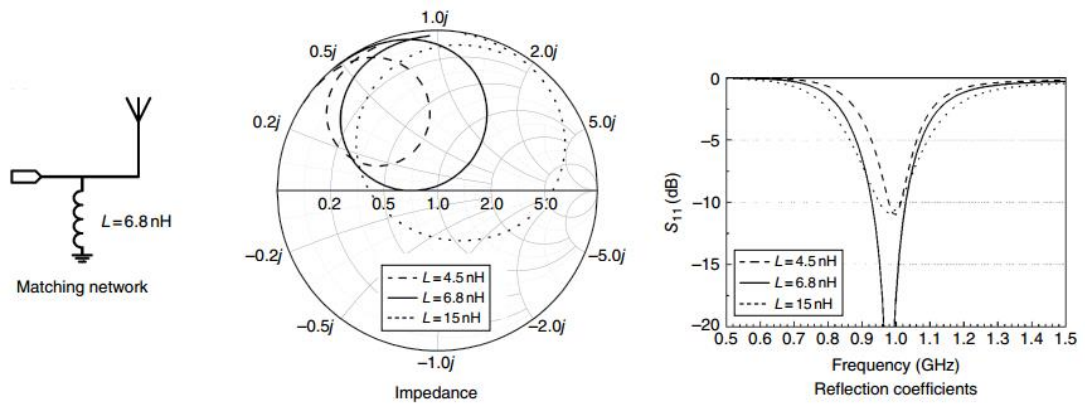


Figure 1.12. Terminal characteristics of an L-shaped monopole antenna with matching circuit

Instead of using external matching circuits on the PCB of the mobile phone, the effect of lumped matching inductor can be realized by grounding a metallic strip on the opposite side of the monopole arm as shown in Figure 1.13.

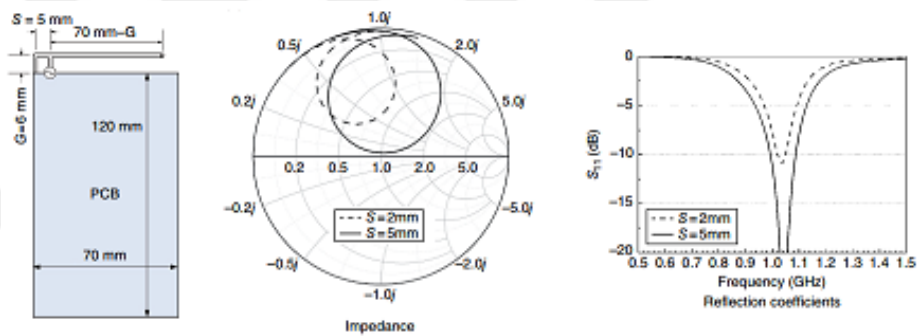


Figure 1.13. Impact of separation G in an Inverted-F Antenna

Since the upper side of the final antenna structure resembles the letter F, the overall structure is called as the “inverted F antenna”. Comparing the impedance characteristics of antennas from Smith chart of Figures 1.12 and 1.13, the grounding strip is seen to function as a shunt inductor. In this type of implementation, the impedance of the antenna for various separation distances can be tuned to that of the feed line by adjusting the length S of the grounding strip accordingly.

In a practical design of an IFA, the procedure starts with a strip that is longer than the quarter of the wavelength at the respective frequency of operation. The strip is placed separated from the ground plane at a particular separation distance of around 4mm and the length of the arm is adjusted to get resonance. According to how the

impedance characteristics of the antenna is seen on the Smith chart, the gap S is fine tuned to get the best resonance possible.

Since there is not much space in the design freedom of the IFA, most of these antennas are used for single-band applications such as GPS, Bluetooth and Wi-Fi. Comparing the two types of implementations of the folded dipole mentioned, the L antenna can be designed to be smaller than the IFA counterpart since the active length of the L antenna starts from the feed point. For the same reason, a PCB with a smaller area is required for L type antennas. However, considering the need of an external tuning circuit for L type antennas, there are some losses related to the lumped matching inductor which reduces the efficiency of the L antenna lower than that of IFA at a few tenths of dB. Therefore, if the size of the PCB is not a concern in design, IFA would be a better choice for its better efficiency and reduced cost from not using a matching component at the feed point.

- **Planar IFA (PIFA)**

The planar inverted F antenna is a low-profile form of the former IFA in which a patch element is used in place of the radiating strip of the IFA. In this configuration, the patch element generally lies above the ground plane and is connected to it by feeding and grounding strips as shown in Figure 1.14.

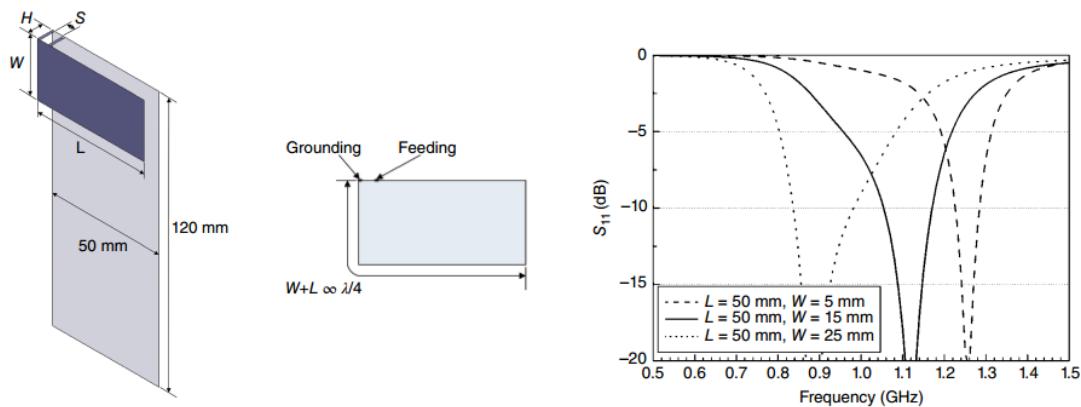


Figure 1.14. PIFA antenna and its resonance frequency for varying widths

As illustrated in Figure 1.14, the resonance frequency of a PIFA can be estimated from the sum of the length and width of the patch which is roughly a quarter of a wavelength at the resonance frequency of interest.

The distance H between the ground and the patch is a critical parameter regarding the bandwidth of the antenna. The bandwidth of the PIFA at a particular frequency of operation is proportional to distance H . Shown in Figure 1.15 is the reflection coefficient of three antennas with patch length (L) and width (W) of 50mm and 25mm respectively, where patches positioned at distances of 5, 7, and 9 mm are considered.

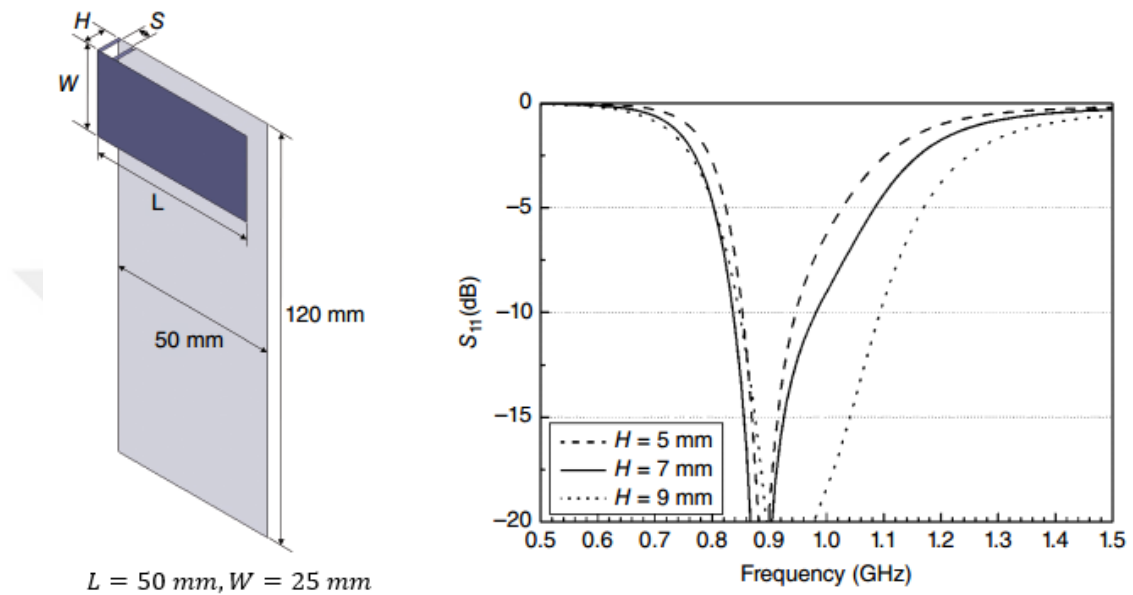


Figure 1.15. PIFA antenna and resonance frequency over varying heights

In overall, the bandwidth of the antenna is shown to almost triple by increasing the ground-patch distance H from 5 to 9 mm under the assumption of -10 dB as the acceptable return loss.

When compared with the IFA structure, there is much higher degree of freedom for designing a multiband PIFA. The most common way of doing this is by the introduction of slits on the patch as shown in Figure 1.16.

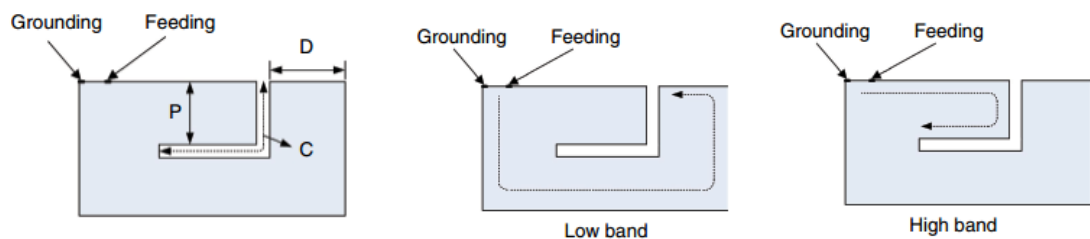


Figure 1.16. Dual band PIFA antenna with paths shown for high and low bands

The terminal and radiational characteristics of the dual band PIFA antenna shown in Figure 1.6 are determined by the dimensions D, C and P. From these three parameters, the distance D between the patch corner and slit opening have the most significant influence on the upper and lower frequency of resonance of the antenna. The effect of D on the two resonance frequencies is towards a shift in opposite directions since the change of this parameter increases the path length of a band while decreasing the other. The C parameter shows its influence mostly in the higher band of operation where an increase in C corresponds to a decrease in the resonance frequency of the upper band. The P parameter also have effect on the upper band despite not being as significant as the C parameter. It is mostly used for fine tuning of the upper band.

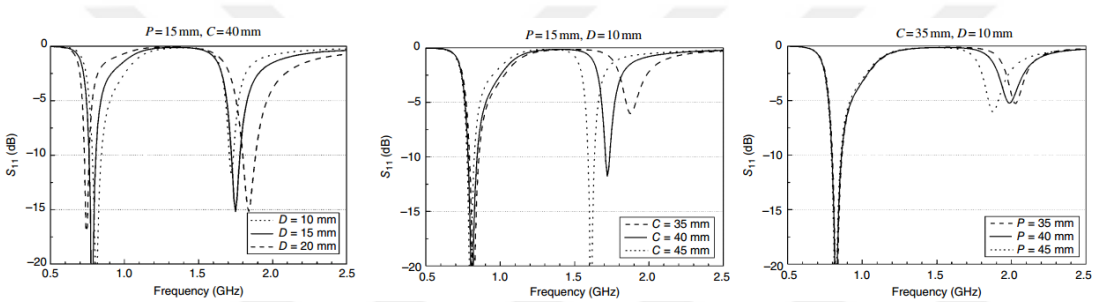


Figure 1.17. Effect of design parameters C, D, and F on a dual band PIFA

By the proper adjustments of these design parameters, the resonance can be tuned in a wide range of interest. In this way, the dimension of the PIFA can be modified as to match its characteristics to that of the fed line. This in turn would save the designer from inherent losses present when matching circuits are used instead.

In addition to the tuning of the antenna by 3 design parameters specified, alternative matching methods are available as shown in Figure 1.18.

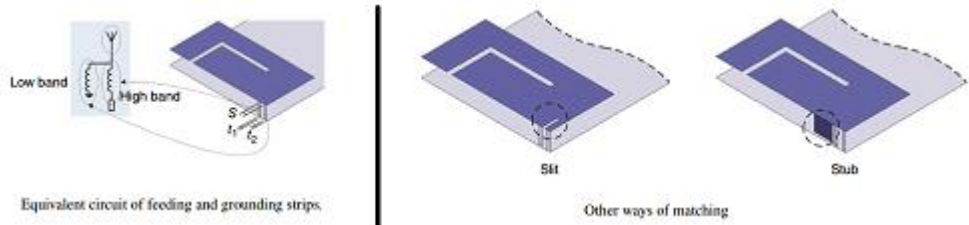


Figure 1.18. Alternative matching methods in a PIFA

The slit introduced between the feeding and shorting terminals of the antenna is used to increase the shunt inductance while addition of a stub is used to add distributed

shunt capacitance to the terminal impedance of the antenna. The addition of stub element decreases the frequency of resonance for both bands as it increases the total current length.

Observation of the current distribution over the patch of a PIFA is made possible by use of commercial simulation software and it provides the design engineer with an insight on how the antenna works in respective bands of operation.

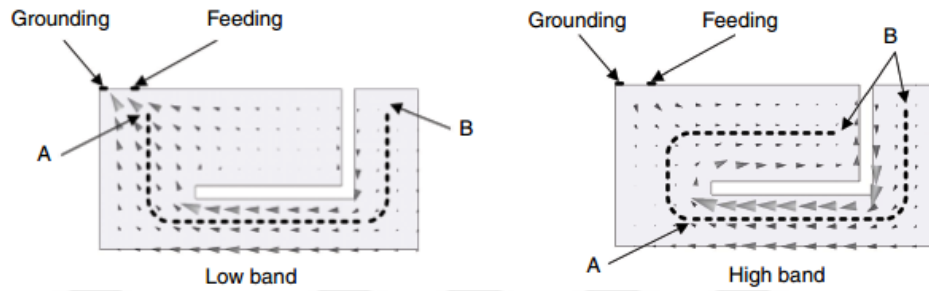


Figure 1.19. Current distribution on a dual band PIFA

One example of the current distribution over the patch of a PIFA is shown in Figure 1.19. For the low band, the current distribution is as in a quarter-wavelength monopole whereas a dipole like distribution is observed for the upper band of operation.

The incorporation of PIFA antennas have been widely employed as internal antennas in the commercial mobile phones. Some of these mobile handsets are shown in Figure 1.20.

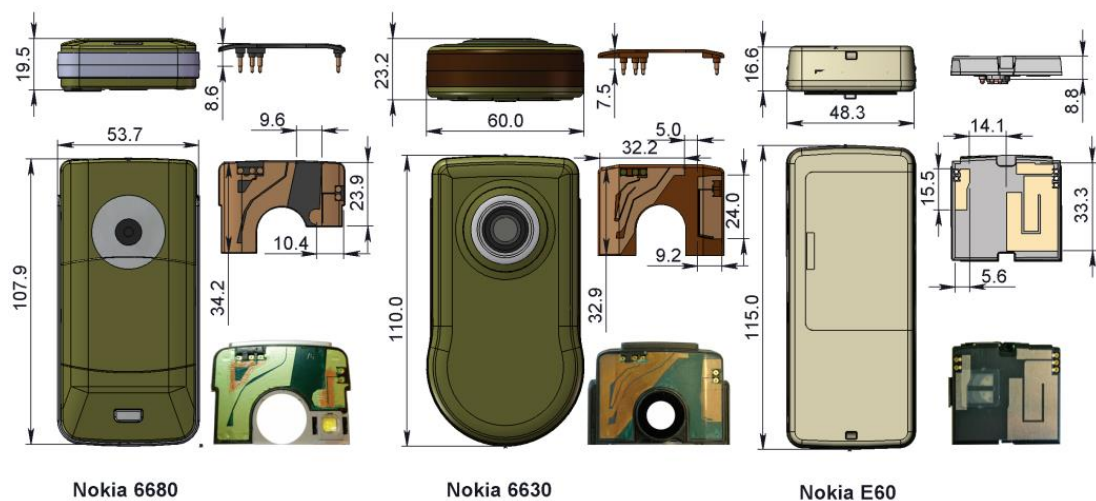


Figure 1.20. PIFA as the 3G GSM antenna in commercial mobile phones (Rowell, 2012)

Following the design of the patch element for resonance at the operational frequencies of interest, the bandwidth of the antenna can be improved by the addition of parasitic elements to the structure of the mobile phone.

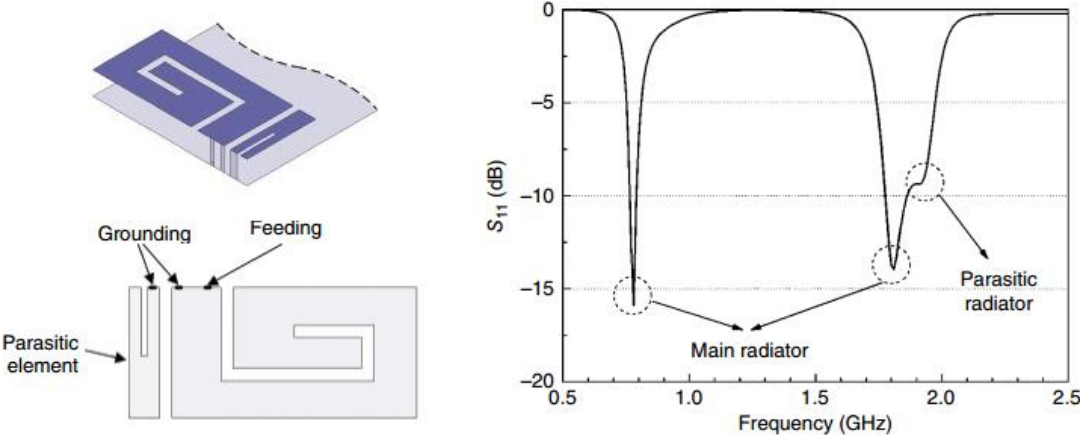


Figure 1.21. PIFA as the 3G GSM antenna in commercial mobile phones (Zhang, 2017)

Shown in Figure 1.21 is the implementation of a parasitic element aside the main patch of IFA. In this configuration, the parasitic element is not electrically connected to the ground plane and is only electromagnetically coupled to the main radiator. As it is evident from the plot of the return loss of the antenna, parasitic elements are mainly used for improvement of available band at the higher frequency of operation.

Some practical implementation of the parasitic element into the structure of commercial mobile phones is shown in Figure 1.22.

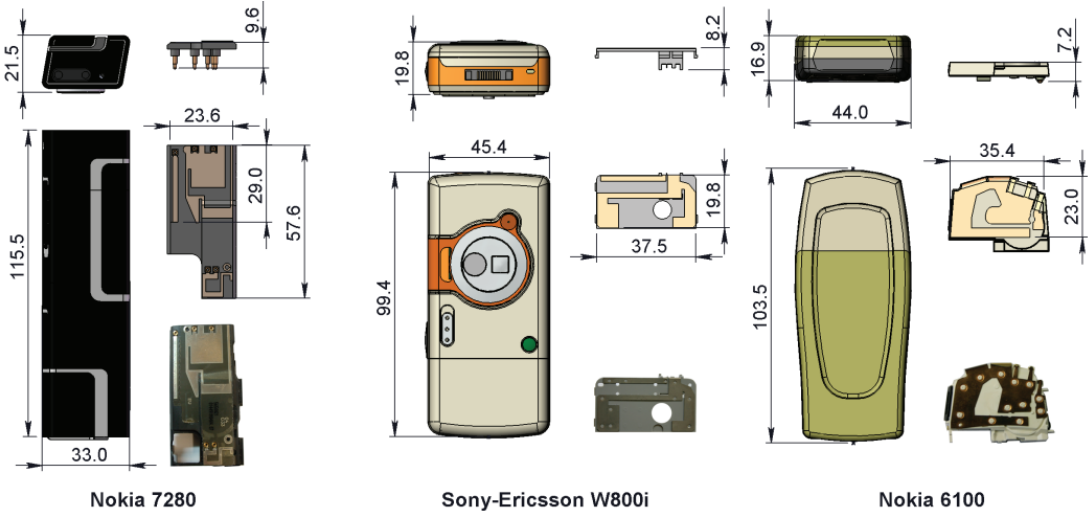


Figure 1.22. PIFAs with parasitic elements in commercial mobile phones

These type antenna configurations generally cover quad-band and penta-band operation of 3G phones at the respective frequencies of 1710-2170 MHz and 1710-1990 MHz.

- **Folded Monopole Antenna**

In a usual talking position, the ground component of the previously introduced PIFA elements are sandwiched between the head of the user and the antenna. This prevents harmful radiation towards the head of the user. However, the bandwidth of the antenna is restricted in this way. In achieving wider bands of operation for the wideband requirements of new generation communication systems, in some mobile phone terminals, the ground is removed and the resulting structure is eventually called as the “folded monopole antenna” instead of a PIFA.

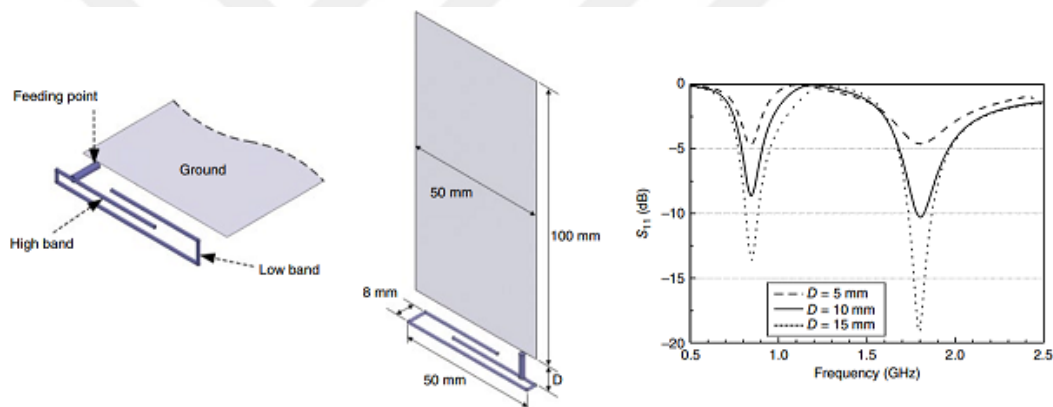


Figure 1.23. A sample internal folded monopole antenna (Zhang, 2017)

A sample structure of a dual band folded monopole antenna is shown in Figure 1.23. In this configuration, the edge of the antenna protrudes over the edge of the ground plane and is built internally on to the inner surface of the plastic casing of the phone. The two branches on two sides of the feed line is designed for the lower and upper frequency of operation. The tuning of the antenna to a specific frequency of interest is implemented by the adjustment of branch lengths accordingly as shown in Figure 1.24.

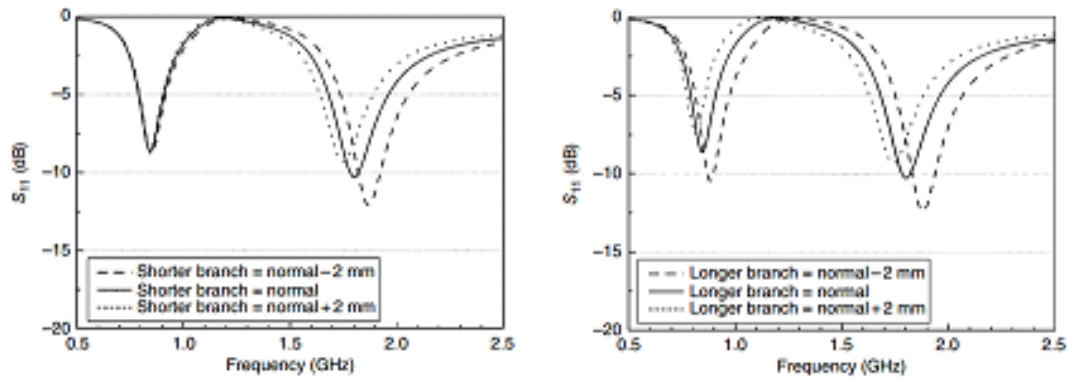


Figure 1.24. Frequency tuning of monopole antenna by branch length (Zhang, 2017)

The length of the shorter branch determines the frequency of resonance at the upper band of operation. In reference to Figure 1.24, a change of 2mm in the length of the shorter branch correspond to a 60 MHz change in the upper resonance frequency. Unlike the shorter branch, the length of the longer branch influences the resonance frequencies at both lower and upper bands.

The bandwidth of the antenna for the selected branch structure mostly depends on the distance D between the folded antenna and the ground plane. The effect of distance D on the bandwidth of the antenna is shown by the plot of a simulated return loss in Figure 1.23.

Figure 1.25 shows various types of implementations of a folded monopole antenna onto the surrounding plastic structure of the handset. As shown in the same figure, Motorola RAZR V3 is an example of a mobile phone employing a folded monopole antenna as its main antenna.



Figure 1.25. Various practical implementations of folded monopole antennas (Zhang, 2017)

Even though the various practical implementations differ in terms of the manufacturing technique used, they are similar from the electrical point of view.

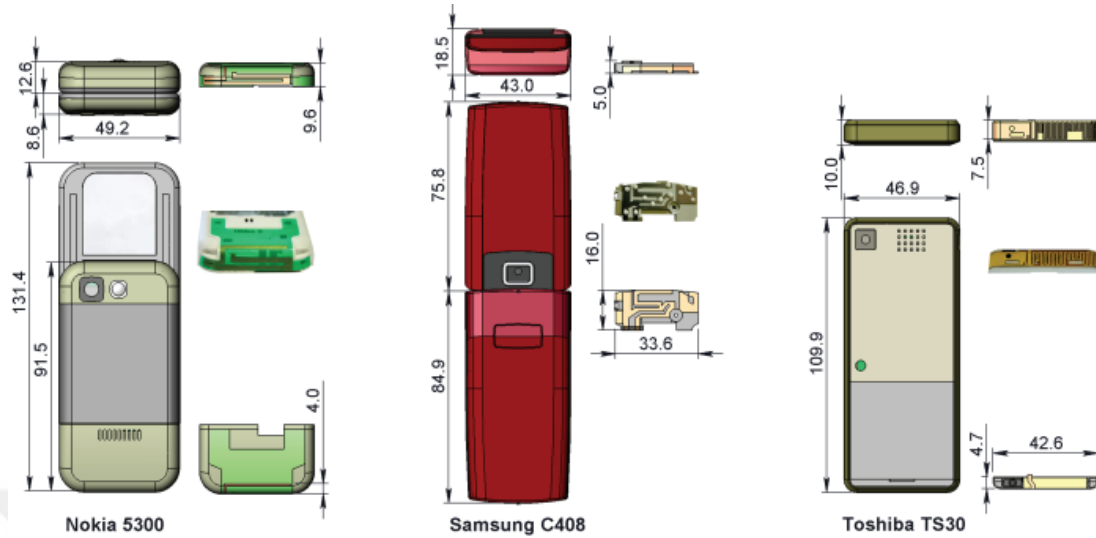


Figure 1.26. Planar monopole antennas in commercial mobile phones (Rowell, 2012)

Planar implementation of the monopole antenna is another type of manufacturing as shown in Figure 1.26.

1.2.3. Antennas in Recent Mobile Phones

Most of today's phone that are out there in the market incorporate multiple and wideband antennas to cover cellular standards of TD-LTE (4G), TD-SCDMA (3G), and GSM (2G). The structuring of the internal antennas operating at these bands are made in a low-profile shape by using printing technologies such as flexible print circuit (FPC) and Laser Direct Structuring (LDS). The latter printing technology of LDS is introduced in Chapter 2. As an example, the primary antenna of Hongmi 2A mobile phone produced by Xiaomi is shown in Figure 1.27 (Zhang, 2017).

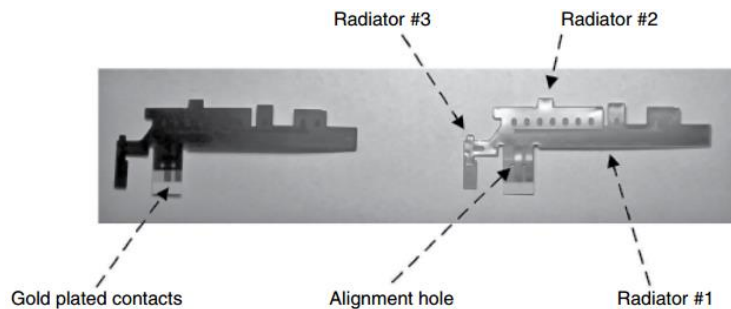


Figure 1.27. A multiband IFA implemented in a Hongmi 2A mobile phone as the main antenna (Zhang, 2017)

In this structure, a multiband IFA structured is adopted with each of radiator branches shown in figure. This elastic structure is built onto the back side of the plastic frame and is fed through a galvanic contact from the PCB. The antenna is matched to the feed line by use of a matching circuit placed on the PCB as shown in Figure 1.28.

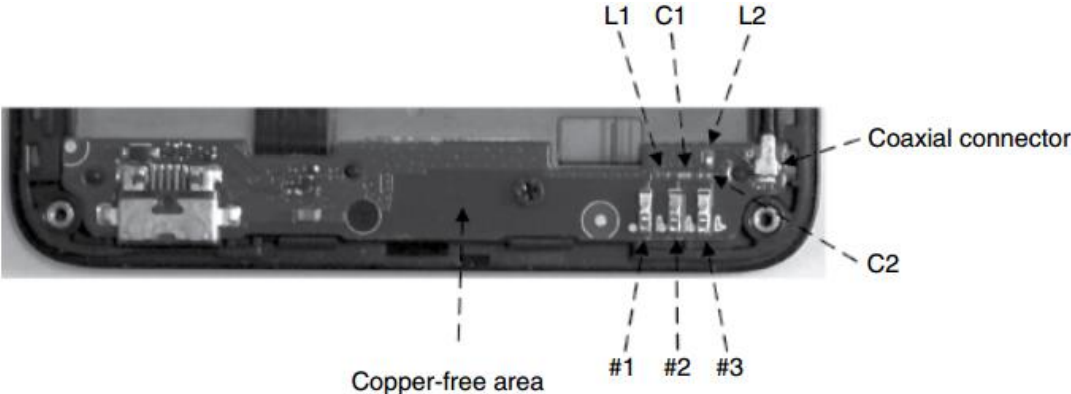


Figure 1.28. Matching circuit of antenna built onto the PCB by SMD components

In addition to the main antenna used for transmission with the based station, the mobile phone structure also comprises at least two antennas for operation in services of GPS and WLAN. Even though independent antenna designs can be implemented for each service, in the case of an unavailable space for two antennas, a single dual-band antenna can be implemented.

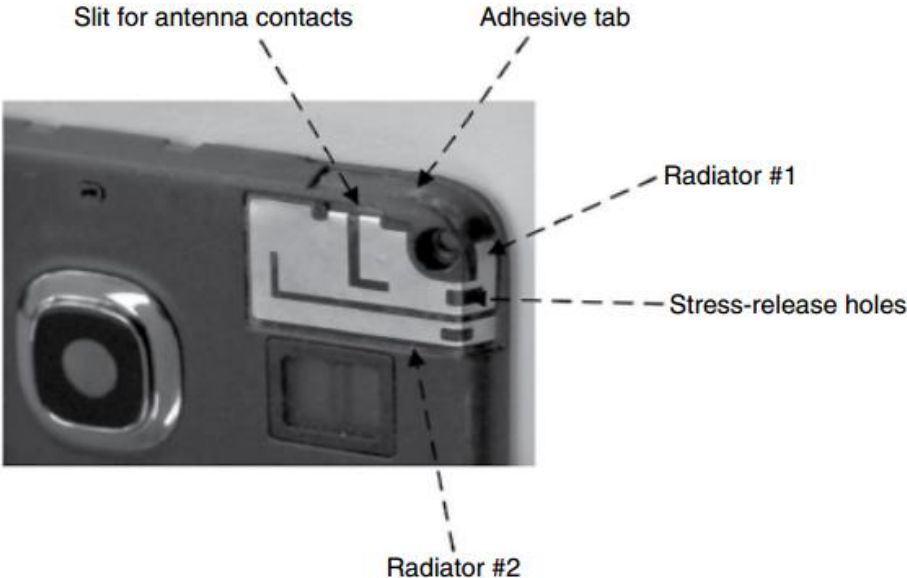


Figure 1.29. A single dual band antenna used for GPS and WLAN services

In this scheme, the antenna can be tuned to the two bands of operation by structural changes in the flex structure or by use of a dual-band matching circuit.

1.3. Multiple-Input Multiple-Output (MIMO) Antennas

When a mobile phone is operated in an urban environment with buildings, walls, and cars around, the signal transmitted by the base station will arrive at the mobile terminal from many directions with different polarization and at different times. This is regarded as the multipath propagation in a communication environment and may exhibit strong fading in the received signal by the antennas of the mobile handset. The effect of fading is best observed when there is no direct line of sight propagation between the base station and the mobile phone. In the case of a destructive interference of signals coming into the mobile phone terminal from different paths, the loss of signal strength may cause decrease in data traffic speed and interruption of calls in progress. In order to keep the occurrence of such conditions at a minimum, MIMO systems are employed at the mobile phone terminal for antenna diversity such that, two antennas are used to connect the mobile phone terminal to the base station. In this way, by continuous monitoring and comparison of the received power by each antenna element, the decision of which antenna to use for communication with the base station can be made at the mobile terminal.

In a practical design, the most significant parameter regarding the design and positioning of multiple antennas at the mobile phone terminal is the isolation between the two antennas. Since both antennas are operation over the same frequency band, a poor isolation between the two would cause a reduced antenna efficiency as the power from an antenna would be absorbed by the other. This compromises the overall system capacity which is actually the ultimate goal of using multiple antennas at the mobile phone terminal.

The simplest and easiest way of increasing the isolation between the two antennas is by placing the two at a far distance as much as possible. Since the main antenna element of recent mobile phones is placed at the bottom side of the phone for preventing harmful radiation towards the head, the diversity antenna which is mostly used in the receive mode only is placed at the upper part of the mobile phone. In addition to this, at a constrained space for placing the two antennas, orthogonal modes of radiation can be implemented by the two antennas so that a good isolation will be obtained when the two are placed together.

1.4. Aim of Research

The aim of this research is to design and realize the physical implementations of cellular, GPS and WIFI antennas to be used in the body of a modern mobile phone terminal. Following the evaluation of terminal and radiational characteristics of the designed antennas by simulations in Computer Simulation Technology (CST) and verification by laboratory measurements, the SAR analysis of the main antenna element is to be carried out by simulations made in microwave studio of CST. This study is carried out as part of a collaboration that is established between VESTEL and researchers from Ege and Yasar university as to realize antenna designs of new generation (based on 4G/4.5G technology) smart phones as part of the R&D activity carried out for the production of domestic phones. In this process, a thorough review of literature is made in order to lay out different schemes of innovative solutions brought to the frequent problems faced with the design and manufacturing of modern mobile phone antennas. By the completion of this work, a cumulative knowledge in theoretical design and techniques of practical implementation and measurement is to be obtained which will in turn lay down the required groundwork for possible future work emanating from this study. In addition to maintaining long-term collaborations in consolidating the cooperation of universities in the development of this critical technology, the in-house knowledge produced within this study is expected to reduce international dependency on antenna designs for Wi-Fi, GPS, Cellular Communication (LTE, GSM, UMTS).

1.5. Outline of Thesis

In Chapter 1, a review of evolution in the parallel development of mobile communication systems and mobile phone antennas are given in terms of their operational diagrams and various types of use.

In Chapter 2, following the definition of fundamental concepts, modern methods of matching and measurement are introduced together with the integration issues faced with the implementation of antennas with other components into the body of the mobile phone.

In Chapter 3, The design considerations of the main and diversity antennas are described together with the simulated and measured performance characteristics obtained at the respective frequency of operation.

In Chapter 4, The design of GPS, 2.4 GHz WIFI and 5.2 GHz WIFI antennas are described for operation at their respective desired frequency of operation. The terminal and radiational characteristics obtained from both simulations and measurements are given.

In Chapter 5, the simulated Specific Absorption Rate (SAR) characteristics of the main antenna in CST is given for various configurations including standard head and hand models.

Conclusions are drawn in Chapter 6.



CHAPTER 2

MOBILE PHONE ANTENNA DESIGN OVERVIEW

The antenna technology has shown a significant progress in parallel to the fast-paced development of new generation communication systems. In each step of the progress, the mobile phone antenna has been improved in terms of the following factors;

- Compactness
- Low profile, small size
- Flexibility
- Robustness
- Multiband

In the recent decade, the changes observed in the antenna design for mobile phone terminals have been in the selection of antenna type, integration with nearby materials into the mobile terminal, and the design procedure followed.

The design of commonly used antennas such as PIFA, planar meander-line, modified dipole antennas of today's mobile phones are based on the concept of small antenna technology. In reducing the size of an antenna element, slow wave structures (meander-line, zigzag) are employed to extend the current path on the antenna. After the antenna is tuned to resonate at the desired bands of operation, its terminal and radiation characteristics are prone to change by the effect of nearby materials such as the ground plane, housing and accessories. Additionally, components with conductive materials in its structure such as camera and speaker should be regarded as part of the radiator when placed near the antenna. The most influential of these nearby materials is the ground plane which may enhance the radiation or degrade the performance of the antenna due to a coupling with the user's hand.

In the evaluation of antenna performance by terminal and radiation measurements, conventional measurement techniques should be used to ensure that the measurement tools have no effect on the behavior of the antenna that is being measured.

In the subparts of this chapter, following the definition of basic concepts in antenna design, fundamental design and implementation issues are introduced together with practical methods of evaluation of a mobile phone antenna.

2.1. Definitions and Concepts

In the quantitative analysis of an antenna in the stage of its design, some terminal and radiational performance characteristics are defined. Reflection coefficient, voltage standing wave ratio (VSWR), efficiency, gain and bandwidth are among the most frequently used performance parameters that are generally used in the specification of an antenna to be designed.

2.1.1. Reflection Coefficient and Return Loss

From the point of view of an electric circuit, an antenna is modeled as a single-port device showing an impedance of Z_{ant} across its terminals. The input signal is fed into the antenna through a transmission line at its input terminal carrying an incident wave of amplitude $V_{incident}$. Due to a possible mismatch between the impedance of the antenna and the transmission line, some part of the incident energy is radiated by the antenna, whereas the rest of the energy is reflected back at the antenna port and travels along the transmission line towards the source. Assuming the amplitude of $V_{reflected}$ for the reflected wave, the reflection coefficient is defined by

$$\Gamma = \frac{V_{reflected}}{V_{incident}} \quad (2)$$

In the design of an antenna, the primary goal is to minimize the reflection coefficient at the antenna port as to keep the amount of power radiated by the antenna at a maximum. The reflection coefficient takes on values in the range from zero to one. A reflection coefficient of 1 means a mismatch at the antenna terminal where all the incident power is reflected back at antenna terminal, whereas a reflection coefficient of 0 means a perfect match at the antenna terminal where all the incident power is radiated by the antenna.

In terms of the S parameters used for the quantitative description of a network with multiple ports, the reflection coefficient is equivalent to the S_{11} parameter.

$$S_{11} = \Gamma \quad (3)$$

In practice, the S_{11} is generally given in the decibel scale calculated as

$$S_{11}(dB) = 20 \log(|S_{11}|) \quad (4)$$

The absolute value of $S_{11}(dB)$ is called as the return loss (RL) which takes on values between 0 and minus infinity. A return loss of 0 means total reflection while a minus infinity means no reflection at the antenna terminal.

The bandwidth of antenna at a particular frequency of operation is defined based on a return loss criterion as shown in Figure 2.1.

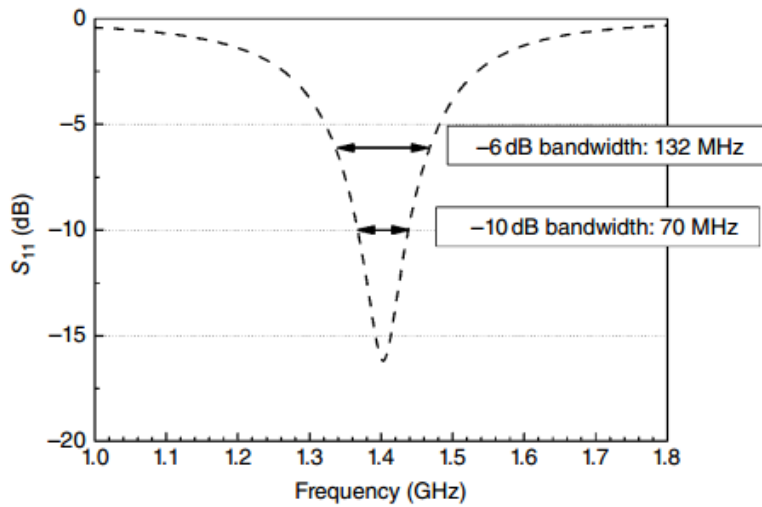


Figure 2.1. Definition of antenna bandwidth under a certain return loss criterion

By reference to Figure 2.1, the antenna is said to have a -10 dB bandwidth of 70 MHz or -6 dB bandwidth of 132 MHz.

2.1.2. Voltage Standing Wave Ratio (VSWR)

VSWR is another measure of how well the impedance of the antenna is matched to that of the transmission line that is defined by the characteristics of the standing wave formed along the transmission line by the superposition of the incident and reflected waves. The VSWR is mathematically defined as the ratio of the amplitudes of the maximum voltage V_{max} to the minimum voltage V_{min} in the amplitude of a partial standing wave.

$$VSWR = \frac{|V_{max}|}{|V_{min}|} \quad (5)$$

Since the standing wave by which the VSWR is defined is formed by the superposition of the incident and reflected waves, the mathematical expression for VSWR can be written in terms of $V_{incident}$, $V_{reflected}$, and Γ as shown below.

$$VSWR = \frac{|V_{incident}| + |V_{reflected}|}{|V_{incident}| - |V_{reflected}|} = \frac{1 + |\Gamma|}{1 - |\Gamma|} \quad (6)$$

The VSWR takes on values between 1 and infinity where 1 means no reflection and infinity means total reflection at the terminal of the antenna. The measured VSWR is generally given in the X:1 format where, for example, a VSWR of 2:1 means a maximum voltage twice the amplitude of the minimum voltage.

2.1.3. Efficiency

Antenna design with terminal impedances that are well matched to that of the transmission line does not necessarily mean a good antenna. Efficiency is used as a measure of how well the power accepted by the antenna is radiated to the air. The efficiency parameter is mathematically expressed as,

$$Efficiency = \frac{P_{radiated}}{P_{accepted}} \quad (7)$$

where $P_{radiated}$ is that portion of the accepted power radiated to the air and $P_{accepted}$ is the total power entering through the terminal of the antenna. The efficiency of an antenna takes on values between 0 and 1 and is practically given in dB scale as,

$$Efficiency (dB) = 10 \log_{10}(efficiency) \quad (8)$$

In scaling efficiency to the dB scale, a constant of 10 is used in front of the logarithm term since the efficiency is defined as the ratio of two power terms.

The gain of the antenna as a measure of its efficiency and radiation characteristics is mostly determined based on the positioning of the antenna and size of the ground structure. Gain has no practical importance in a mobile phone antenna design since the antenna engineer does not have much freedom in deciding the gain of the antenna by structural changes to the antenna element itself (Zhang, 2017).

2.2. Physical Limits of Antenna Design

For an antenna to be designed with given performance requirements over an operating frequency, the size of the antenna cannot be made arbitrarily small since the performance of the antenna element is sensitive to its electrical size compared to wavelength (Fujimoto, 2001). The bandwidth and efficiency of the antenna is directly related to its size and will show reduced performance in terms of bandwidth and efficiency when made smaller than a half wave dipole.

The quality factor (Q) of an antenna is of significant value to the antenna designer as it provides knowledge on how small an antenna can be constructed for a given bandwidth. It is defined as the ratio of the time-average of dissipated energy to the power radiated by the antenna. The physical size of the antenna relative to a given wavelength can be quantified by means of the lower boundary of the radiation quality, regarded as the “Chu” limit (Zhang, 2017).

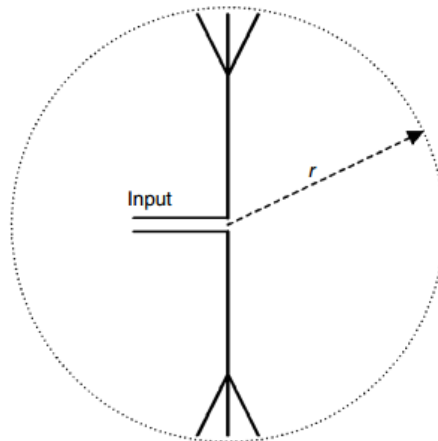


Figure 2.2. Minimal sphere enclosing an antenna

For a minimal sphere of radius r enclosing the antenna, the lower limit for the quality factor (Q) is defined as r/λ . For Q values much greater than 1, the percentage bandwidth of the antenna around the center frequency of f_{center} can be approximated by,

$$\% \text{ Bandwidth} = \frac{f_{upper} - f_{lower}}{f_{center}} = \frac{1}{Q} \quad (9)$$

In a practical design, it is difficult to define an enclosing sphere from which the bandwidth of the antenna can be approximated. Considering that the ground plane is part of the radiating structures in antenna structures of modern mobile phones, an all

enclosing sphere would have such a long radius that it would result unachievably wide bandwidth estimates by Chu's expression. Similarly, excluding the ground terminal from the enclosing sphere completely would underestimate the actual bandwidth of the antenna. In addition, the radiating effects of nearby components such as battery and speaker further affect the bandwidth of the antenna making it harder to pre-estimate the bandwidth.

2.3. Antenna Matching

The progress shown in the technological tools can be used for the development of low profile, multiband antennas. In this way, the antenna designer is provided with design freedom as to change the antenna structure to satisfy given performance criteria. In some cases, the structural changes to the antenna element are not enough to match the impedance of the antenna to that of the feed line for better radiation and efficiency. In such cases, matching circuit networks are constructed in front of the feedline where inductors and capacitors are used. Resistors are not used in this network since it would bring additional losses to the systems thus reducing the efficiency which is one of the ultimate goals of antenna design.

2.3.1. Smith Chart

The essential goal of antenna matching is to convert the terminal impedance of the antenna to that of the transmission line that is feeding the antenna, which is set as 50 Ω by industry standards. The reflection coefficient defined previously is a complex quantity represented as,

$$\Gamma = \frac{V_{reflected}}{V_{incident}} = |\Gamma| \angle \Theta_{\Gamma} \quad (10)$$

The reflection coefficient can be graphed in a two-dimensional complex plane as shown in Figure 2.3 where the amplitude of Γ is constant over any of the concentric circles shown.

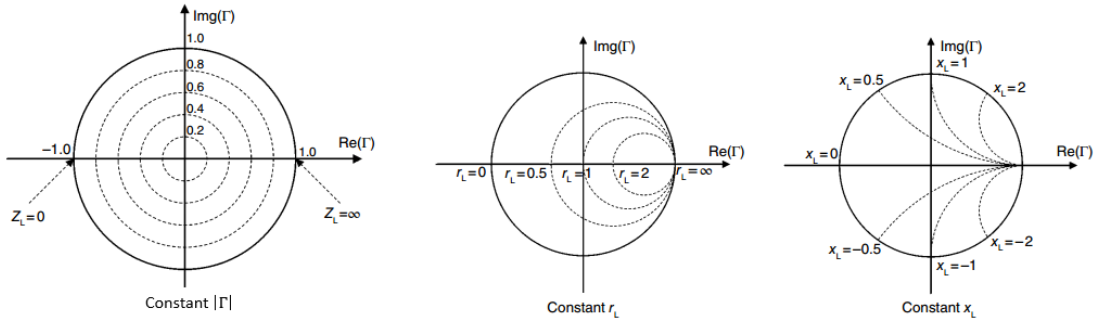


Figure 2.3. Constant $|\Gamma|$, r_L , and x_L curves

The complex reflection coefficient can also be written in terms of the following equation,

$$\Gamma = \frac{Z_L - Z_0}{Z_L + Z_0} = \frac{Z_L/Z_0 - 1}{Z_L/Z_0 + 1} = \frac{z_L - 1}{z_L + 1} \quad (11)$$

Here, Z_L is the load (antenna in this case) impedance, Z_0 is the characteristic impedance of the transmission line and z_L is the antenna impedance normalized with respect to that of the transmission line. The normalized impedance is a complex quantity and can be written as the sum of its real and imaginary components expressed as,

$$z_L = r_L + jx_L \quad (12)$$

The variation of normalized impedance z_L over the complex plane shown by constant r_L and x_L curves are shown in Figure 2.3. The Smith Chart is constructed by the overlay of the constant r_L and x_L curves on to the same graph as shown in Figure 2.4.

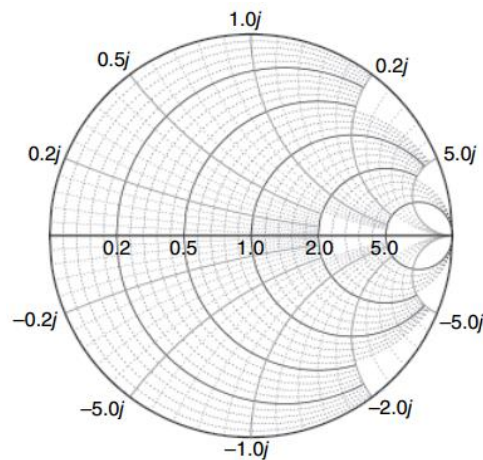


Figure 2.4. The Smith Chart

A given load connected at the end of a transmission line is represented by a unique corresponding point in the Smith Chart and the variation of overall load impedance by connection of reactive matching components is evaluated by moving the respective curve over constant r_L curves. In finding the total impedance at the source, the matched impedance point on the Smith Chart is moved over the constant x_L curves by a ratio of the wavelength corresponding to the length of the transmission line.

In working with components placed in parallel at the matching network, it is easier to work in the admittance Smith chart which is simply obtained by rotating the Smith chart by 180 degrees. In this case, the curves represent the real g_L and imaginary b_L parts of the normalized load admittance y_L expressed as,

$$y_L = \frac{1}{z_L} = g_L + jb_L \quad (13)$$

For ease of use, ZY Smith charts are constructed by a combination of the impedance and admittance Smith charts as show in Figure 2.5.

The ZY Smith charts are useful in making transitions between impedance and admittance charts in working with matching circuits composed of several series and parallel reactive components.

2.3.2. Single-Band Matching

In the reactive lumped element matching of an antenna by use of reactive components, a matching component can move the normalized impedance or admittance along the constant curves of r_L or g_L of the ZY Smith Chart. For possible combinations of the parallel and series connection of a capacitor or an inductor, a load point can move along 4 directions over two curves as shown in Figure 2.6.

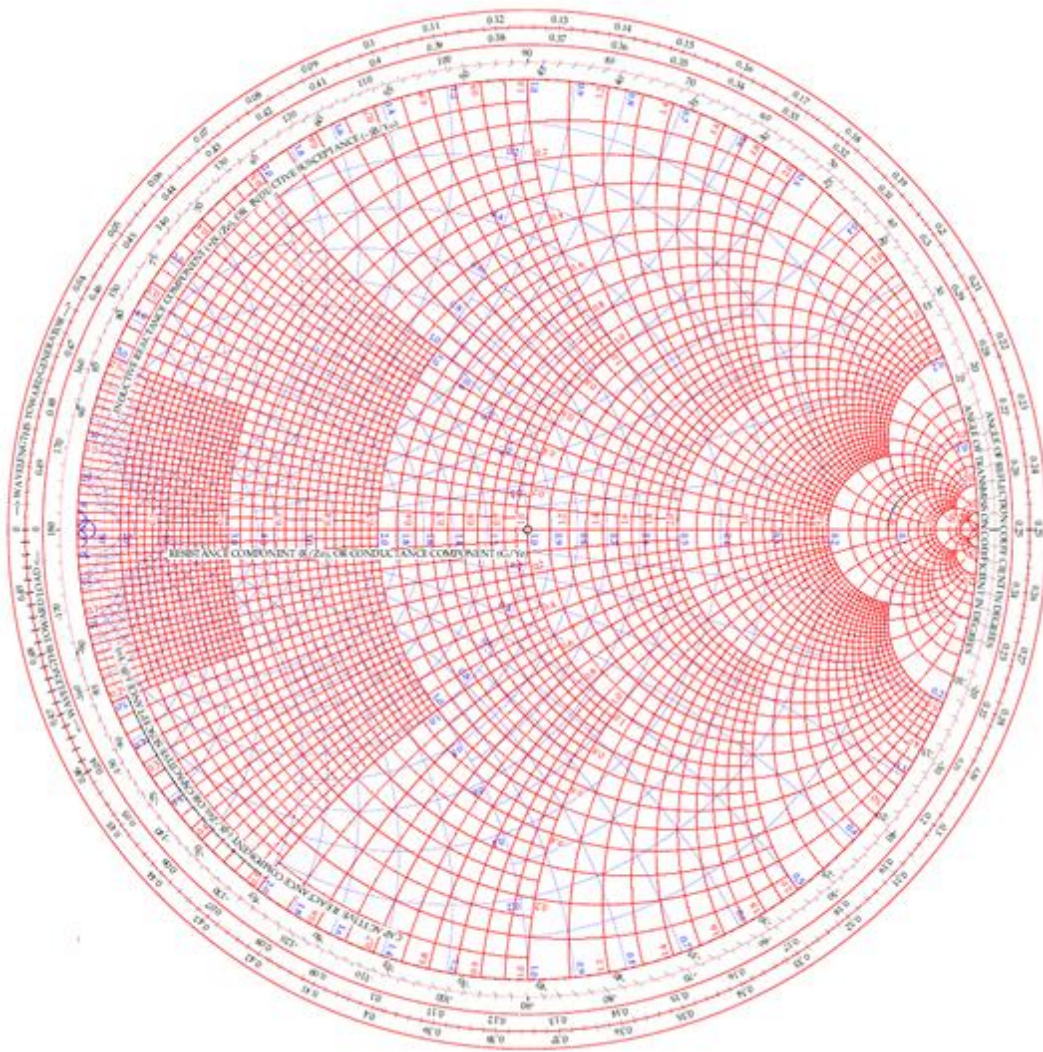


Figure 2.5. The ZY Smith Chart

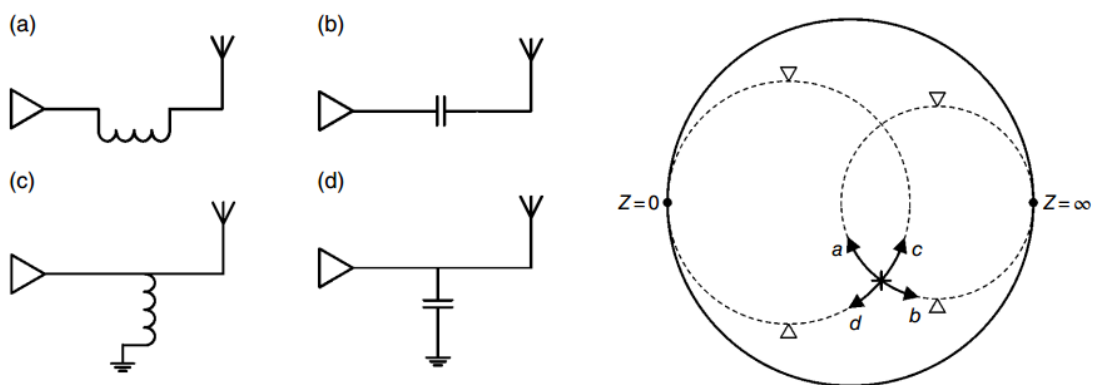


Figure 2.6. Respective ZY chart directions for 4 possible connections of lumped reactive matching elements

For the single band matching of an impedance that is inside the $|\Gamma| = 1$ circle, there are four possible ways of moving the normalized impedance to the center of the chart as shown in Figure 2.7.

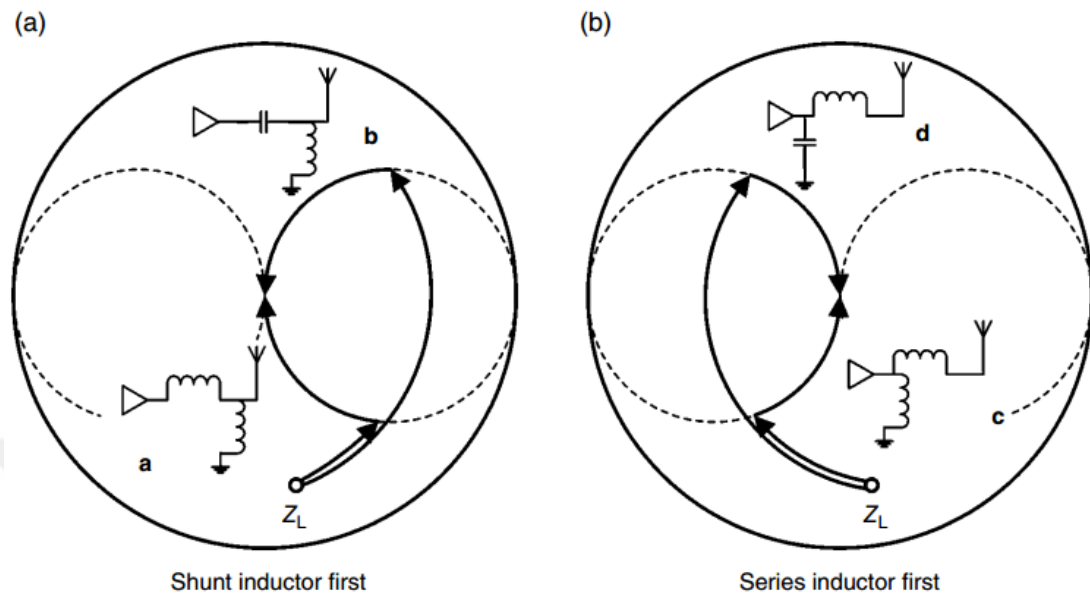


Figure 2.7. Four possible matching circuit options for a single load impedance

Each matching circuit combinations have their own advantages under certain circumstances. As an example, in the case of a potential electrostatic discharge hazard, matching circuits (a) and (b) can be preferred since there is a shunt inductor, which shorts the antenna to the ground terminal from the DC current of view.

2.3.3. Dual-Band Matching

In a design environment where there is a physically constrained volume that is available for the antenna, the limited bandwidth of the antenna needs to be utilized in multiple bands operation by use of appropriate matching circuits. For the case of a dual-band matching, when selecting a matching component for the particular band of operation, the selected component should have the desired impact at the respective frequency while imposing less effect on the other band. As an example, use of shunt capacitors or series inductor is preferred in a high frequency band matching.

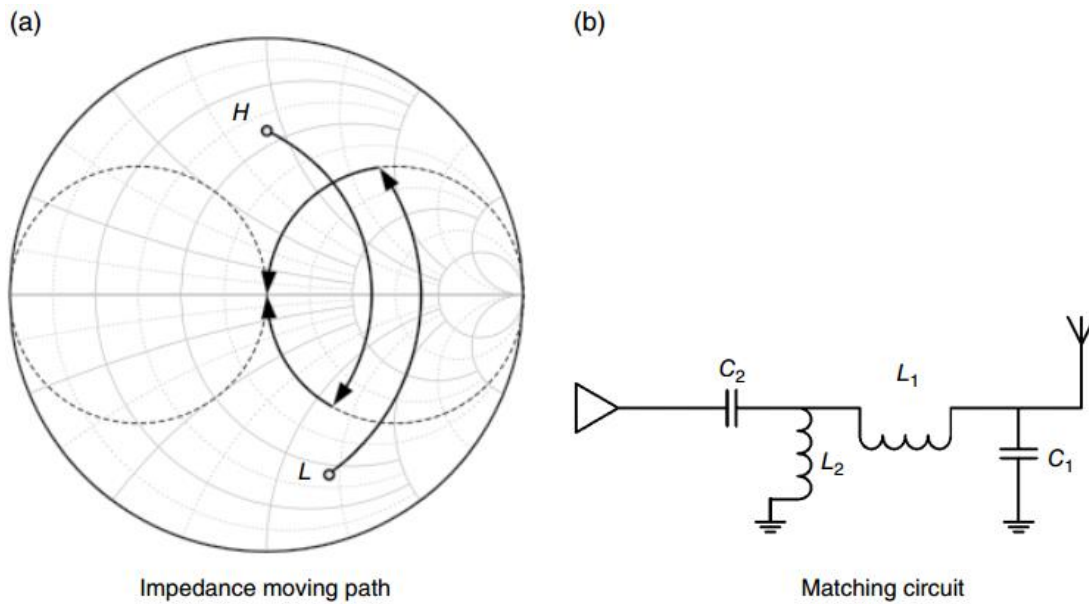


Figure 2.8. Dual band matching with four elements

An example of a dual band matching scheme is shown in Figure 2.8. In this figure, the high and low bands are marked by L and H, respectively. In deciding for the four matching circuit components, two of the reactive components are used for the lower band of operation while the other two are used for the higher band of operation. In doing so, the ideal operation of reactive components is assumed where the impact of a component used for a particular band is assumed not to occur on the other band of operation. In the high frequency band, the impedance is moved to the bottom part of the $r = 1$ circle by capacitor C_1 and is then moved to the center of the chart by L_1 . At the lower band, the normalized impedance is moved to the top of the Smith Chart by L_2 and is then moved to the center by C_2 .

2.3.4. Reconfigurable Matching

Considering the physically limited volume allocated to the design of antennas in modern mobile phone structures, it is hard to find a single matching circuit that will enable the use of limited available bandwidth of the antenna over the multiple bands of operation. This calls for the use for different matching configurations regarded as the reconfigurable matching for each band that are controlled electronically by a control circuitry. In this configuration, the system covers a wide frequency band by shifting the available bandwidth over narrower operational bands by each matching circuit.

An important issue to be considered with the use of reconfigurable circuits is the degradation in efficiency of the antenna due to inherent losses brought by inductors, capacitors and optional use of active components such as varactors, pin diodes, and field effect transistors (FET).

In the switch based reconfigurable matching of an antenna, a separate matching circuit for each band of operation is employed by use of electronic switches. In the design stage of this configuration, the impedance curve of the antenna over its operational frequency range is divided into sub frequency ranges as shown in Figure 2.9. This sample configuration is constructed by use of two single-pole four-throw switches where the antenna and the feed line are connected to the single-pole terminal of respective switches.

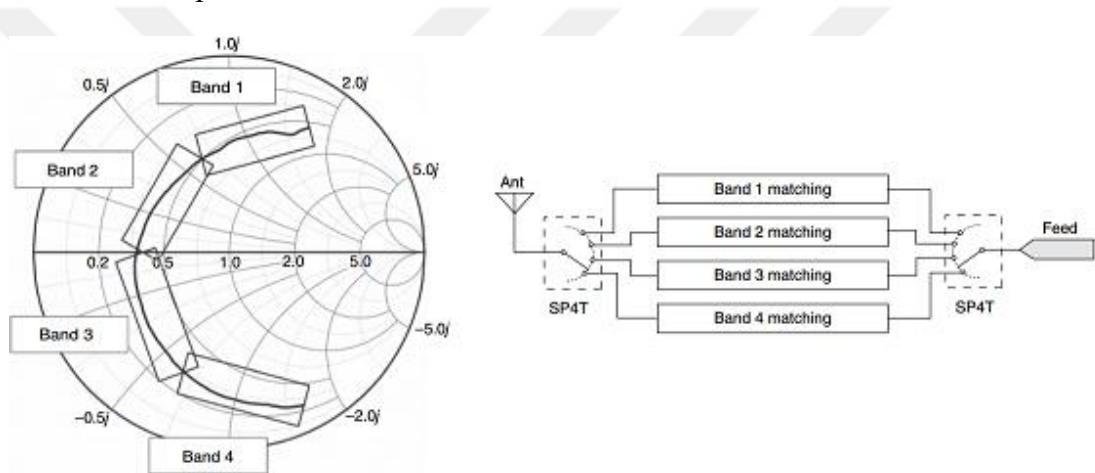


Figure 2.9. Reconfigurable Matching Circuit in four bands

The four matching circuits designed for each band of operation are connected between the corresponding four-throw terminals of the switches. The switches on both sides of the matching circuit are operated synchronously in selecting a particular matching circuit at the operational frequency band of interest. In this way, the matching circuits are isolated which enables the independent design of each circuit for each respective band. A total of eight reactive matching components are used under the assumption of using two components for each matching circuit.

Assuming the use of matching circuits shown in Figure 2.10 for each of four bands,

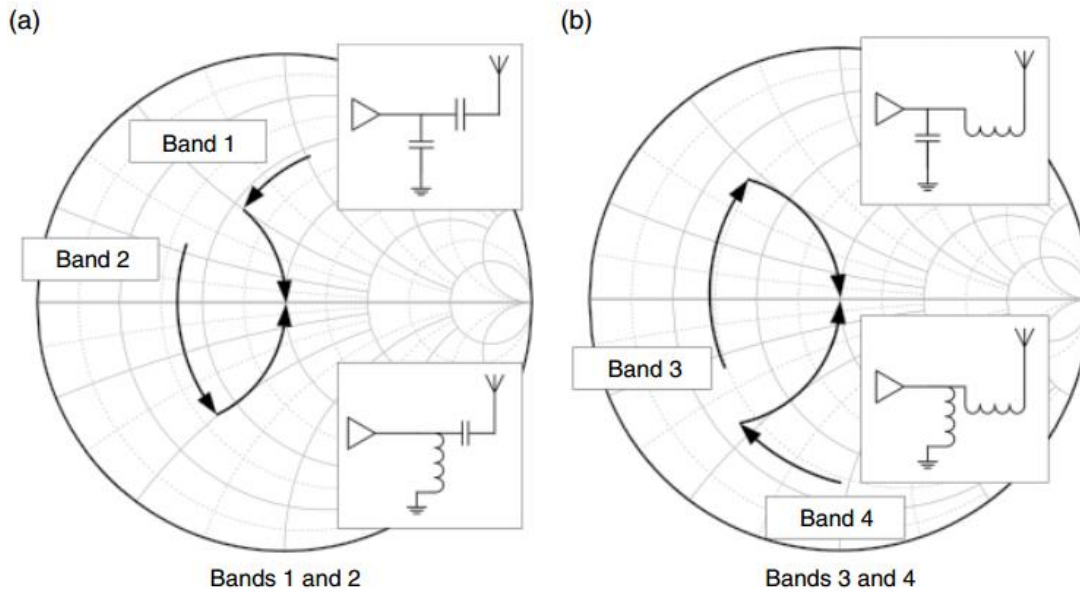


Figure 2.10. Impedance curves for each matching circuit in four bands

The overall circuit configuration can be simplified based on the concept of reuse with the lumped reactive components in matching circuits. A sample simplified configuration built by using four reactive elements and two single-pole double-throw switches is shown in Figure 2.11.

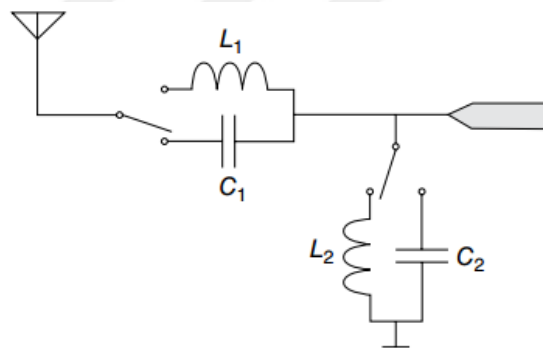


Figure 2.11. Simplified reconfigurable switching by reuse of matching components

Based on the antenna impedance curve shown in Figure 2.10, the use of $L_1 = 5.1 \text{ nH}$, $L_2 = 15 \text{ nH}$, $C_1 = 4.7 \text{ pF}$, $C_2 = 5.6 \text{ pF}$ as the matching circuit elements shown in Figure 2.11 results in a return loss characteristic as shown in Figure 2.12.

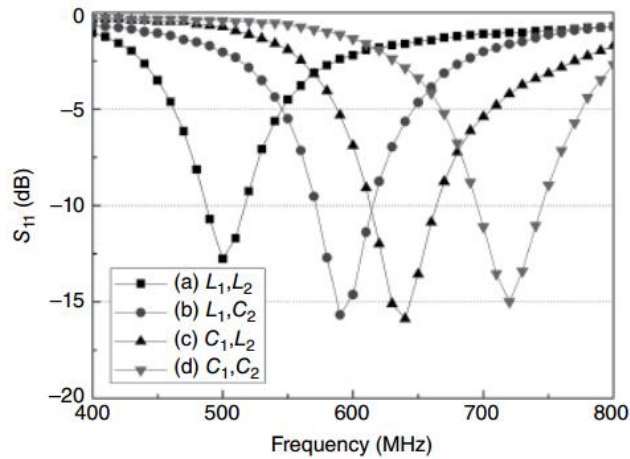


Figure 2.12. Return loss for matching circuit with reused components

Even though the design concept of switch-based matching is straightforward, the implementation of the circuit with several components into the PCB of the mobile phone brings some complications in the process of circuit design.

2.4. Antenna Manufacturing Technology

The manufacturing technologies available for use in the design of antennas for mobile phones is a decisive parameter on the type of antenna to be used and its structural properties since each method of manufacturing has its own set of limitations. Metal Stamping, Molded Interconnected Device (MID), Flex-film are among the commonly used methods of manufacturing in recent mobile phones

2.4.1. Metal Stamping

Metal stamping is the cheapest technology used in the manufacturing of internal antennas for mobile terminals. In this technology, the metallic radiator as the antenna is assembled onto the plastic carrier of the phone by use of multiple heat stakes.

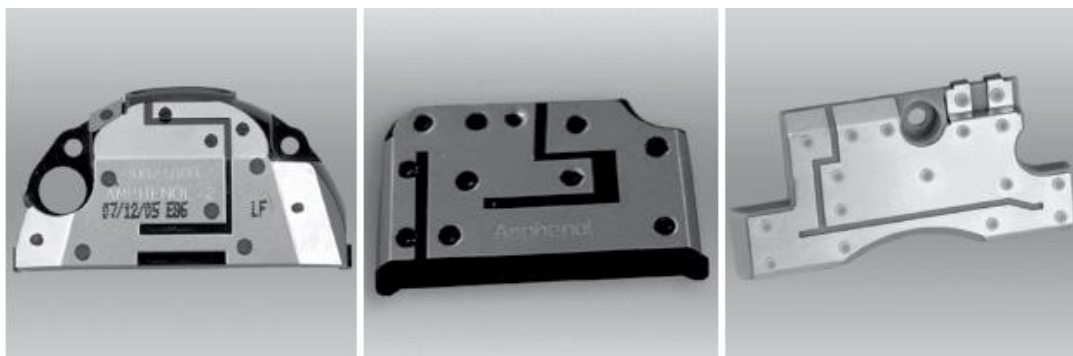


Figure 2.13. Antennas printed by metal stamping on plastic carrier

The printed antennas are fed through gold-plated spring fingers placed on the PCB of the mobile phone. Even though the metal stamping technology provides some degree of freedom in laying out antenna pattern on a combination of two-dimensional surfaces, it does not allow design on double-curved surfaces. Additionally, a minimum line width is required in ensuring the stability of the structure. Thus, the use of this method is encouraged for antenna designs that does not depend small dimensions, such as placing a 0.35 mm gap between a capacitive load and the antenna.

2.4.2. Molded Interconnected Device (MID)

In the area of electrical circuit design, Molded Interconnected Device technology is the integration of electric circuit traces onto high temperature thermoplastics by structured metallization. There is a variety of methods available for use in the structuring of circuit traces on plastic carrier body. As one of these methods, Laser Direct Structuring (LDS) is one of the most commonly used methods in the antenna layout manufacturing of modern mobile phone terminals.

The process of antenna manufacturing by LDS starts by the molding of a doped thermoplastic by either one-shot or two-shot molding. In the single-shot MID, the trace is laser etched into electroplated metal on a single type of plastic. Despite providing flexibility for surface design with double-curved profiles, single-shot molding is not well suited for three-dimensional designs with via holes and feeding structures of the antenna. In the two-shot molding, two types of plastics are molded which is cheaper than its one-shot counterpart in cases of production in large quantities. As the initial step of the metallic plating, the thermoplastic is doped with an additive where a physical-chemical reaction forms the metallic nuclei. A laser then creates a rough surface over which the copper is anchored during the metallization procedure. In the metallization step of the process, following the cleaning of the surface, tracks with height of 5-8 μm are built-up with the help of current-free Cu baths



Figure 2.14. Three-dimensional structuring on carrier plastic by LDS (LKPF,2017)

With this method of manufacturing, both sides of the carrier plastic can be metallized in a three-dimensional layout and be connected to each other by interconnecting vias through connection holes. Shown in Figure 2.14 is a sample structuring of an antenna element onto the plastic casing of a mobile phone terminal. The LDS technology is now one of the standard processes of antenna manufacturing for high-end phones. In terms of antenna operation, LDS method can be regarded as the most consistent scheme since the antennas are built as part of the plastic structure.

2.5. Antenna Measurement

In the design process of antennas, the terminal and radiation characteristics of the antennas are evaluated by passive and active methods of measurement. In the passive measurement of a mobile phone antenna, the host device is in an inactive state and the performance parameters such as standing wave ratio (VSWR) or reflection coefficient, efficiency and gain are measured by external signal generators. In the active measurement of performance parameters such as total radiate power (TRP), effective isotropic radiated power (EIRP), total isotropic sensitivity (TIS), and effective isotropic sensitivity (EIS), the measurements are made when the device is kept in a working state. In the following subsections, the active and passive methods of antenna measurements are introduced together with practical issues of frequent occurrence.

2.5.1. Passive Antenna Measurement on a Vector Network Analyzer

Network analyzer is a crucial piece of equipment used for the measurement of a variety of parameters of an antenna such as the reflection coefficient and transmission loss. There are two types of this device as scalar network analyzer

(SNA) and vector network analyzer (VNA). In a vector network analyzer, amplitude and phase characteristics of terminal response can be measured such that it can be used to display the impedance of the antenna on the Smith Chart, whereas, a scalar network analyzer can only show the amplitude characteristics of the measured quantity. By the use of VNA, the tuning process of antenna design can be simplified by visualization of its impedance while tweaking various parameters of the antenna for desired performance.



Figure 2.15. Sample vector network analyzer with its simplified schematics

For the VNA shown in Figure 2.15, there are two ports which enables the measurement S_{11} and S_{21} parameters. In the measurement these quantities, three vector receivers are employed, namely A, R, and B, inside the network analyzer. Here R is the reference receiver that is connected to the signal source through a power divider. A is the reflection receiver that is connected to port 1 through a directional coupler which is designed to couple the reflected power from the device under test. B, on the other hand, is the transmission receiver that measures the amount of power going through the device under test and reaching port 2. S_{11} parameter is internally calculated by the analyzer by using the measured complex values from A and R. Similarly, S_{21} is calculated from complex values measured from B and R.

In the specification of the terminal characteristics of an antenna, both the reflection coefficient and VSWR are used. The two quantities can be converted into one another by use of the following equations.

$$\text{Reflection Coeff.} = 20 \log \left(\frac{VSWR - 1}{VSWR + 1} \right) \text{ (dB)} \quad (14)$$

$$VSWR = \frac{1 + 10^{\frac{RL}{20}}}{1 - 10^{\frac{RL}{20}}} \quad (15)$$

In terms of the S_{11} parameter, -6 dB and -10 dB are the commonly used limits over which the bandwidth of antenna is evaluated.

2.5.2. Measurement Setup and Location of Testing Cable

Since the antenna is a radiating element, its terminal response may be affected by nearby objects around the antenna. In order to isolate the antenna from surrounding objects, the device under test should be placed far from the surface of the bench by use of a supporting foam with permittivity close to one.



Figure 2.16. Antenna testing setup on a vector network analyzer

Maintenance of a good fixture in the evaluation of an antenna is an essential skill required for providing the duplicate of the environment which is electromagnetically equivalent to the actual working environment of the device. In doing so, one should keep in mind that the body of the phone is also a part of the radiator and modifications made to it may shift the resonance frequency of the antenna by disturbing the radiation current on the phone.

In the process of building the early prototypes of antenna and phone combination, single sided printed circuit boards can be used to represent the multilayered PCB of the actual terminal. Use of such a board is sufficient as a valid approximation of the PCB since the ground layer is of importance in the operation of the antenna. For the cases of using multilayer PCB boards in prototypes, the conductors on both sides of

the PCB must be well connected by interconnecting vias in order to prevent the occurrence of unwanted parasitic resonances.

The remaining parts of the mobile phone terminal such as battery, housing and screen of the phone also effect the operation of the antenna by coupling or dielectric loading. The influence of these components in the integration process of the antenna is further introduced in subsection 2.5.3.

In the passive measurement of antennas where an external source is connected to excite the antenna, the location of the testing cable on the mobile phone terminal under test is another important aspect of taking reliable measurements of terminal characteristics. For that purpose, semi-rigid cables are used as an alternative to flexible coaxial cables for their superior performance especially at higher frequencies.

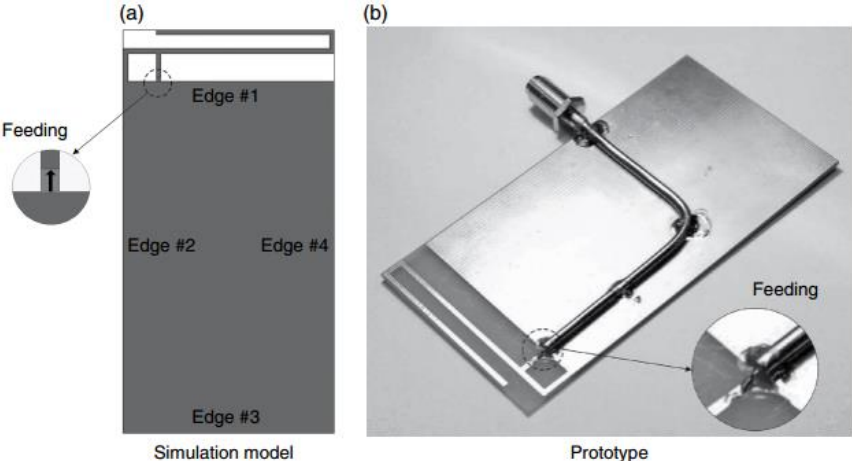


Figure 2.17. Sample test configuration of a PIFA antenna

A sample configuration built for the testing of a PIFA antenna is shown in Figure 2.17. In this configuration, the inner conductor of the semirigid cable is connected to the antenna and the outer conductor is soldered to the ground plane of the system. The cable is then laid in parallel to the ground plane and is soldered at multiple points to the ground plane of the system. At the end of the semi-rigid cable, an SMA connector is used to connect the antenna to the external signal source.

The placing of the semi-rigid cable along the surface of the ground plane should be done in a way that current distributions on the ground will not leak to the semi-rigid cable. Evaluating the suitability in Figure 2.17 as exit points of the semi-rigid cable, edge 1 is adjacent to the antenna element so the placement of the cable's end at this

point will affect the response of antenna. Edge 2 carries strong currents at both high and low bands of operation. Connection to edge 3 will alter the effective length of the ground plane and change the resonance frequency of the antenna. Thus Edge 4 is the best choice for connecting the edge of the connector. In general, the placement of the test cable is said to depend on the type of antenna used and the corresponding current distribution on the ground plane of the system.

In the case of taking measurement from a real mobile phone, the decision of where to connect the test cable is made easy by the switch connectors placed on the PCB for purposes of tuning and calibration.

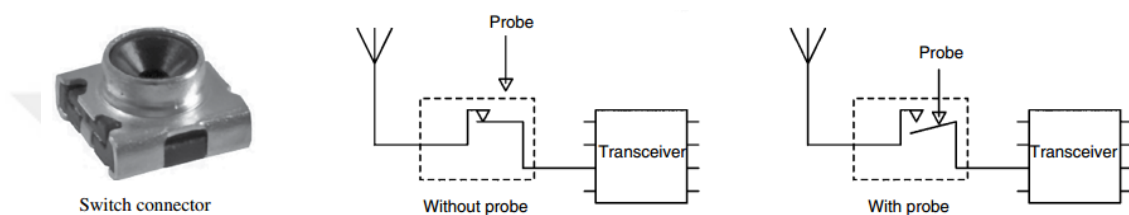


Figure 2.18. Sample switch connector and its operation (Zhang, 2017)

A sample switch connector is shown in Figure 2.18 along with its intended use of operation. For the normal operation in the disconnected state, the signal from the transceiver passes through the switch connector. When the probe is connected, the antenna is disconnected from the transceiver and the probe is directly connected to the transceiver unit. By removing the switch connector from the PCB and tracing the lead connections to the board, one can solder the semi-rigid test cable to the connector location such that the probe will be connected directly to the antenna. However, in this method, since the PCB surface is coated by an insulative material, it may not be easy to solder the testing cable to the ground plane at several points. In such a case, one can reconnect the switch connector to the PCB after rotating it 180 degrees around its center axis.

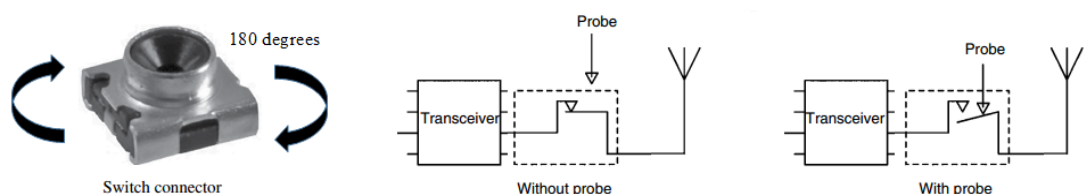


Figure 2.19. Switch connector operated in opposite direction by rotation

This will ensure a reverse operation of the switch where, in the connected state, the transceiver will be disconnected and the probe will be connected directly to the antenna. This process is illustrated in Figure 2.19 and will provide much more stable measurement than the previous one.

2.6. Aspects of Antenna Integration into Mobile Terminal

In addition to the physical limitations of a mobile phone antenna introduced in chapter 1, there are other issues that needs be taken into account in the structuring and integration phases of design.

2.6.1. Impact of Ground Plane

For the types of mobile phone antennas introduced in Chapter 1 such as folded monopole and PIFA, the description of the antenna element is made around a ground plane and operational characteristics of the two in each band of operation have been described in terms of the surface current distribution on the ground plane and the antenna element itself. Thus, the ground plane of a mobile terminal plays a significant part in the effective length, bandwidth and radiation characteristics of the antenna.

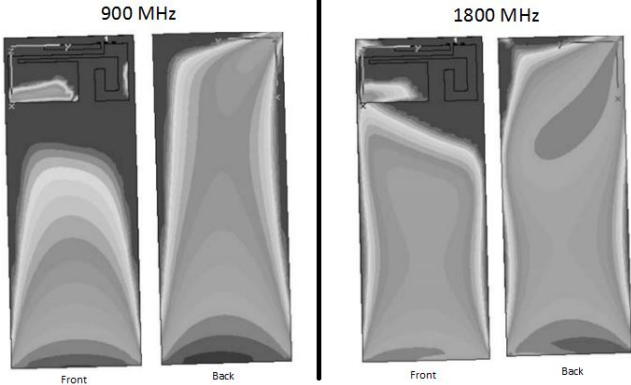


Figure 2.20. Current distribution of a PIFA over a finite ground plane (Fujimoto, 2001)

An example of the current distribution for a PIFA over a finite ground plane at operational frequencies of 900 MHz and 1800 MHz is shown in Figure 2.20. Comparing the current distributions in both frequencies of operation of the given PIFA, it is seen that although the current distribution is almost the same on the antenna pattern over the ground plane, it is seen to show a significant difference in

the ground plane itself. The combined effect of current distributions on the antenna pattern and the ground terminal determines the frequency of resonance and the radiational characteristics of the antenna.

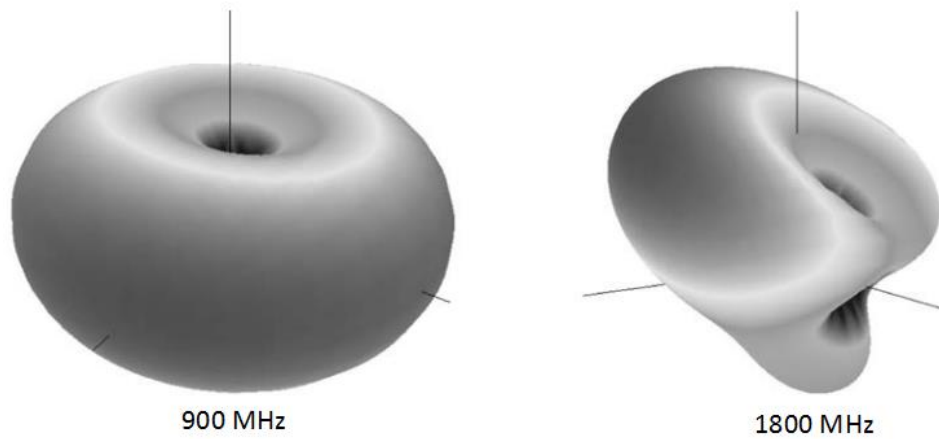


Figure 2.21. Radiation pattern of PIFA at 900MHz and 1800 MHz

The radiational characteristics corresponding to the given current distributions are shown in Figure 2.21. The antenna is seen to have a nearly omnidirectional pattern at 900 MHz while an irregular directive pattern at 1800 MHz respectively.

In addition to the radiation pattern, the ground plane of an antenna also has influence on matching characteristics and impedance bandwidth of the antenna. In some studies, the antenna performance is optimized by a proper excitation of wave modes on the ground plane where the antenna element itself merely acts as a matching element to the configuration on the ground plane (Fujimoto, 2001).

For a mobile phone terminal with limited physical volume available for its ground plane, the ground plane can be made of resistive lossy components for increasing the bandwidth of the antenna. However, this comes with a reduced efficiency of the antenna since some part of the power accepted through the terminal of the antenna will get dissipated on the lossy ground plane.

Two commercial mobile phones, namely Nokia 8850 and Geo GC688, incorporating lossy ground planes in their structure are shown in Figure 2.22. In the Nokia 8850, a lossy ground plane is integrated into the antenna over a chrome-plated middeck beneath the antenna and is connected to PCB ground via pogo pins. In the Geo GC688, a resistive foam material is used as the ground plane for achieving the quad-band bandwidth performance [Rowell, 2012].

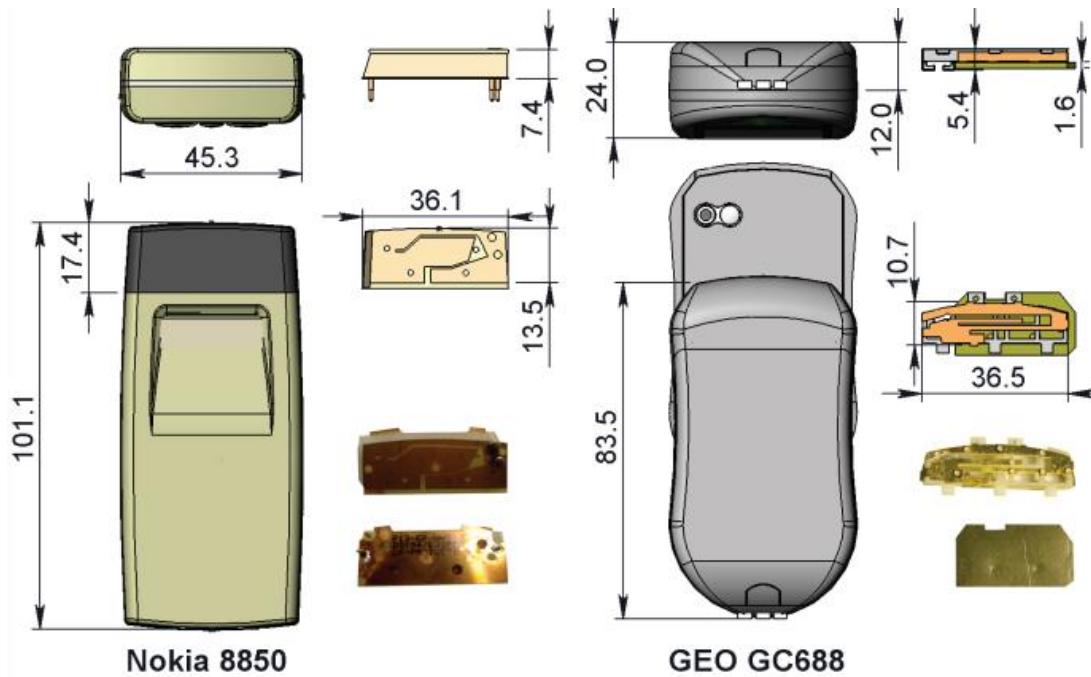


Figure 2.22. Mobile phones with a lossy ground plane (Rowell, 2012)

Following the performance evaluation of an antenna together with its ground plane, the integration of antenna and ground plane combination with other nearby systems in the mobile terminal is performed. These components may detune the matching of the antenna by introducing losses to the system and acting as lossy passive loading elements and noise source to the antenna. Thus, a practical knowledge of the aspects of each component on the antenna characteristics is important for a quick troubleshooting of the possible issues faced in the process of integration.

2.6.2. The Effect of Acoustic Components

The loudspeaker of a mobile phone terminal consists of a coil with a permanent magnet and is connected to the audio base band circuit on the PCB through balanced connections. In the presence of the speaker, the antenna element may get detuned and have some part of its power dissipated at the loudspeaker. In order to decrease the effect of this element on the antenna, the speaker should be kept away from the area of the antenna body with dense current distributions. Thus, positioning of antenna and loudspeaker should be co-designed by antenna engineers and acoustic engineers for minimal impact on the antenna and optimal performance in audio.

2.6.3. The Effect of Camera

The common stick phones of the industry have a camera lens at the backside of the terminal where the antenna is located. The effect of this component shows itself in the form of passive detuning by the reduction in the effective volume of the PIFA (Fujimoto, 2001). It also degrades the receiving sensitivity of the terminal by creating RF emission. An example of the emission from a mobile phone camera at the low band is shown in Figure 2.23 where the noise floor is at 120 dBm.

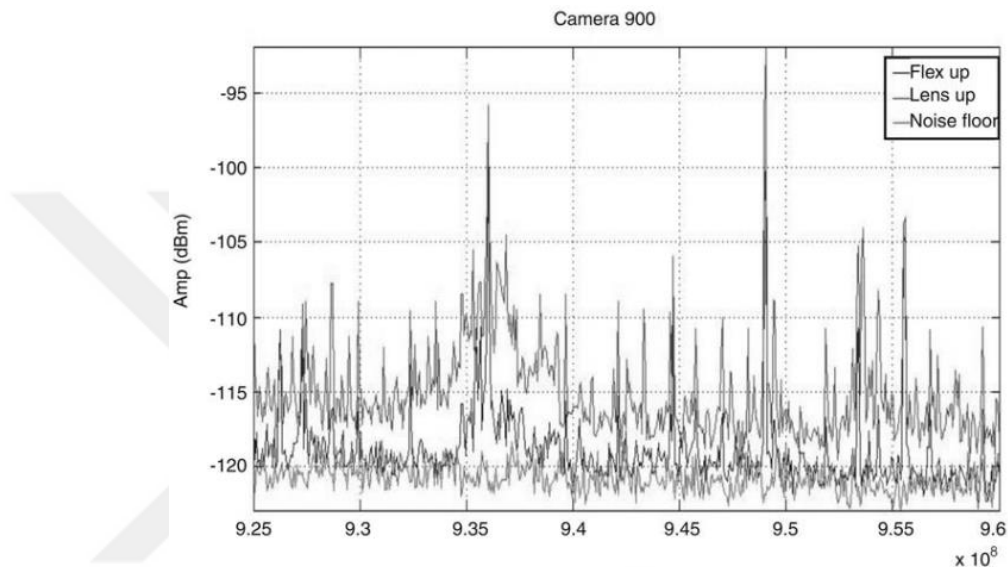


Figure 2.23. Spurious emission from a mobile phone camera (Fujimoto, 2001)

In reference to Figure 2.23, the radiation level is seen to be 10 to 20 dB above the noise floor which cause some problems at the receiving bands.

2.6.4. The Effect of Battery

As a structure of high volumetric volume made of conductive materials, the battery is shown to have significant effects on the bandwidth and gain at Bluetooth and WLAN bands of the PIFA antenna in a small bar type handset (Fujimoto, 2001). This is mostly due to the size of battery being close to that of the wavelength at high bands of operation, such as the 2.4 GHz band.

2.6.5. The Effect of Display

The large screens of the modern multimedia phones occupy a big surface on the backside of the system ground plane. Since the screen is firmly integrated into the phone body that is a part of the antenna, it may have some induced currents on it,

which may vary the radiation performance of the antenna. The liquid crystal display (LCD) placed in parallel to the system ground is made of lossy dielectric materials and may change the electromagnetic near field of the mobile phone. In this sense, its effect should be taken into consideration for analysis of specific absorption rate (SAR) and hearing aid compatibility. Like the camera, screen is a high data speed component which may introduce unwanted RF emission.

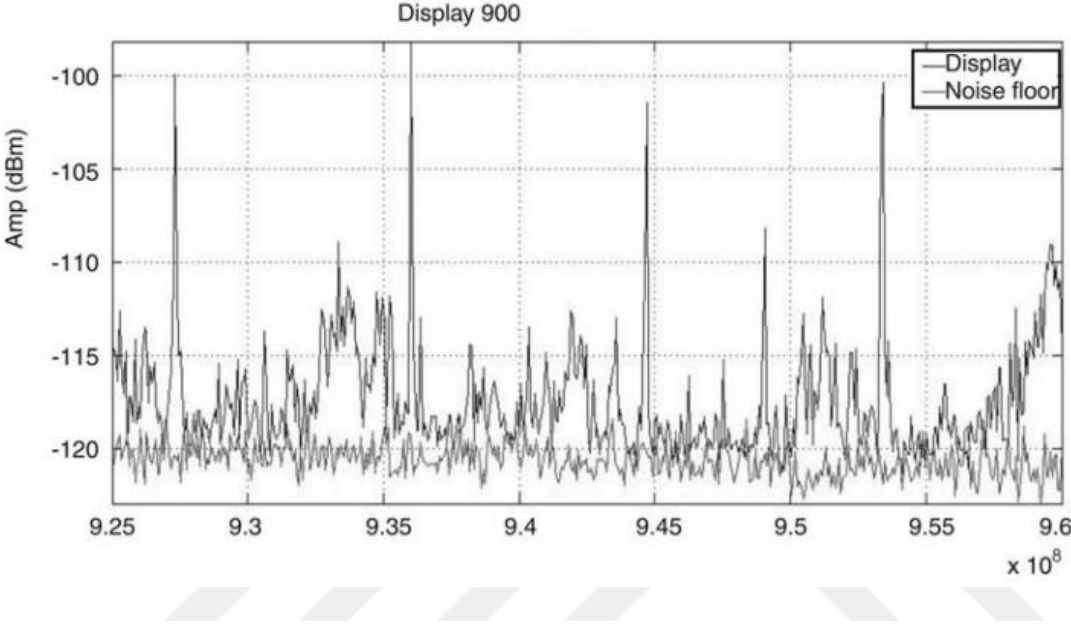


Figure 2.24. Spurious emission from a LCD display (Fujimoto, 2001)

A measurement of the emission at the receiving band of 900-MHz GSM of a bar type phone is shown in Figure 2.24 where the noise floor is at 120 dBm. The level emission from this figure is seen to be 10 to 20 dB above the noise floor which may cause problems on the receiving band.

CHAPTER 3

DESIGN AND EVALUATION OF CELLULAR ANTENNAS

Recent mobile phones employ a built-in multiband cellular antenna that can cover frequency bands of systems such as GSM (800, 900, 1800, and 1900 MHz bands), UMTS (1.8, 1.9, 2.1, 2.5 GHz bands). Traditionally, the internal multiband antennas have been implemented using self-resonant planar inverted F type antenna elements in which utilization of parasitic resonator or meandering was among the alternatives of covering the operating bands of GSM, PCS, and UMTS systems (Ciais, Park, Guo). An attractive alternative for multi-band planar inverted F antenna are internal monopole type antenna structures. Alternatively, matching circuits can be used to create some or all of the antenna resonances which allows the utilization of non-resonant antenna elements. The operation of these elements is usually based on making use of the radiation of the entire metallic chassis of the mobile handset (Valkonen). In this chapter, a multi-band, frequency reconfigurable main antenna is introduced along with a receive diversity antenna for use in 4G (4th generation) mobile terminals. The main antenna is a Planar Inverted F Antenna (PIFA) mounted on bottom of the mobile phone and grounded by a variable reactance for operation in 790-960 MHz and 1710-2690 MHz bands covering GSM, DCS, PCS and UMTS standards. The receive diversity antenna on the other hand is a monopole antenna to be operated in the 1710-2690 MHz band. Use of LDS (laser direct structuring) structure in both antennas is proposed for fine-tuning of their response. Simulated frequency responses of reflection coefficients and radiation patterns of the prototype antennas are given.

3.1. Main Antenna

The design of the antenna starts with the construction of components that play role in the operation of the antenna element. This is done by use of electromagnetic 3D modeling software such as CST Microwave Studio and HFSS. The construction of the mobile phone terminal is presented in Figure 3.1 in a successive fashion. The model comprises a ground plane with sizes 134mmx71mmx0.8mm, which represents

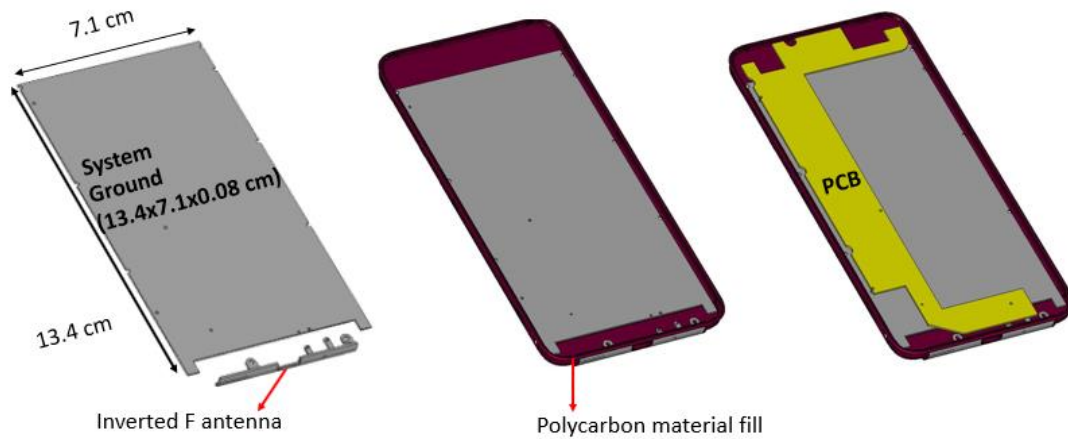


Figure 3.1. 3D structure modeling of main antenna and mobile phone

the system ground of the whole system in an actual mobile phone terminal. A polycarbon material surrounds the ground plane which, in an actual construction, holds the internal components and casing of the phone together. The poly-carbon material is modeled as a lossy dielectric and is given the electrical properties of $\epsilon_r = 2.95$, $\mu_r = 1$, loss tangent ($\tan \delta$) = 0.009. The PCB board of the phone is constructed from perfect electric conductor material of width 0.8mm and is given the particular shape given in Figure 3.1 where some openings are left for battery and cameras.

In this structure the metallic bottom part of the phone is desired to be used as the main antenna by proper matching for operation at the respective bands of operation. Selection of the bottom part of the phone as the location of main antenna is a common practice as to prevent harmful radiation towards the head. The bottom part of the mobile phone as the main antenna is shown in detail in Figure 3.2

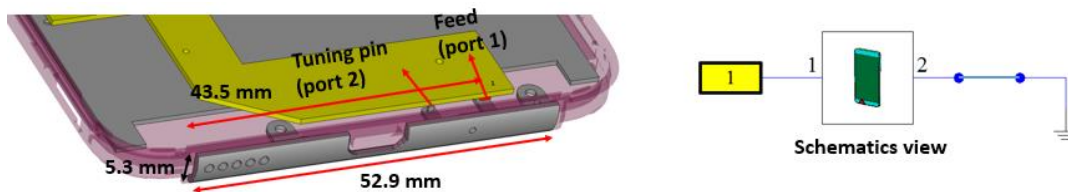


Figure 3.2. Metallic bottom case as the main antenna

In the initial step of analysis for terminal characteristics of the antenna, the IFA structure is fed through a discrete port from the PCB of the mobile phone with its schematic representation shown in Figure 3.2.

From this simulation model, the return loss of the antenna is calculated at the feed terminal of the antenna as shown in Figure 3.3 where the other pin of the PIFA is grounded to the PCB of the phone.

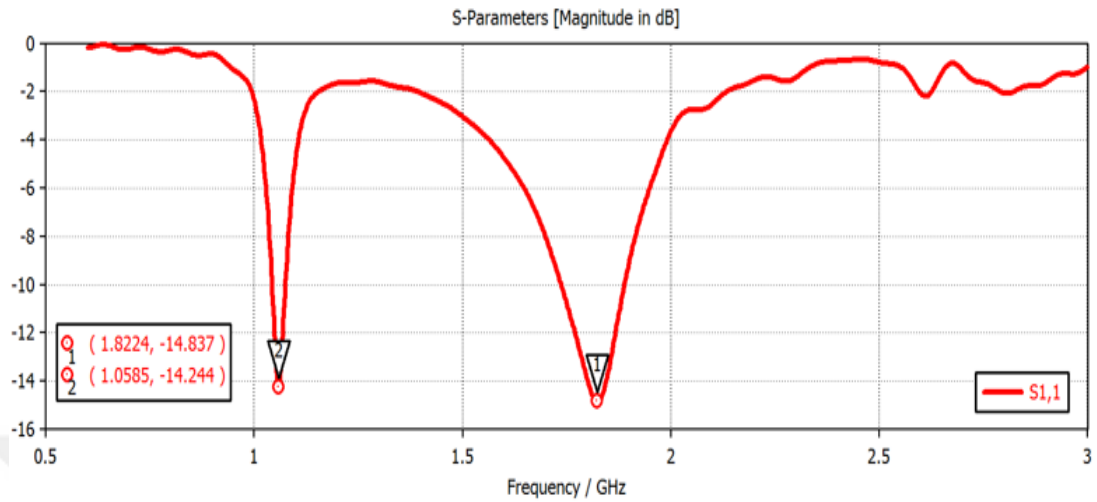


Figure 3.3. Return loss of antenna (poly-carbon fill included in simulation)

In reference to the return loss given in Figure 3.3, the antenna is seen to show dual band resonance at the respective frequencies of around 1.05 GHz and 1.82 GHz.

In order to see the effect of how the poly-carbon material fill effects the impedance characteristics of the antenna, the simulation was run one more time where the poly-carbon material is replaced by vacuum. The resulting return loss measured from this simulation is shown in Figure 3.4.

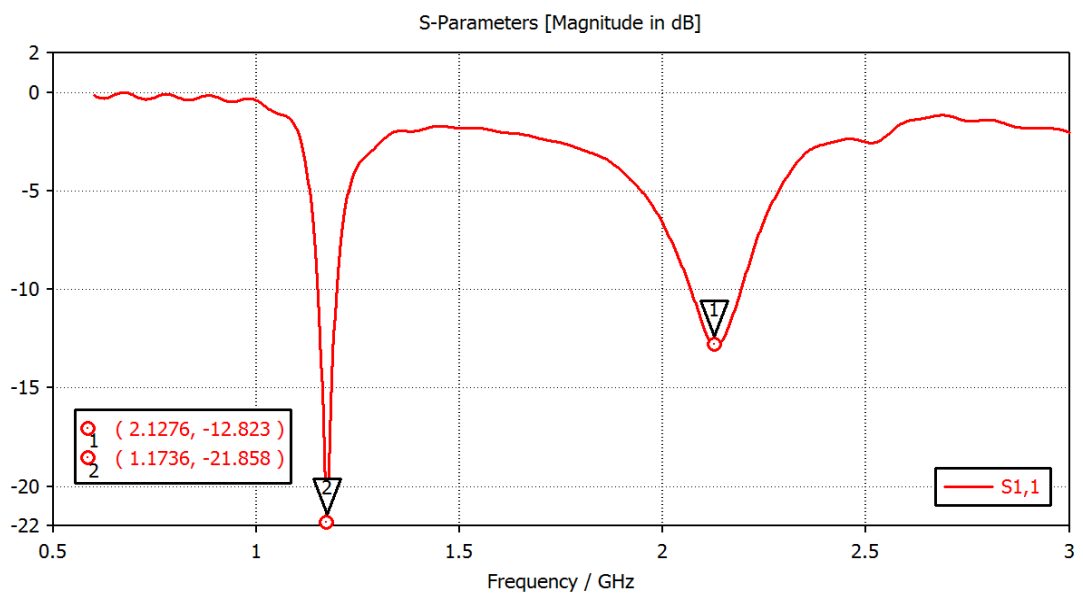


Figure 3.4. Return loss of antenna (poly-carbon fill excluded from simulation)

In reference to the return loss given in Figure 3.4, the antenna is seen to show dual band resonance at the respective frequencies of around 1.17 GHz and 2.12 GHz.

Comparing the return losses obtained in Figures 3.3 and Figure 3.4, the poly-carbon fill material is seen to shift down the resonance frequency of the antenna in both bands by causing dielectric loading on the antenna. The amount downshift in the frequency of resonance is 120 MHz and 300MHz for the lower and upper band of operation respectively. From this result, it is concluded that the effect of dielectric loading from the poly-carbon fill is significant and should be taken into consideration in simulations. Thus, the poly-carbon material fill is used in all the simulations performed.

In order to utilize the limited total bandwidth of the antenna in various bands (multiband) of services, the grounding of the PIFA antenna can be made by a capacitive/inductive load as shown in Figure 3.5. In this way, the resonance frequency of the antenna element together with the phone chassis can be shifted to the range of frequencies of a particular service of interest.

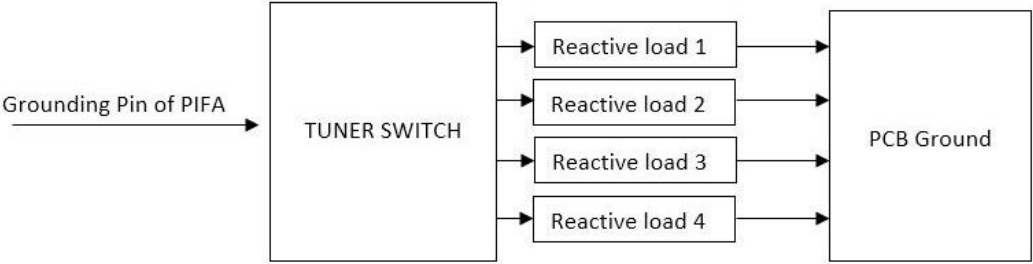


Figure 3.5. Tuner Switch Configuration

The selection of reactive components connected to the grounding pin can be made electronically controllable by use of low-loss RF switches employed on the PCB of the phone.

For the desired performance at the upper band of operation in the range 1710-2690 MHz, the use of a 0.3pF capacitor as the reactive loading to the grounding pin of the PIFA is shown to satisfy the return loss criteria of $|S_{11}|(dB) < -6dB$ with reference to Figure 3.6. However, for the lower band of operation in the range 790-960 MHz, it was not possible to create resonance by any of the commercially available reactive components as loading to the grounding pin of the PIFA antenna element. This is shown in Figure 3.7.

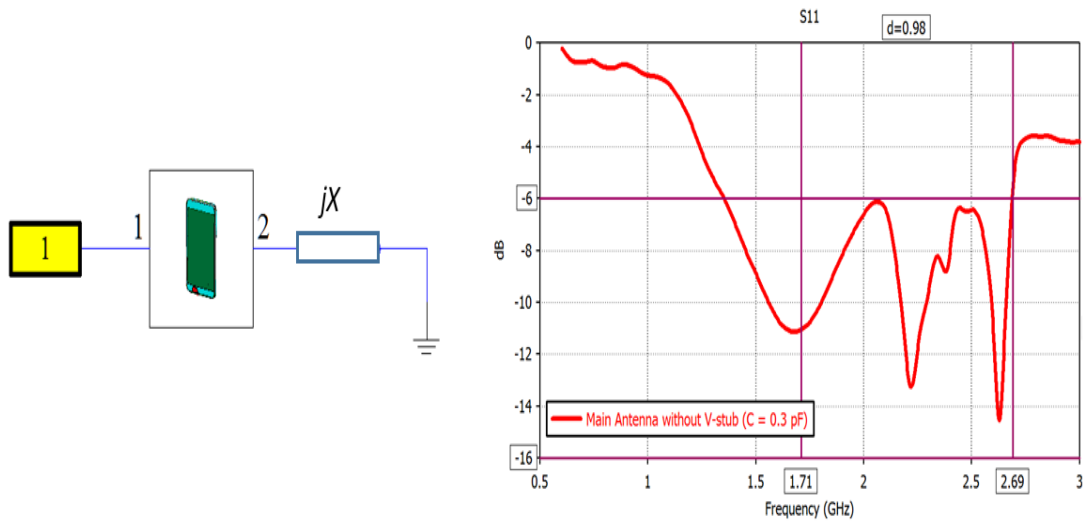


Figure 3.6. Upper band coverage by capacitive loading at grounding terminal

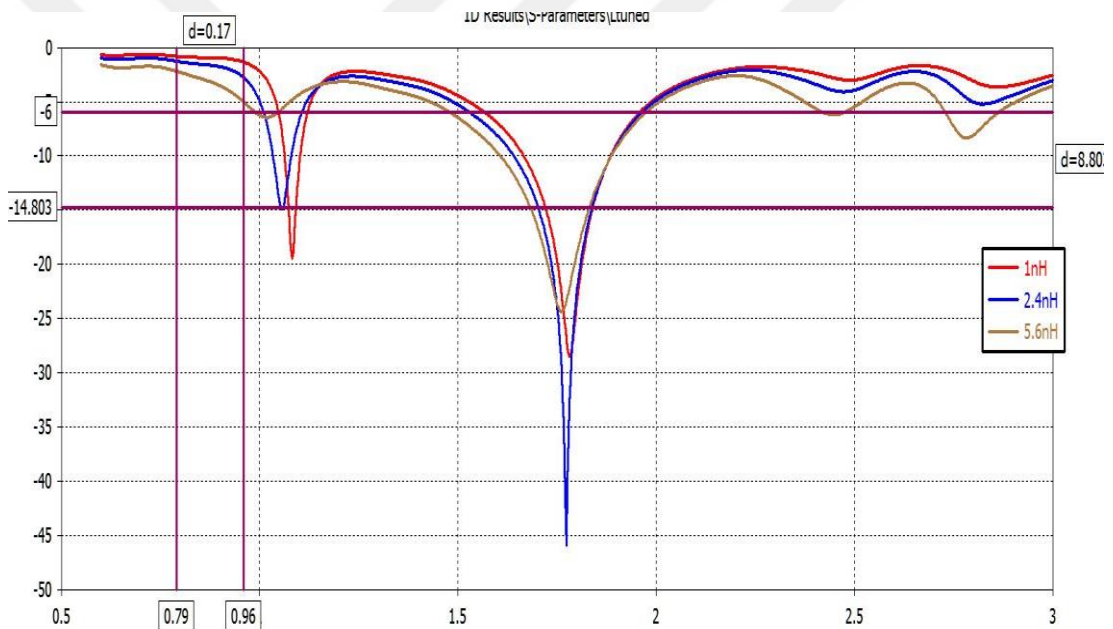


Figure 3.7. Return loss for a number of inductive loads at the grounding terminal

The physical setup for the measurement of the return loss of the main antenna is shown in Figure 3.8 where a switch connector is used at feed point of the PCB. In this configuration of passive measurement, the reactive tuning element connected to the grounding pin of the PIFA through a switch IC is uncontrollable.

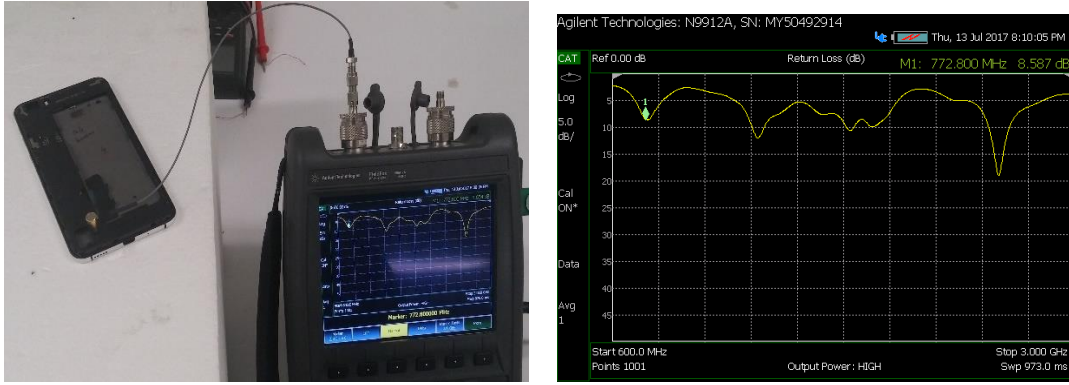


Figure 3.8. Physical implementation and measured return loss of Main antenna

Thus, the measurement shown is the result of the return loss corresponding to the tuning element that was active when the phone was last turned on. This response is similar to the simulated return loss of Figure 3.9 obtained when a 18nH inductor is connected at the grounding pin of PIFA.

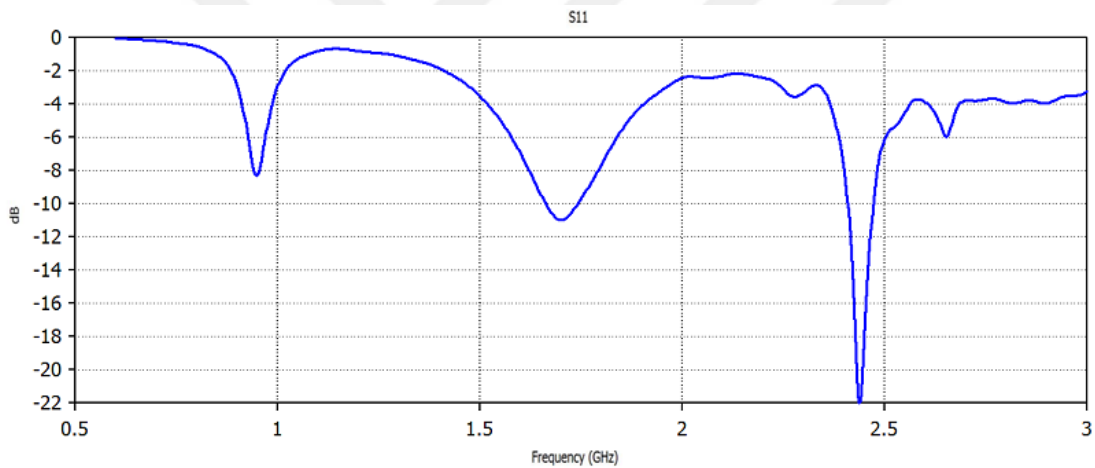


Figure 3.9. Simulated return loss of main antenna with 18nH connected at its grounding terminal

In addressing the resonance at the lower band of operation, some structural changes on the antenna were required. In that sense, a V shaped stub element is added on the ground end of the PIFA antenna element as shown in Figure 3.10.

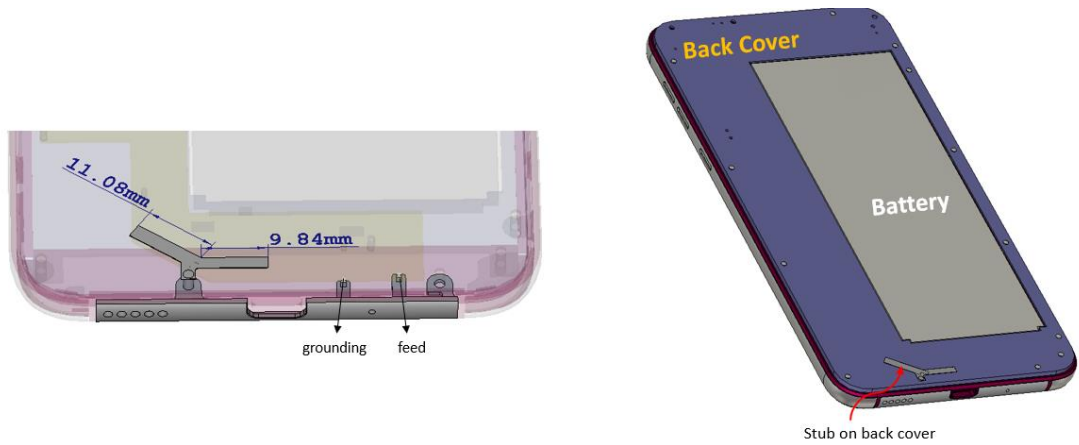


Figure 3.10. Main antenna with stub element built on plastic back cover

The stub element shown in Figure 3.10 is given such a shape so that it will be in the same orientation as the PCB ground plane beneath it. The length and width of the two arms are then optimized for best performance in terms of the return loss at the feed terminal of the antenna. In an actual design, the stub element can be structured on the back cover of the antenna by using Molded Interconnect Device (MID) technology (i.e., Laser Direct Structuring (LDS)). For this configuration where an additional stub element is used, the lower band of operation can be covered by use three different valued inductive loading at the grounding terminal of the antenna. This is shown in Figure 3.11.

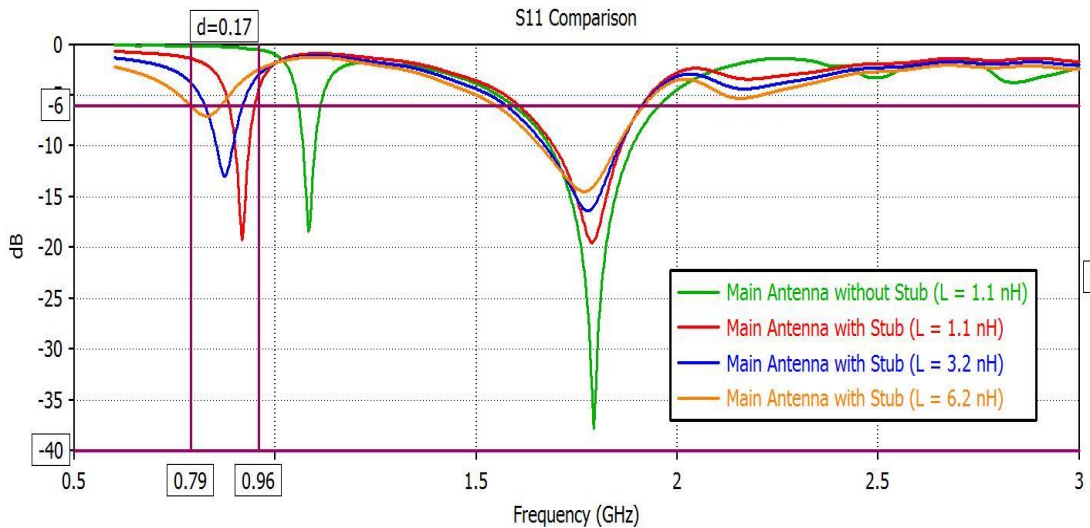


Figure 3.11. Lower band coverage by use of stub element and inductive loading

For the configuration with a stub element, the capacitive loading with $C = 0.3$ pF still covers the upper band of operation as shown in Figure 3.12.

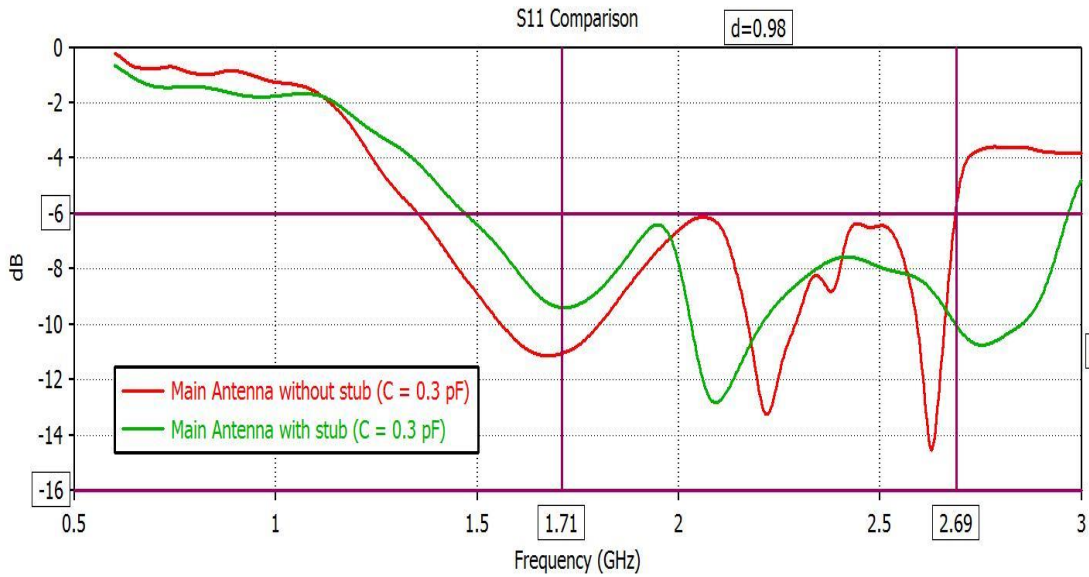
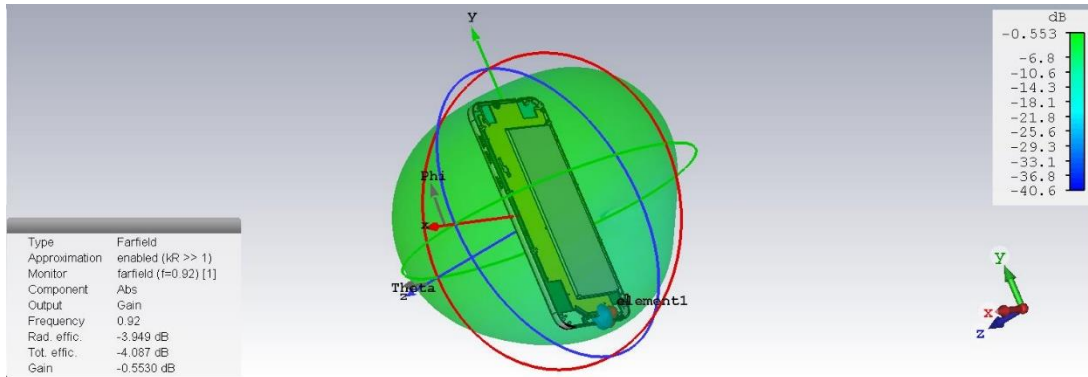


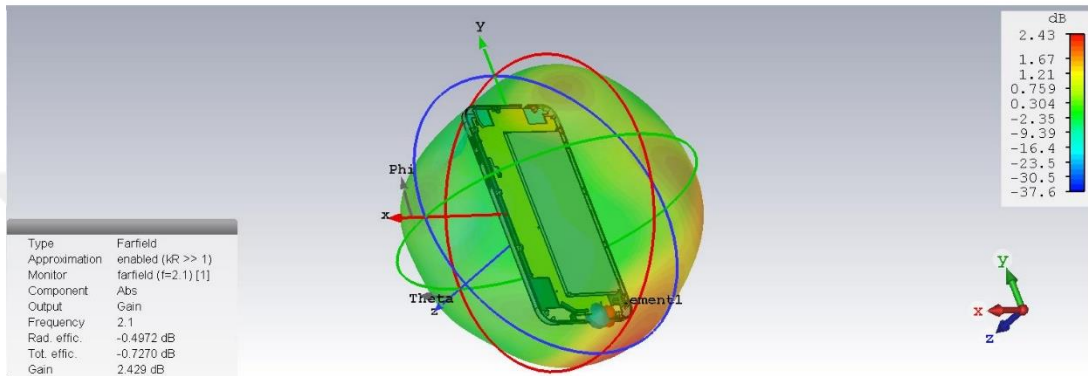
Figure 3.12. Upper band coverage by capacitive loading in two configurations

In simulating the effect of reactive loading to the grounding terminal of PIFA, impedance characteristics of the antenna has been evaluated by using the schematics view of the CST Microwave Studio. In doing so, a two-port simulation of the antenna is followed by reactive loading to the port at the grounding location of PIFA by using the two-port representation of the antenna in the schematics view. If such a two-port representation and lumped element loading options are not available in the simulation program used, complex S-parameter data from a two-port simulation of the antenna can be used with the method given in appendix to evaluate the antenna impedance and return loss in software environments such as MATLAB.

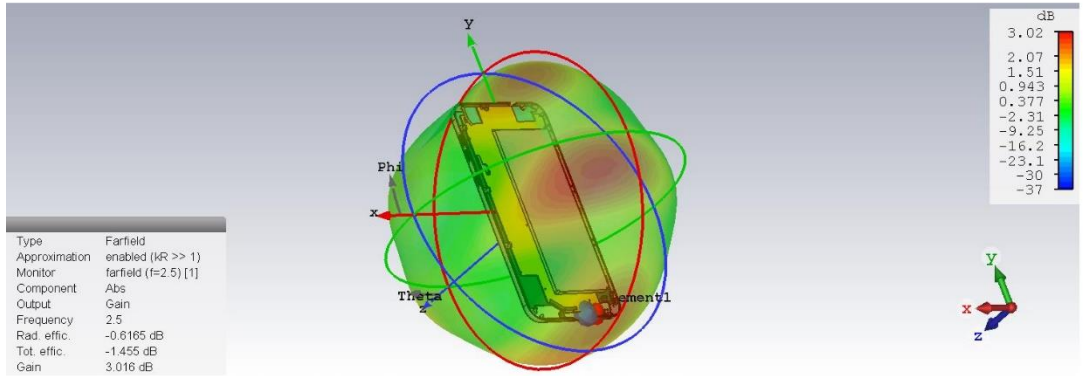
The far-field gain radiation patterns of main antenna at various bands of service are given in Figure 3.13.



(a) $f = 920 \text{ MHz}$, grounding load:1.1nH



(b) $f = 2.1 \text{ GHz}$ grounding load:0.3pF



(c) $f = 2.5 \text{ GHz}$ grounding load:0.3pF

Figure 3.13. Far-field gain radiation patterns of main antenna

3.2. Diversity Antenna

The communication between the cell site and mobile is not by a direct radio path but via many paths. In this way, constructive or destructive combination of various incoming radio waves leading to a rapid variation in signal strength. To cope with this issue, the current standards of LTE communication is built upon the use of multiple antennas on the mobile phone terminals. In this sense, most of modern mobile phones employ the use of a receive diversity antenna for the purpose of

providing an independent sample of data from the signal in the vicinity of the phone. In the case of not being able to acquire signal with adequate strength from the main antenna of the phone, the phone will do a switched diversity (choose the received signal with the most energy) or combined diversity (sum the powers from two receiving antennas) in order to ensure the uninterrupted operation of the service in use. The use of diversity antenna as a radiator is theoretically possible by employing orthogonal radiational characteristics to that of the main antenna. However, such an implementation is not a common practice as it brings additional power consumption which in turn results in a reduced battery life of the mobile phone. The method of measuring isolation is typically done by connecting both antennas to a Vector Network Analyzer, and measuring S12 (the transmission coefficient) without taking the radiational characteristics of the antennas into account. However, antenna isolation can further be increased by reducing the correlation coefficient between the antenna's radiation patterns by directing the peak radiation from two antennas in different or opposite directions.

For this study, the metallic upper casing of the mobile phone introduced in the previous chapter is configured as a receive diversity antenna for use at the upper band of operation in the frequency range 1710-2690 MHz. The upper portion of the phone is selected as the diversity antenna location in order to maximize isolation between main and diversity antenna by placing the two far from each other as much as possible.

For the sake of an easier feed configuration and simpler antenna structure, the metallic case is used in a folded monopole scheme as shown in Figure 3.14.

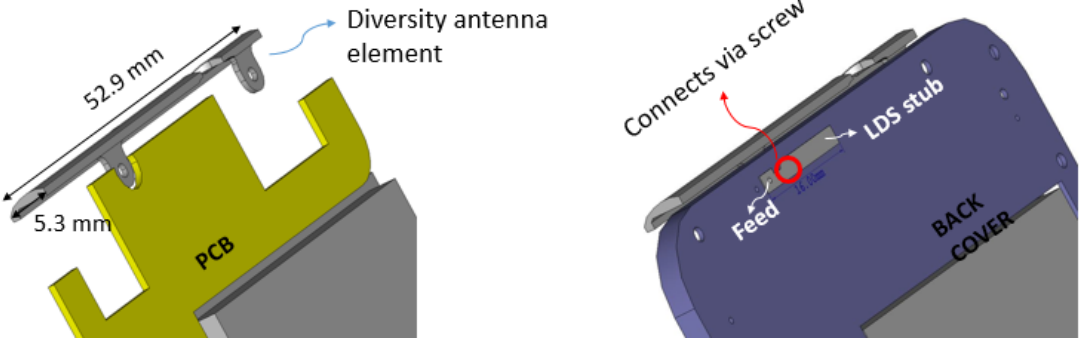


Figure 3.14. Metallic bottom case as the diversity antenna

Shown in Figure 3.14 is the geometry of the proposed diversity antenna that is intended for use as a receiver only in the 1710-2690 MHz band. The antenna has identical size of 52.9 x 5.3 x 0.9 mm³ as the main antenna.

The isolation of diversity antenna from the main antenna is an important aspect regarding antenna efficiency. With poor isolation, some of the energy that would have been radiated by the main antenna gets to be absorbed by the diversity antenna causing a loss in antenna efficiency. In order to maximize isolation with the main antenna located at the bottom of the phone, the diversity antenna is placed at the upper side of mobile phone. The antenna is fed at the top of the PCB to obtain an efficient antenna-chassis combination with maximum bandwidth behavior (Kivekäs,2003). As was done with the main antenna, the diversity antenna element is fine tuned for the satisfaction of the impedance matching criterion of 6 dB return loss in the 1710-2690 MHz band by use of a stub element of size 2.0 x 10.9 mm at the feed point of the antenna.

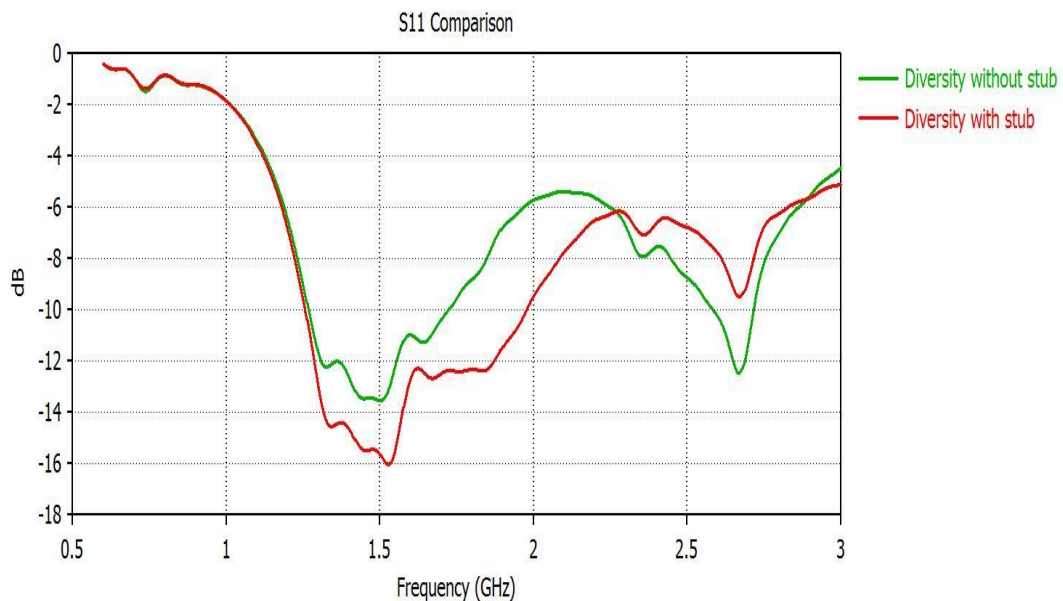


Figure 3.15. Return loss (dB) of diversity antenna with and without the stub element

The simulated S-parameter of the antenna in the range from 600 MHz - 3 GHz is shown in Figure 3.15. Using the typical impedance matching criterion defined by 3:1 VSWR (6-dB return loss), the antenna is seen to cover the desired band of 1710-2690 MHz by the addition of stub element into the structure.

The physical setup for the measurement of the return loss of the diversity antenna is given in Figure 3.16. In this configuration, the network analyzer is connected to the

through a coaxial cable probe which is in turn connected to the antenna through a switching connector as defined in Section 2.5.2.



Figure 3.16. Physical setup for measurement of Return loss (dB) of diversity antenna

The measured return loss of the diversity of the antenna from the setup shown in Figure 3.16 is shown in Figure 3.17. From this figure, it is seen that the antenna is shown to satisfy the return loss criteria of $|S_{11}| < -6dB$ over the operational frequency range of 1710-2690 MHz.

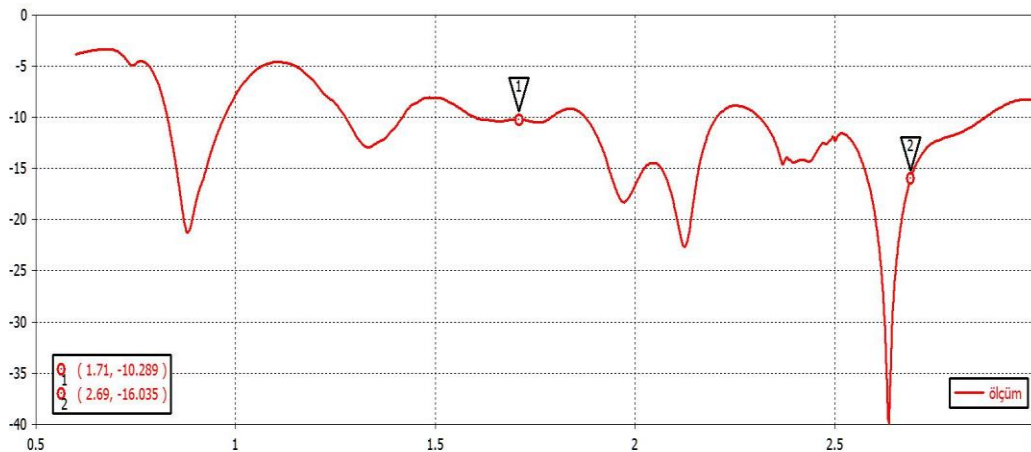
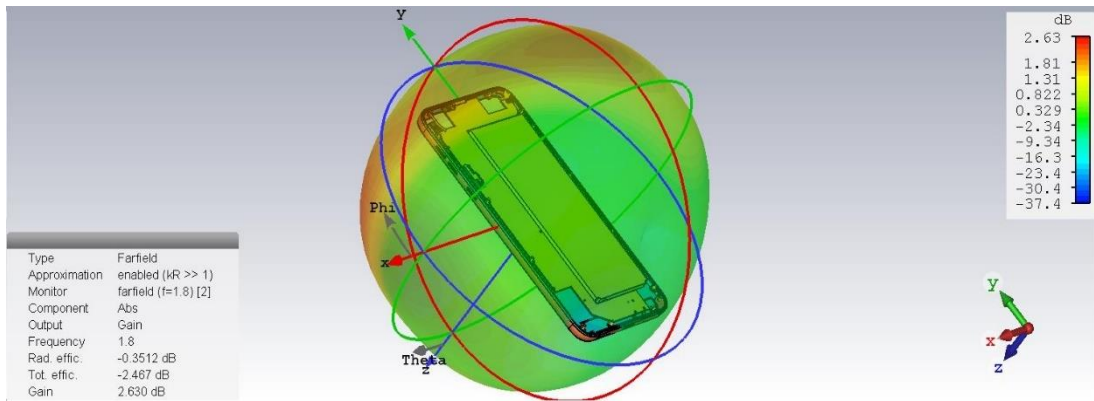
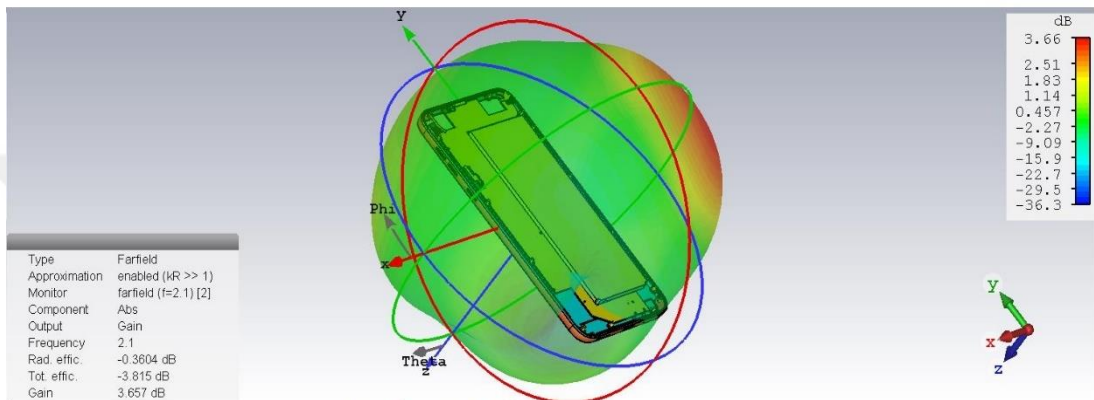


Figure 3.17. Measured Return loss (dB) of diversity antenna

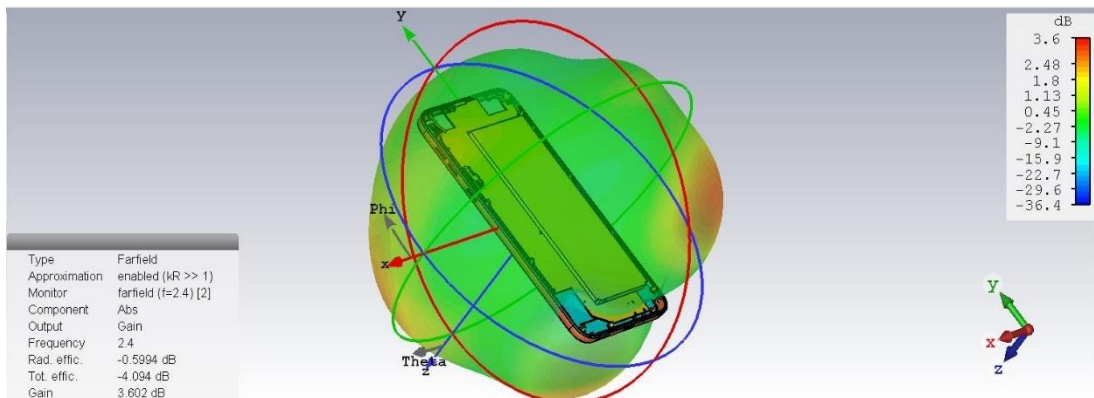
Figure 3.18 shows the far-field gain radiation pattern of the diversity antenna at 1.8, 2.1, and 2.4 GHz. Similar to the main antenna of the previous section, the receive diversity antenna element has omni-directional characteristics in its radiation pattern as desired. The radiation pattern cuts of the antenna resemble a dipole antenna.



(a) $f = 1.8 \text{ GHz}$



(b) $f = 2.1 \text{ GHz}$



(c) $f = 2.4 \text{ GHz}$

Figure 3.18. Far-field gain radiation patterns of diversity antenna

With reference to Figure 3.18, the diversity antenna is said to have moderate in the frequency band of operation.

As an overall description of the work presented in this chapter, cellular antenna designs of a mobile phone operating at the frequency of 719-960 and 1710-269 MHz for the main antenna and 1710-2690 MHz for the diversity antenna was implemented without the use of a matching circuit (Özbağış, 2017).

CHAPTER 4

DESIGN AND EVALUATION OF GPS AND WLAN ANTENNAS

In addition to the main and an optional transmit or receive diversity antenna used for data transfer with the base station for cellular services, a mobile phone terminal employs additional antennas for operation of Global Positioning System (GPS) and Wireless Local Area Network (WLAN) services.

In the GPS service, the mobile phone terminal receives its location information from GPS satellites that are positioned at far and high orbits. Thus, the power of the signal incident on the phone is very weak and requires GPS antennas to have low return losses and high radiation efficiencies at the frequency of operation.

Unlike the GPS antennas, the WLAN service antennas of a mobile phone capture signals broadcasted from wireless service hotspots that are located at the close vicinity of the mobile phone terminal. Thus, antennas with lower terminal and radiational performances may provide satisfactory operation for this service.

Due to the different set of requirements set for the GPS and WLAN service antennas on a mobile phone, antennas for these two services are designed independently on the mobile phone terminal. Single element dual band antenna or two different antenna configurations are available for operation at the respective WIFI frequencies of 2.4 GHz and 5.2 GHz.

In this chapter, three independent antenna configurations are introduced that are designed for operation for GPS service at 1.575 GHz, and Wi-Fi services at respective frequencies of 2.4 GHz and 5.2 GHz.

4.1. GPS Antenna

The design configuration for the GPS antenna is similar to that used for the main and diversity antennas of the mobile phone where the metallic case of the phone is used. Since the bottom and upper parts of the phone are used with main and diversity

antennas, the remaining metallic side parts of the phone are used for the WLAN and GPS antennas.

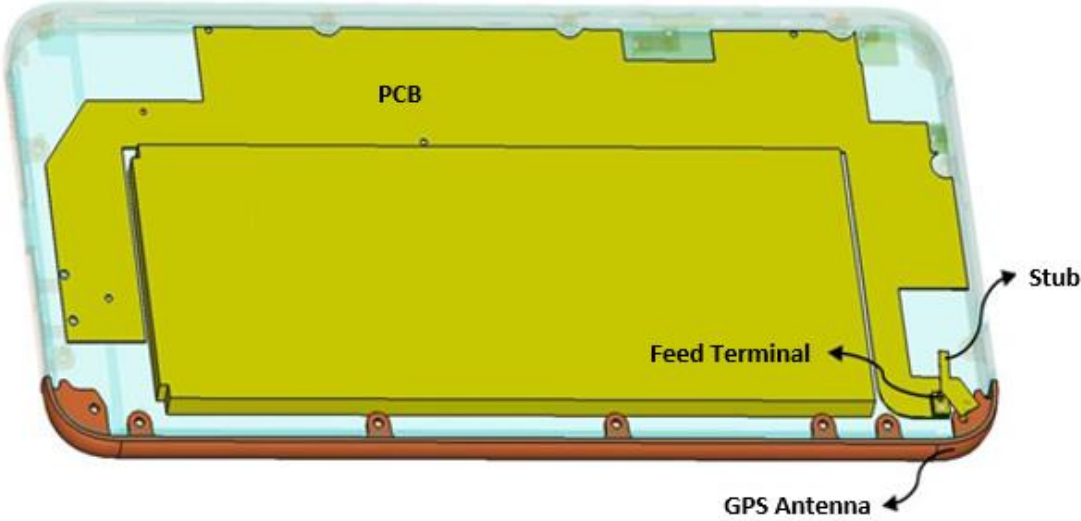


Figure 4.1. Geometry of GPS Antenna

The geometry of the GPS antenna is shown in Figure 4.1. In this configuration, the corner part of the metallic structure around the phone is used as a folded monopole radiator, which is tuned to the frequency of operation by use of a stub element on the plastic cover and a matching circuit built on the PCB of the mobile phone.

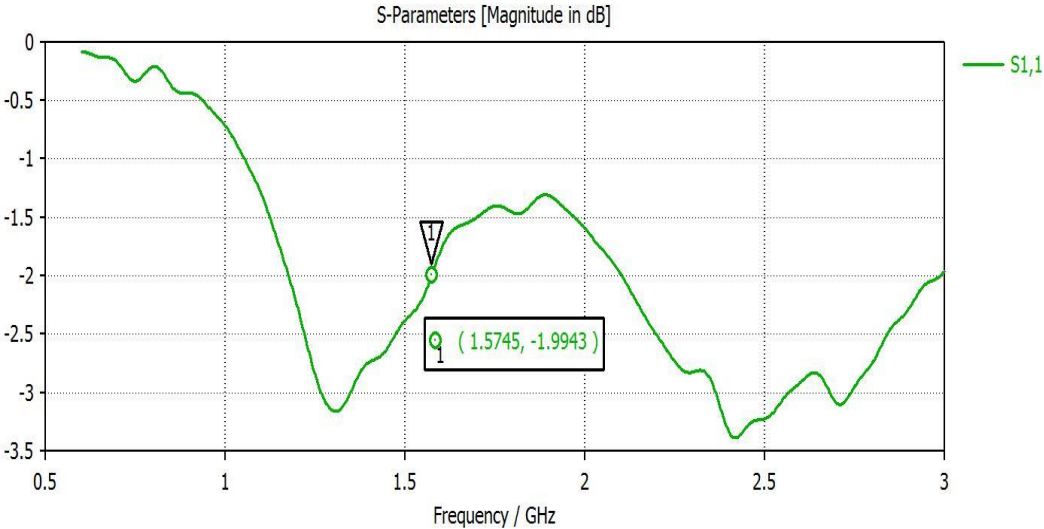


Figure 4.2. Return loss of GPS Antenna without a matching circuit

Shown in Figure 4.2 is the simulated return loss of the configuration shown in Figure 4.1 where no matching circuit is used in front of the feed terminal.

In order to provide resonance at the frequency of operation, a two-element matching circuit is used in front of the feed terminal as shown in Figure 4.3.

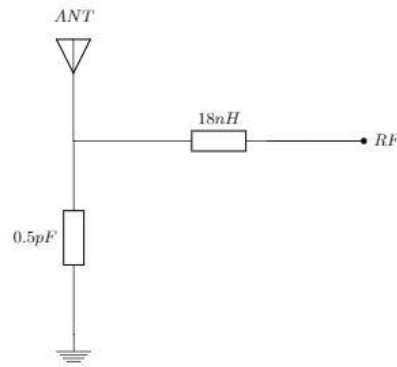


Figure 4.3. Matching circuit of the GPS antenna

By the use of the matching circuit used in Figure 4.3, the return loss at the frequency of operation is improved as shown in Figure 4.4.

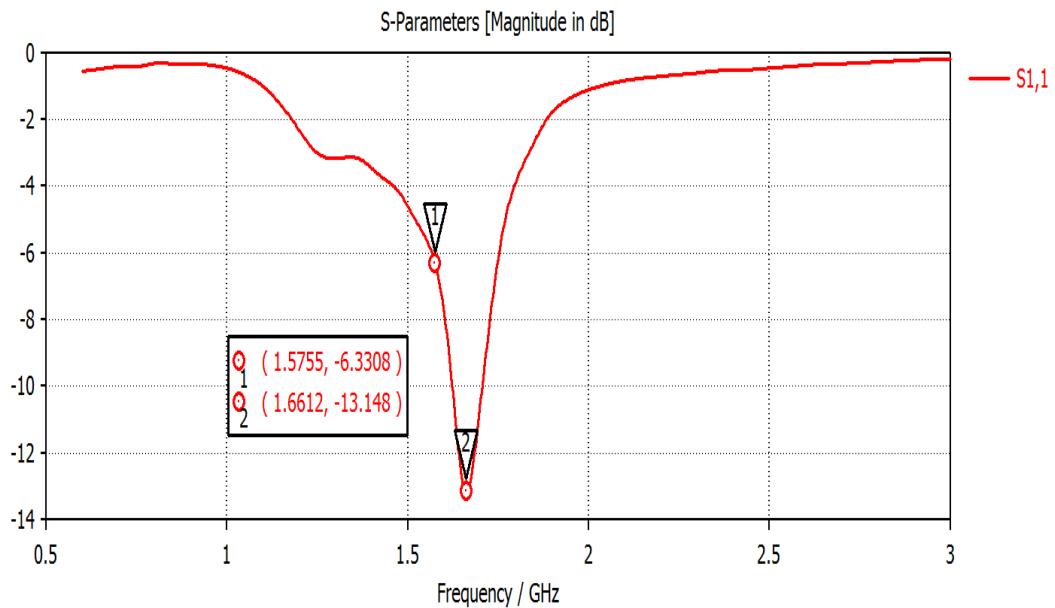


Figure 4.4. Return loss of GPS antenna with matching circuit

Even though the best terminal response of the antenna occurs at a frequency higher than the operational frequency of 1.575 GHz, the resonance at this frequency is expected to shift to the vicinity of the operational frequency by the dielectric loading caused when the plastic back cover of the phone is added to the simulation model.

The physical implementation of the GPS antenna is constructed and the return loss is measured at the feed terminal as shown in Figure 4.5.

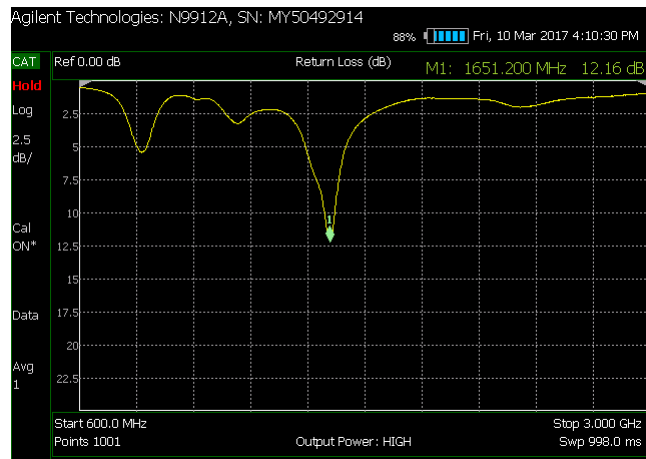
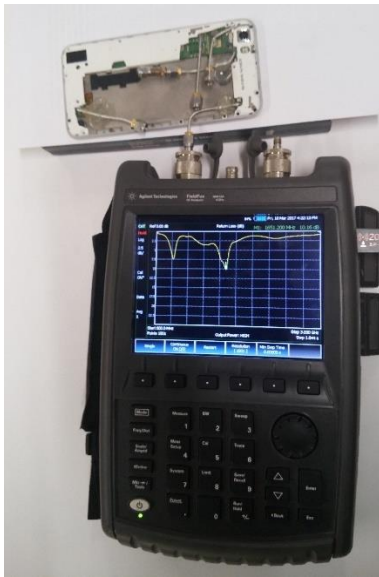


Figure 4.5. Physical implementation and measured return loss of GPS antenna

In order to compare the two return losses obtained from the simulations and physical measurements, the two results are shown on the same plot as shown in Figure 4.6.

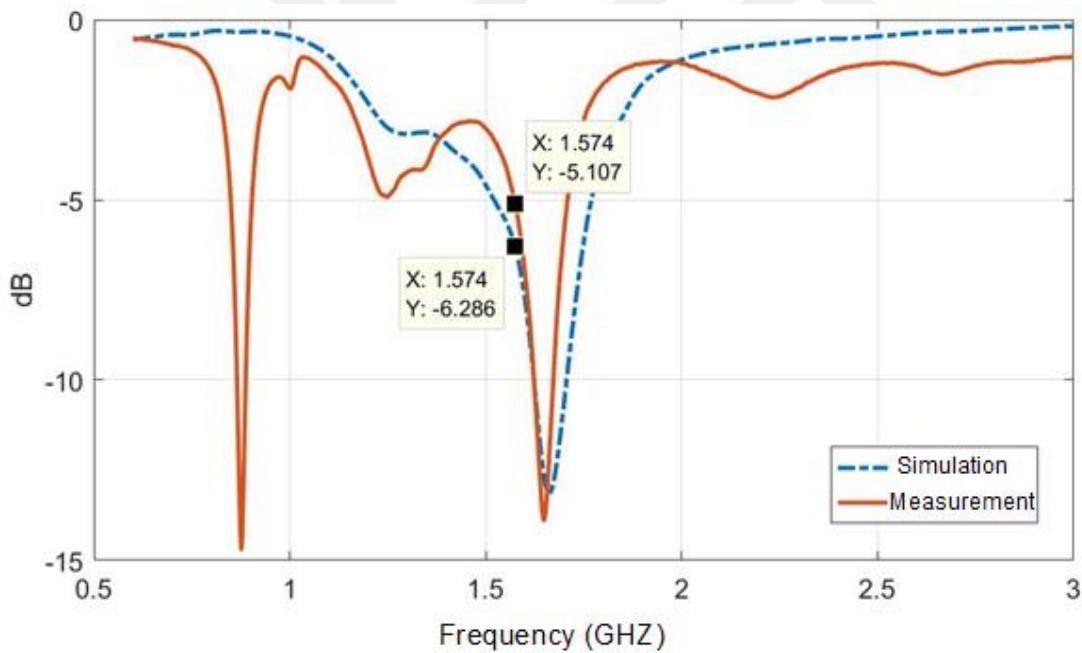


Figure 4.6. Simulated and measured return losses for the GPS

By comparison of the two plots shown in Figure 4.6, the results obtained from measurements are in a good agreement with the simulations except the occurrence of an additional dip for measurement at around 900 MHz.

In taking the measurements from the configuration of the GPS antenna setup where the antenna is fed by a semi-rigid cable at its feed terminals, the positioning of the

cable provides different results in terms of the measured return loss as shown in Figure 3.19.

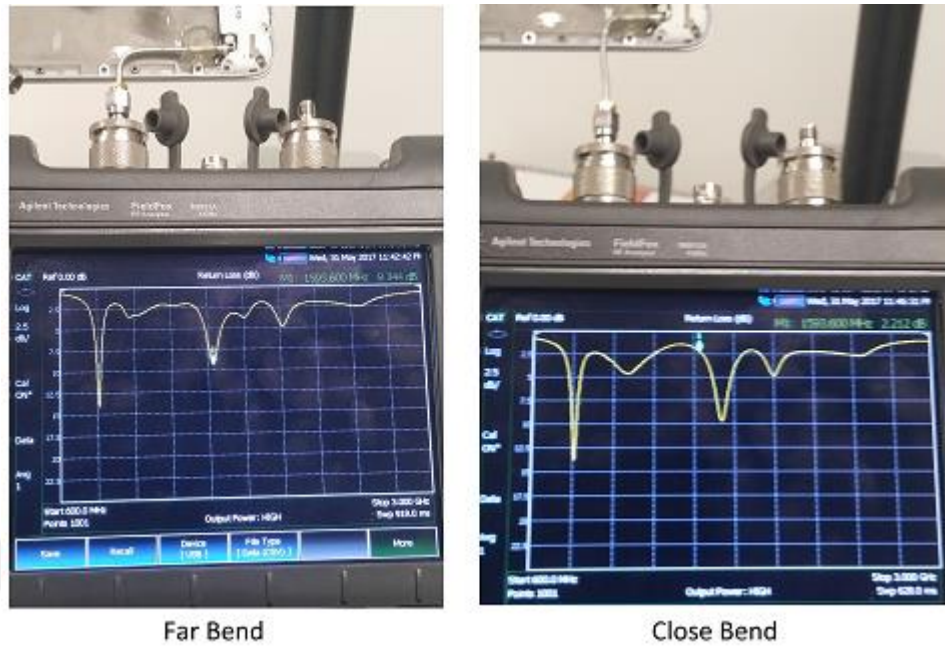


Figure 4.7. Measured return loss of GPS antenna for different cable positions

In reference to two configurations shown in Figure 4.7, the positioning of the cable is seen to be significant for the return loss at higher frequencies. Among the two, the far bend configuration gives the most reliable results as explained in part of 2.5.2 of this document.

As an alternative to this configuration built for measurement of return loss, switch connectors can be employed on the PCB with its operation introduced in part 2.5.2. Such a configuration is shown in 4.8.

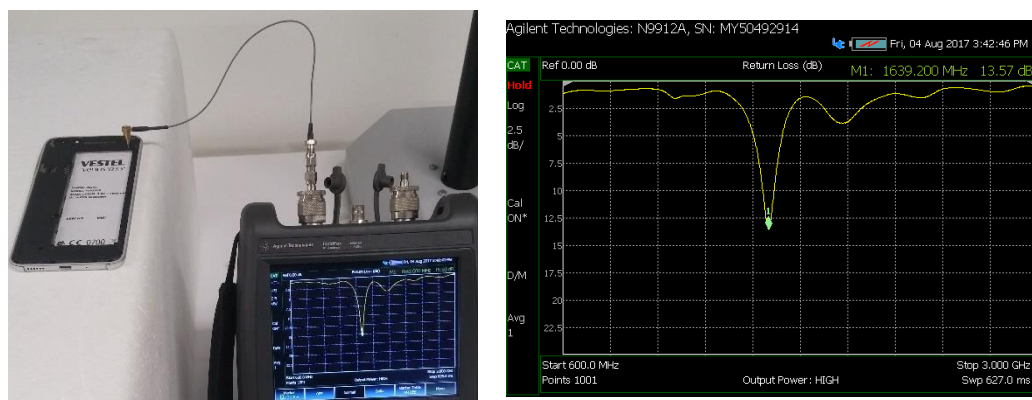


Figure 4.8. Measured return loss of GPS antenna by use of switch connectors

In order to compare the two return losses obtained from the simulations and physical measurements where the switch connector is used, the two results are shown on the same plot as shown in Figure 4.9.

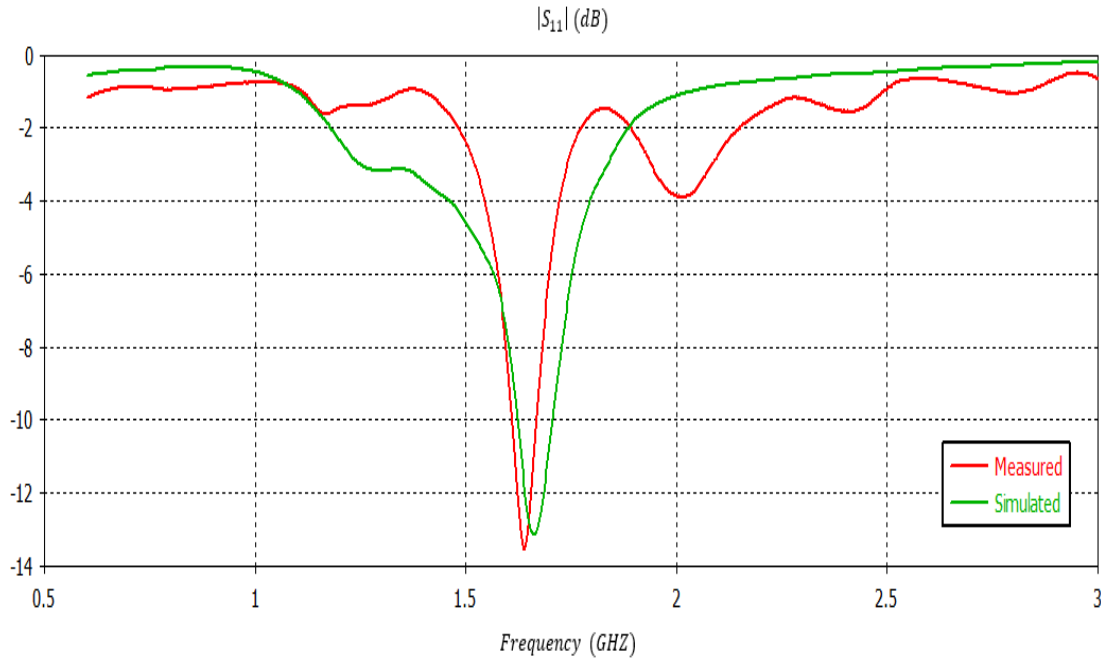


Figure 4.9. Simulated and measured (with switch connector) return losses for GPS antenna

Comparing the plot in Figure 4.9 with the previous comparison of simulated and measured return losses, the second type of measurement configuration where switch connectors are used is seen to provide better results in terms of consistency with that measured.

4.2. 2.4 GHz Wi-Fi Antenna

Due to the success obtained by using the top right corner of the phone as the GPS antenna where it is matched to the frequency of operation by use of stub element and matching circuit, the other top left corner of the phone is a good candidate for the 2.4 GHz Wi-Fi antenna due to its frequency of operation being close to the GPS antenna. In that sense, the configuration of the top left corner of the metallic case of the phone as the folded monopole Wi-Fi antenna operating at 2.4 GHz is shown in Figure 4.10.

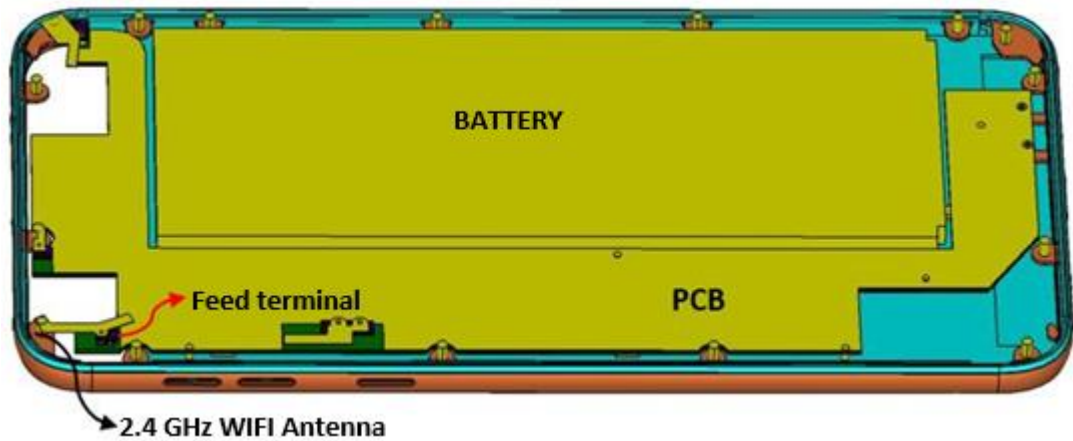


Figure 4.10. Geometry of 2.4 GHz WIFI Antenna

In the configuration shown in Figure 4.10, the antenna is fed through the stub element pattern built on the back cover of the mobile phone.

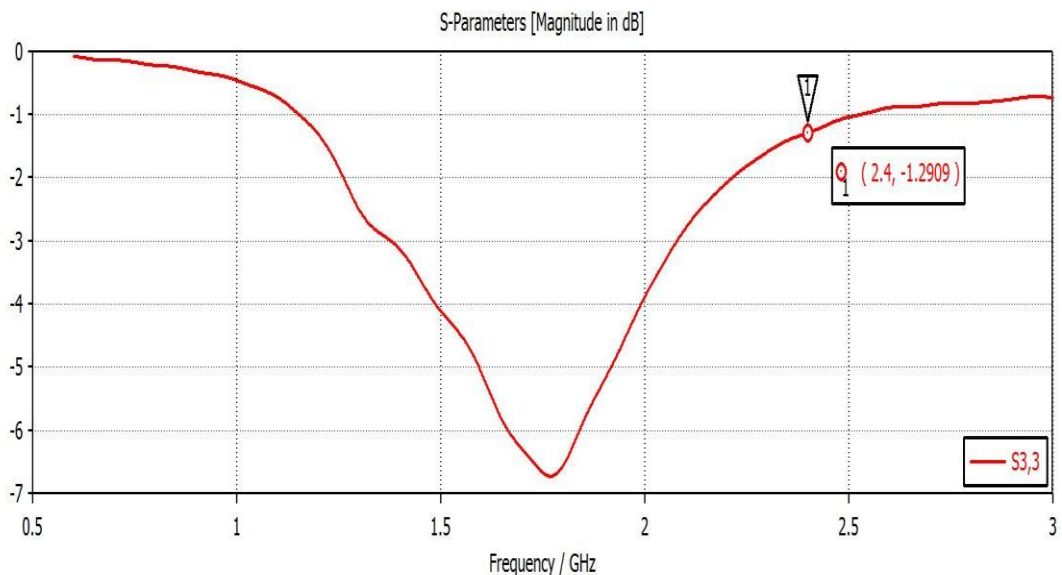


Figure 4.11. Return loss of 2.4 GHz WIFI antenna without a matching circuit

The simulated return loss of the configuration given in Figure 4.10, where no matching circuit is used is given in Figure 4.11. As it was done for the GPS antenna, a three-element matching circuit is implemented in front of the feed terminal in order provide resonance in the operational frequency of 2.4 GHz.

The matching circuit configuration of the antenna is shown in Figure 4.12. In the actual implementation of the configuration, the matching circuit can be built on the PCB structure of the phone by use of SMD components.

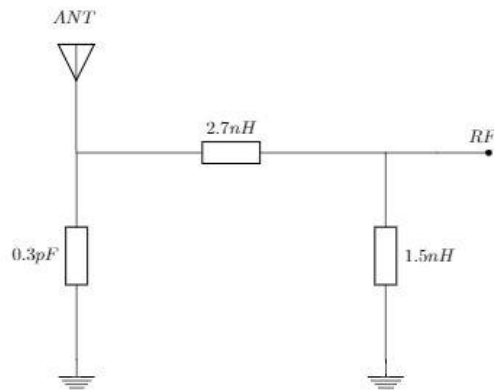


Figure 4.12. Matching circuit of the 2.4 GHz WIFI antenna

The simulated return loss of the antenna after the addition of the matching network is given in Figure 4.13.

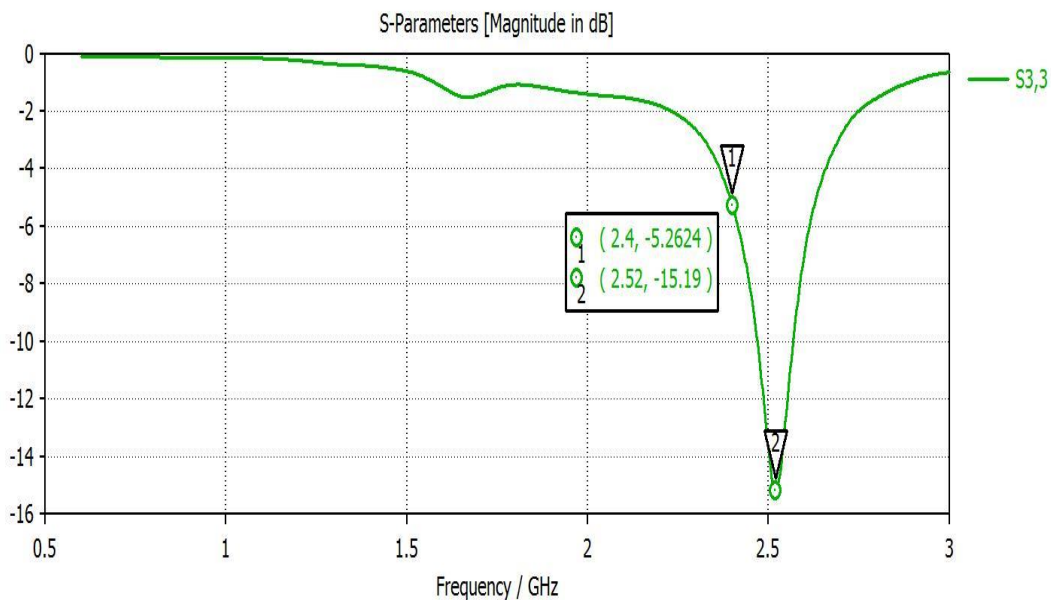


Figure 4.13. Simulated return loss of 2.4 GHz WIFI antenna with matching circuit

Even though the best terminal response of the antenna occurs at a frequency higher than the operational frequency of 2.4 GHz, the resonance at this frequency is expected to shift to the vicinity of the operational frequency by the dielectric loading caused when the plastic back cover of the phone is added to the simulation model.

The physical implementation is shown in Figure 4.14 has been constructed in an attempt to measure the return loss of the antenna. In doing so, switch connectors are used at the PCB of the mobile phone as introduced in part 2.5.2 of this report.

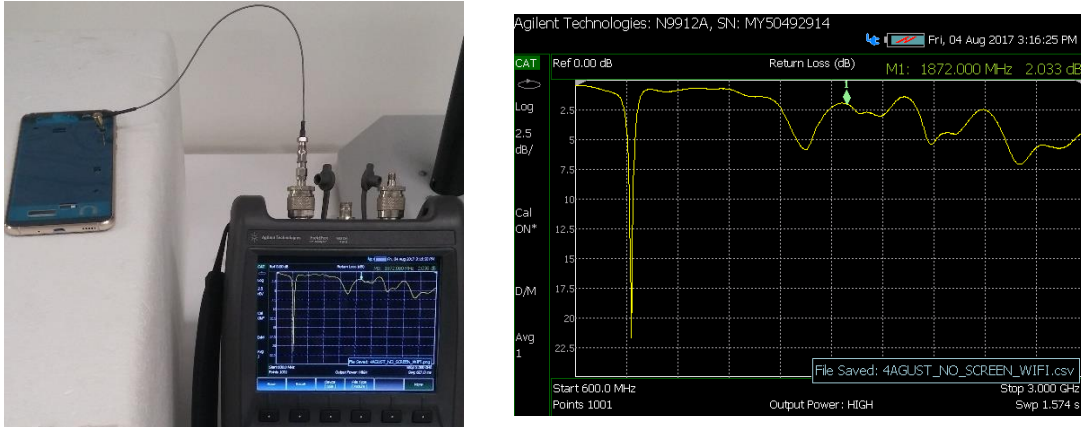


Figure 4.14. Measured return loss of Wi-Fi 2.4 GHz antenna by use of switch connectors

Regarding the measured return loss of the antenna given in Figure 4.14, the result is seen to be inconsistent with the simulated return loss given in Figure 3.24. The difference between the two return losses may be due the removal of the screen for measurement. The removal of the screen from the structure was necessary as to connect the coaxial cable since the switch connector is located on the screen side of the PCB. This results in the occurrence of resonance at 2.6 GHz instead of the intended frequency of 2.4 GHz.

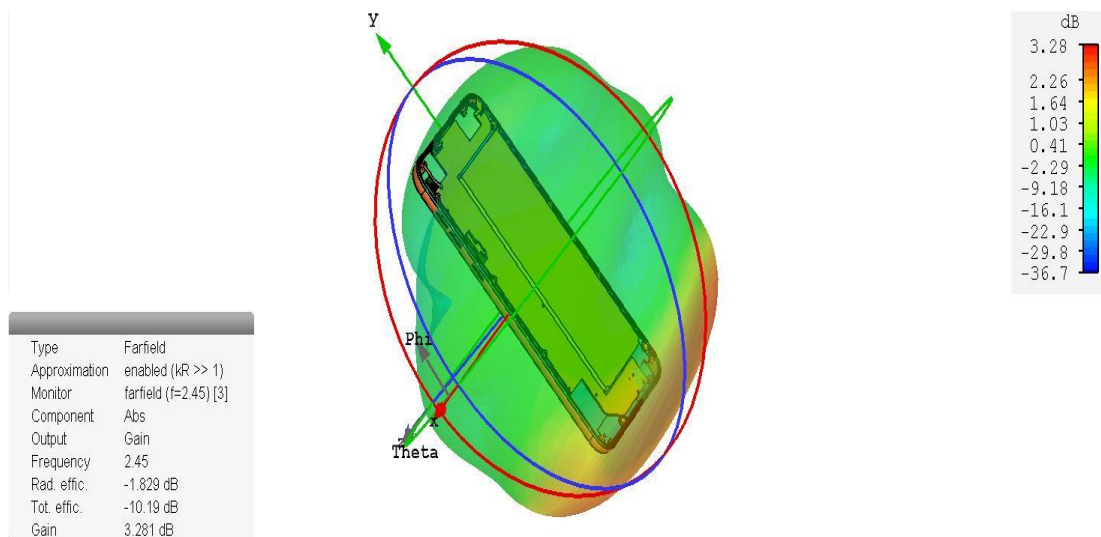


Figure 4.15. Simulated far-field gain of the 2.4 GHz WIFI antenna

The simulated far-field gain of the antenna is given in Figure 4.15. It has a moderate gain of 3.281 dB at the frequency of operation.

4.3. 5.2 GHz Wi-Fi Antenna

Considering the high frequency of operation of the 5.2 GHz Wi-Fi antenna, the size of the antenna, which is directly proportional to some fraction of its wavelength, gets relatively smaller when compared with other antennas built on the mobile phone. Since the effect of dielectric loading caused by lossy dielectric materials in close vicinity of the antenna increases with frequency, the use of outer metallic case of the phone as an antenna at the high frequency of 5.2 GHz would make the antenna vulnerable to detuning by external contacts with the phone.

As an alternative approach, an LDS pattern applied on the plastic back cover of the phone can be configured for use as the WIFI antenna that is fed from the PCB of the phone at the LDS pattern applied to the phone side of the plastic cover. In this way, LDS patterns can be used as independent antenna elements due to the availability of double side plating of the plastic material. Such a configuration is shown in Figure 4.16 where a PIFA is constructed as the WIFI antenna operating at the frequency of 5.2 GHz.

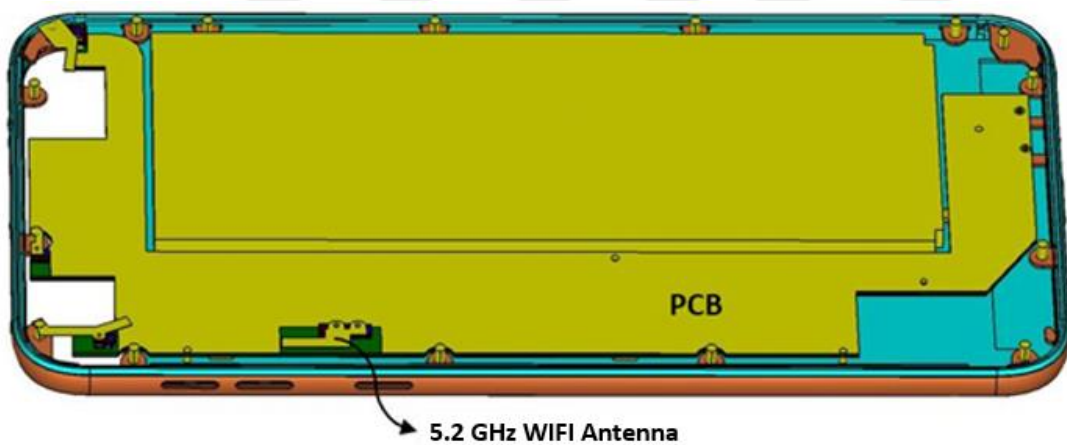


Figure 4.16. Geometry of 5.2 GHz WIFI Antenna

The feed and grounding of the PIFA configuration is made from the PCB side of the LDS pattern. The ground plane of the PCB at the bottom of the LDS pattern is trimmed for better radiation pattern in all directions.

In this PIFA configuration by LDS pattern on back cover plastic, the designer has the freedom of coming up with alternative patterns and can control the crucial structural parameters of antenna in adjusting the terminal characteristics of the antenna.

The simulated return loss of the PIFA given in Figure 4.16 is given in Figure 4.17.

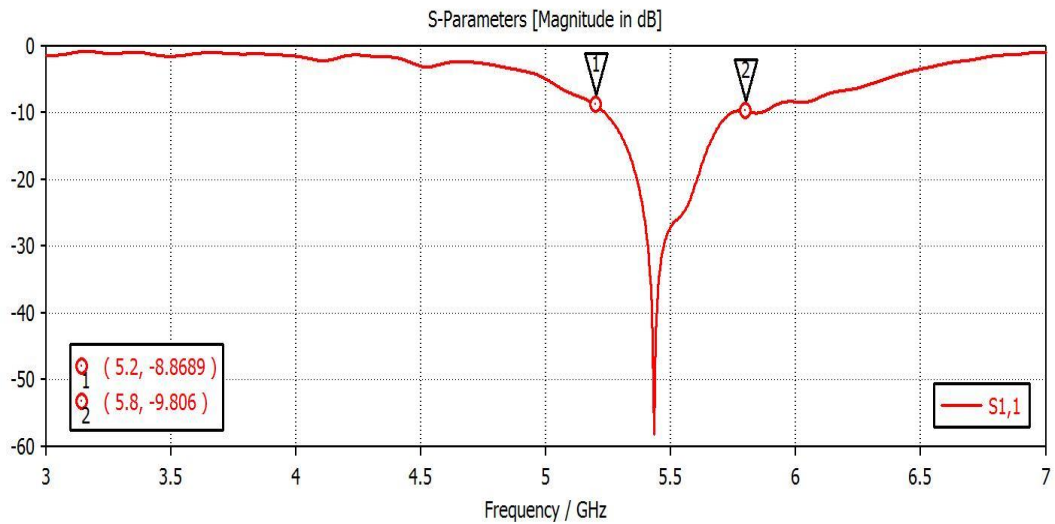


Figure 4.17. Simulated return loss of 5.2 GHz WIFI antenna

The antenna is shown to have a quite wide bandwidth around the frequency of operation. Despite the best terminal response of the antenna occurring at a frequency higher than the operational frequency of 5.2 GHz, the resonance at this frequency is expected to shift to the vicinity of the operational frequency by the dielectric loading caused when the plastic back cover of the phone is added to the simulation model.

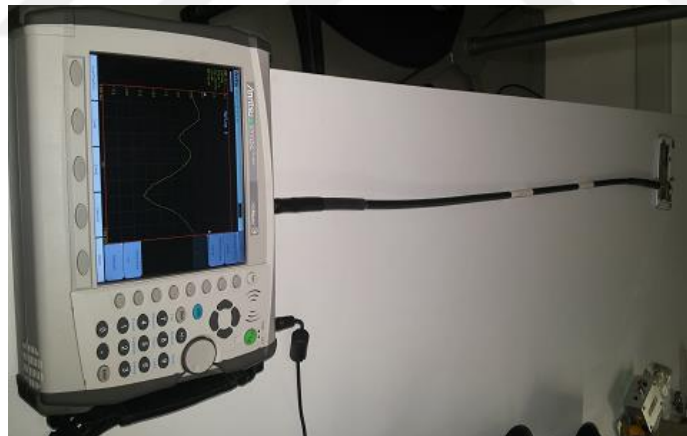


Figure 4.18. Measurement setup of 5.2 GHz WIFI antenna

In the configuration used for the laboratory measurement of the return loss, a different network analyzer was used due to the upper frequency of the previous one being restricted at 4 GHz. Shown in Figure 4.19 is the plot of the simulated and measured return losses of the antenna.

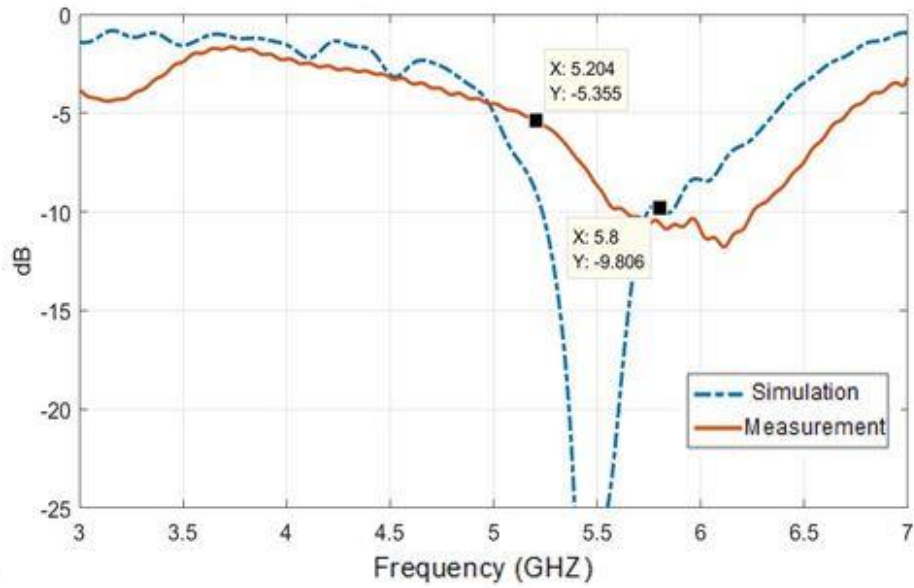


Figure 4.19. Simulated and measured return losses of 5.2 GHz WIFI antenna

Comparing the return losses obtained from simulations and measurements, the small shift in the resonance band of the two plots can be attributed to the decreased effect of dielectric loading due to the trimming of some part of the cover for placement of the coaxial test cable.

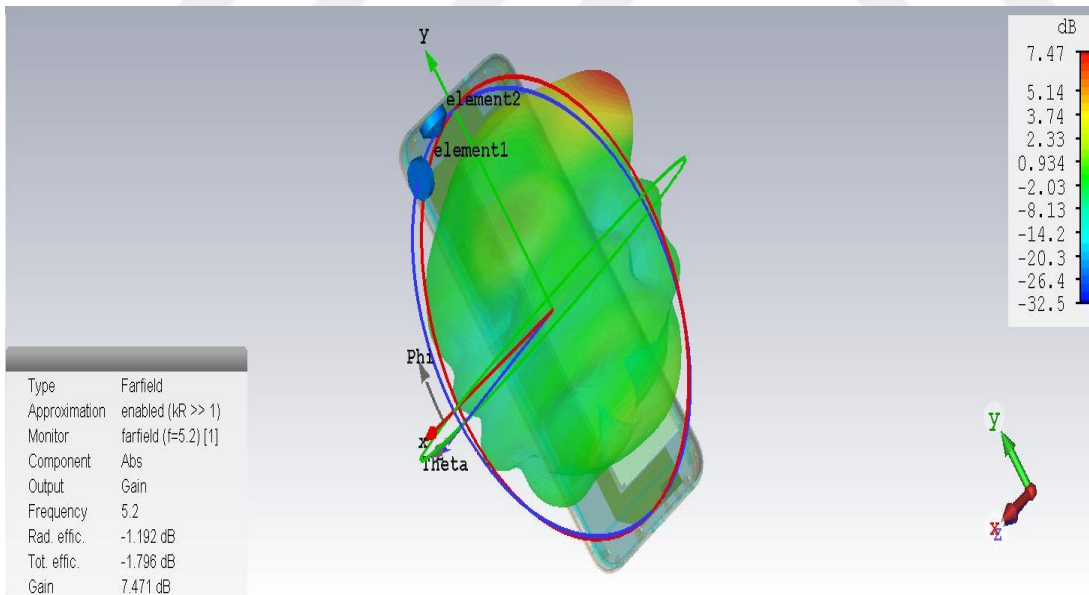


Figure 4.20. Simulated far-field gain of the 5.2 GHz WIFI antenna

The simulated radiation pattern of the antenna is shown in Figure 4.20. From this figure, the antenna is seen to possess the relatively directive radiation characteristics of antennas operating at relatively high frequencies.

CHAPTER 5

SAR ANALYSIS

The cellular device antennas receive and radiate electromagnetic energy at different frequencies depending on the type of application in use. At these frequencies, human body tissues are characterized as lossy dielectric materials. Since cell phones are used in close proximity of the head, high energy electromagnetic waves are able to penetrate through and be absorbed by the tissue which may result in serious health hazards by causing a temperature increase in various parts of the brain.

As a measure of the rate at which the energy is absorbed by the body exposed to radio frequency electric fields, Specific Absorption Rate (SAR) is defined as the time derivative of incremental energy absorbed by an incremental mass contained in a volume element of a given density (IEEE, 2013), given as,

$$SAR = \frac{d}{dt} \left(\frac{dW}{dm} \right) = \frac{d}{dt} \left(\frac{dW}{\rho dV} \right) \quad (16)$$

In terms of the induced electric field, it is given as,

$$SAR = \frac{\sigma E^2}{2\rho} \quad (17)$$

In (17), E represents the peak electrical field strength in the body tissue (V/m), σ is the tissue conductivity (S/m), and ρ is the mass density of the tissue (kg/m^3). SAR is usually quoted as a peak spatial average value averaged over the whole body or a small sample volume of tissue containing a certain amount of mass (1g or 10g) and it is given in units of W/kg. In order to ensure a safe operation, the compliance testing and certification of mobile terminals in each country are subject to measurement protocols of peak spatial average SAR specified by authoritative bodies (i.e. IEEE, FCC, ICNIRP). It is the intention of these protocols to represent a conservative estimate of the peak SAR induced in the head by describing in detail the concepts and techniques of measurement together with the simulated-tissue, anatomically

equivalent and simple phantom models to be used in laboratory and simulated calculations of SAR.

The SAR distribution in the human body due to exposure to electromagnetic fields is affected by several factors such as, anatomy of the head, phone position, frequency, tissue composition, EM source structure, and electrical properties of tissues. The analysis of SAR characteristics with respect to these factors has been the subject of many previous studies. In (Hossain, 2015) and (Satriya,2013) significant SAR changes with nonlinear dependence characteristics were observed due to the effect of inclination angle between antenna and head model. Muscle and tissue distribution inside anatomical models is one major factor influencing spatial peak SAR (Lee, 2011). In (Christ, 2006), a significant increase of 2.2-4.7 dB of peak spatial SAR was found when tissue distribution of exposed regions was considered instead of standard liquids in different parts of the body.

Regarding the inclusion of a hand model in SAR analysis, research shows that it may result in a decrease (Hossain, 2015) as well as an increase (Li, 2012; Panagamuwa, 2013) for specific types hand grip. Considering the power levels of current mobile handsets, the changes observed in peak spatial SAR are expected to stay within maximum standard limits set by authoritative bodies as 1.6 W/g (for 1g average) and 2.0W/g (for 10g average). For that reason, inclusion of a hand model is not considered in current SAR measurement practices suggested by authoritative bodies.

Morphological properties of the head model also constitute an important aspect in SAR analysis of mobile phones. In (Ghanmi, 2013), SAR distribution in the brain was shown to vary between two biological head models due to differences in anatomical proportions and geometry of the head models. In (Monebhurrun, 2010), a representative of the adult human head was used that is constructed from 3D laser scanned head models of volunteers. A child model was derived from this model with appropriate transformations in accordance with the growth rate of different parts of human head. As a result of the comparison of SAR obtained from these head models with different sizes, maximum 10 g averaged SAR values were obtained with bigger head model since it provides a large radius of curvature that is similar to a flat phantom where the tissue boundary is closer to the source, thereby absorbing more energy than a smaller head. In (Adibzadeh, 2015), the impact of head morphology on

local brain SAR was investigated where head morphology was found as an important source of uncertainty for dosimetry studies of mobile phones.

Due to the dependence of SAR on the model of human head used, tissue parameters of the head model and positioning of the phone relative to the head causes discrepancies in test results obtained from different laboratories for the same wireless handset. In order to overcome inter-laboratory measurement variations, a specific anthropomorphic mannequin (SAM) head model with a standardized size, shape and tissue equivalent liquid parameters have been defined by the IEEE Standards Coordinating Committee 34, Subcommittee 2, Working Group 1 (SCC34/SC2/WG1) (Beard, 2006). The size, shape and dielectric properties of this phantom together with the test positions are chosen such that it will provide conservative SAR characteristics compared with the heterogeneous anatomical head models. In general terms, the SAM phantom is defined as a low permittivity, low loss plastic shell filled with homogeneous tissue-equivalent liquid. The properties of the homogeneous filler liquid are selected such that it will yield permittivity and conductivity values within $\pm 10\%$ of the target values at the frequency of measurement. The phantom shell on the other hand should be constructed from low-permittivity, low-loss material with loss tangent less than or equal to 0.05 and a relative permittivity between 2 and 5. As an accurate and practical representation of the pinna, the phantom shell also includes a simplified lossless spacer with a thickness of 6mm.

For the evaluation of repeatability in SAR using standardized techniques, an international inter-laboratory comparison [Siegbahn, 2010] was made between 10 laboratories where three different commercially available mobile phone models were used as the radiation source. As a result, agreement in calculated SAR between the participating laboratories was found to be similar to the agreement obtained in inter-laboratory comparisons. Regarding the conservativeness of SAM phantom, in [Lee, 2015], SAM phantom was compared with four anatomical head models at different ages for exposure from a typical bar-type phone. As a result, SAM phantom was found conservative for phone models with the antenna at the top of the phone. However, for phones having antenna at its bottom, SAM phantom was shown to produce lower 1- and 10-g SAR due to the occurrence of hotspot farther from the feed point of the antenna. In (Monebhurrin, 2010), SAM phantom was also found

conservative in the child head when compared with a child head model constructed from 3-D laser scanned head models by morphing technique. On the contrary, in [Lee 2011], a comprehensive comparison was made between SAM phantom and European child head models by considering pinnae compression, cheek position, tilt position, skin properties and morphology. As a result, 75% of the 40 total cases reviewed showed lower SAR results in the SAM phantom.

As a review of literature on the subject matter shows, it is not possible to establish a direct relationship between SAR and effecting parameters as to describe how the peak spatial SAR will change with respect to that particular parameter. The measured and numerically calculated values of SAR are highly dependent on type of mobile phone and antenna type under investigation. In (Ghanmi, 2013), electromagnetic radiations and SAR from mobile phones having different antenna/types and positions were investigated and it was confirmed that shape/design of the mobile phone and the location of the antenna can have a large influence on SAR at high frequency exposure to the brain. In (Keshvari, 2011), SAR distributions from two commercial mobile phones and a half wave dipole antenna were compared where it was concluded that the spatial average values and distribution of SAR from generic source models cannot be extrapolated to real device exposures. For that reason, as a valuable contribution to this field of study, it is important to add to the existing knowledge, the SAR characteristics of various mobile phones analyzed in a way as described in standardized practice. In that sense, it is the purpose of this study to analyze the SAR characteristics produced by the main antenna of a mobile phone where the metallic bottom casing of the handset is configured as a Planar Inverted F Antenna. By numerical simulations, the comparison of SAR distributions caused by the handset in SAM phantom and heterogeneous anatomical models are made together with an analysis of the effect of using a homogeneous hand model next to the SAM phantom. Effect of positioning the antenna element on bottom and upper parts of the handset and SAR averaging methods are considered.

5.1. Main antenna as the source of radiation

As the source of electromagnetic radiation, the main antenna of the mobile phone introduced is configured to operate at the GSM band frequencies of GSM 900 MHz and 1800 MHz by appropriate reactive loading to the grounding terminal of PIFA.

The geometry of the phone is shown in Fig. 5.1 where the height, width, and thickness of the antenna element are 52.9 mm, 5.3 mm, and 0.9 mm respectively.

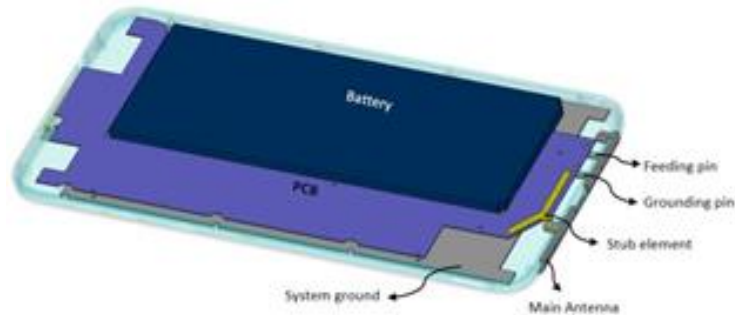


Figure 5.1. Main antenna as the source of electromagnetic radiation

The simulated return loss of the antenna is shown in Figure 5.2.

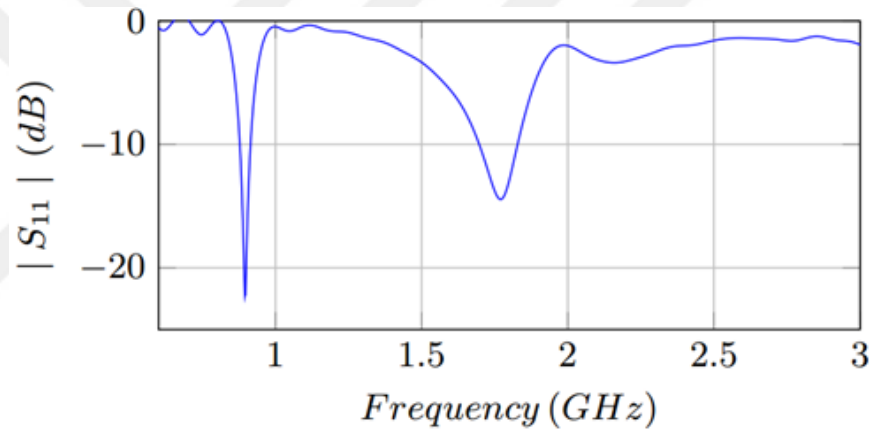


Figure 5.2. Simulated return loss of the main antenna

5.2. Description of Head and Hand Models

As part of this study, the investigation of the effect of using different head models and inclusion of a hand model on peak spatial average SAR is of interest. For that purpose, two different head models and a homogeneous hand model are used in numerical simulations as shown in Fig. 5.3.

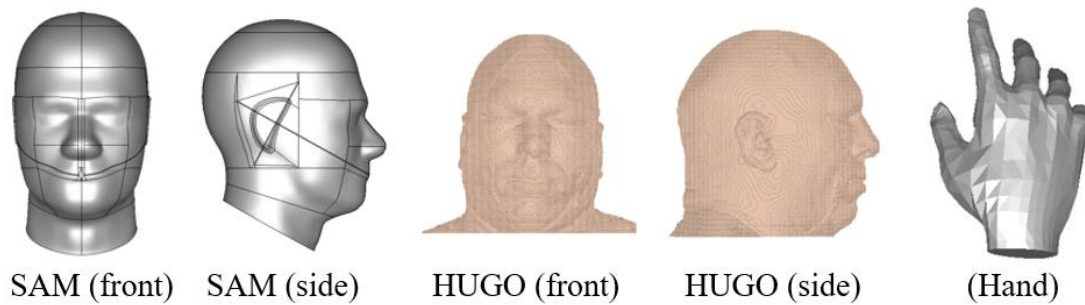


Figure 5.3. Head and hand models

5.2.1. SAM Head and Homogeneous Hand Model

In the set of recommended practices suggested by international authoritative bodies for the measurement of peak spatial average SAR, the use of a standardized SAM head phantom is recommended which is specifically designed to produce a conservative estimate of SAR in the head when compared with anatomically correct heterogeneous head models. As a representation of the adult male head, the shape of SAM phantom and its dimension parameters are from the 90th-percentile anthropometric data tabulated by the US army.

The inner and outer surfaces belonging to the left and right halves of the SAM phantom are publicly available as a computer-aided design (CAD) file. In order to use this available model in numerical simulations, the volume enclosed by the inner surface and the volume between the inner surface and the outer shell are solidified by use of a CAD program. The resulting files are imported to the electromagnetic simulation program and the solidified regions are given material properties as given in Table 1 in accordance with the standards.

Additionally, a homogeneous hand model is constructed whose physical characteristics and holding position is constructed in a 3D character animation program called Poser. The constructed hand model is exported to the electromagnetic simulation program as an object file and is given the same material properties as the SAM liquid. The effect of using the hand model together with the homogeneous SAM head model in two holding positions is investigated.

Table 5.1. Material properties of head and hand models

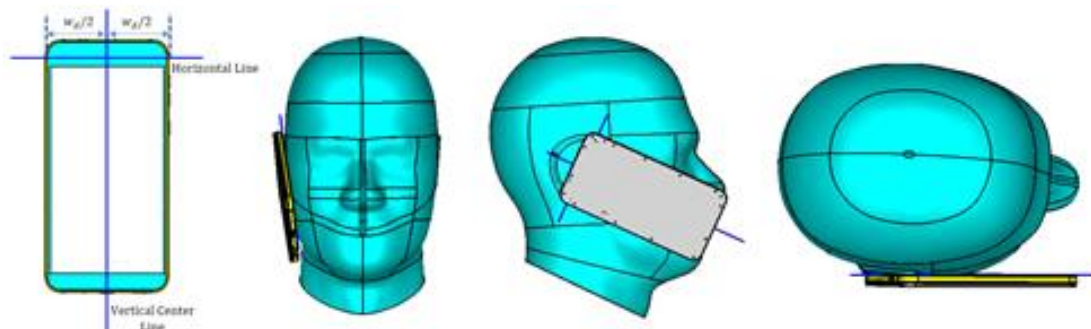
	ϵ_r	σ (S/m)	ρ (kg/m ³)
SAM liquid	41.5	0.97	1000
SAM shell	3.7	0	1000
Hand	41.5	0.97	1000

5.2.2. Heterogeneous Anatomical Head Model

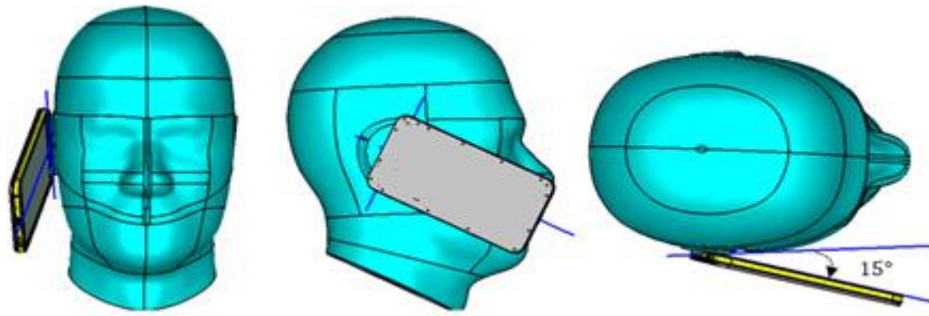
In order to construct a base of comparison to the SAR obtained from SAM phantom, an anatomically correct head model with 1mm resolution is used in this study. This voxel-based human model is the “HUGO” from the Visible Human Project. This phantom provides a detailed description of various types of tissues in the human body and is constructed by use of medical imaging techniques (CT scan and MRI) on cadaver with no physical anomalies. The voxel data file of the HUGO is readily available with defined electrical properties and is commonly used for non-ionising dosimetry applications in CST. The available voxel data is a complete body representation of the human body in an upright standing position and requires the use of additional software (Vuchkovikj, 2013) to put the body into practical (i.e. phone holding) positions. In this study, only the HUGO head model next to the phone without the hand in two talking positions are considered

5.2.3. Test Positions

As a way of simulating the real case talking positions of the phone, two standardized positions (“cheek” and “tilt”) of holding the phone against the head phantom are considered.



(a) Reference positioning lines and cheek positioning



(b) Tilt positioning

Figure 5.4. Positioning of the phone in cheek and tilt positions

In placing the phone in the cheek position, two lines are defined on the handset – the vertical centerline and the horizontal line as shown in Fig. 5.4. The vertical centerline passes through the midpoints of the phone’s width at the level of acoustic output and bottom edge. The horizontal line passes through the acoustic output in a direction parallel to the vertical centerline. The phone is then placed next to the phantom such that the intersection of two perpendicular lines is on the extension of the line passing through right ear center (REC) point and left ear center (LEC) point. By translation along and rotation around REC-LEC axis, the phone is placed as shown in Figure 5.4 such that it is in contact with the pinna and a point below the pinna on the cheek.

In positioning the phone in the tilt position, the phone in the cheek position is moved away from the handset and is rotated around the horizontal line by 15 degrees as shown in Figure 5.4. The handset is then moved towards the phantom on the RE-LE line until any point of the handset touches the ear.

5.2.4. Simulation Settings

The simulations of the described model setup were performed on a hexahedral mesh using the transient solver of microwave studio of computer simulation technology (CST). For the excitation of the antenna, a discrete port with an impedance of 50 ohms was defined at the feed point of the antenna. The frequency range is set between 600 MHz and 3 GHz and far field, electric field, and power loss monitors were set at 900 MHz and 1800 MHz. In the post-processing phase of the simulation, the 1 g and 10 g spatial peak volume averaged SAR calculations of all configurations were performed at the two frequencies of interest. In each configuration, the averaged SAR values are normalized with respect to the power accepted by the antenna. The reference average output power is set to 0.25 W and 0.125 W at the

respective frequencies of 900 MHz and 1800 MHz representing the 1/8 of the peak output power. The normalization with respect to the average power compensates for the occurrence of antenna mismatches when using the phone in close proximity of different head and hand model configurations.

5.3. SAR Results

In the analysis of SAR characteristics observed due to electromagnetic radiation from the described handset, the constructed models of homogeneous head (SAM), heterogeneous anatomical head, and homogeneous hand models are used in a number of various configurations as shown in Figure 5.5. The numerical SAR calculation of these configurations are carried out by considering cheek and tilt positions, 1g and 10g spatial average, antenna position in upper and bottom side of the phone, and frequency of operation. Analyzing the resulting spatial average SAR data given in Table 2 where each row represents a single type of configuration analyzed at different frequencies and averaging schemes, it is immediately obvious that for every configuration, the SAR value is lower for both methods of averaging used at higher frequency of operation. This lower SAR characteristic at higher frequency can be related to lower power output (0.125W) defined at 1800 MHz when compared to that (0.25 W) defined at 900 MHz. The averaging method used also has a slight effect on peak spatial average SAR where averaging over a 10g of tissue results in lower peak values when compare with 1g averaging. This is due to the averaging at points of high power absorption together with neighbor areas with lower power absorptions. The use of 10g averaging causes the spatial smoothing of SAR distribution, making the detection of closely spaced points of peak SAR in the head. Except for the HUGO model with antenna placed at upper part of the phone, the tilting position of the phone is seen to reduce SAR to some degree when compared with cheek positioning. This is mostly due to the decrease in coupling between the head tissue and antenna element together with the system ground plane caused by the decrease in parallel positioning between the two by tilting. This effect of tilting is better recognized at 900 MHz since at relatively low frequencies, the chassis mode currents are more pronounced than the antenna element itself for PIFA antennas. For all configurations of SAM and HUGO head where the inclusion of hand is not considered, the placement of the antenna at the upper part is seen to produce higher SAR near the pinna due to the decreased distance between antenna and head tissue.

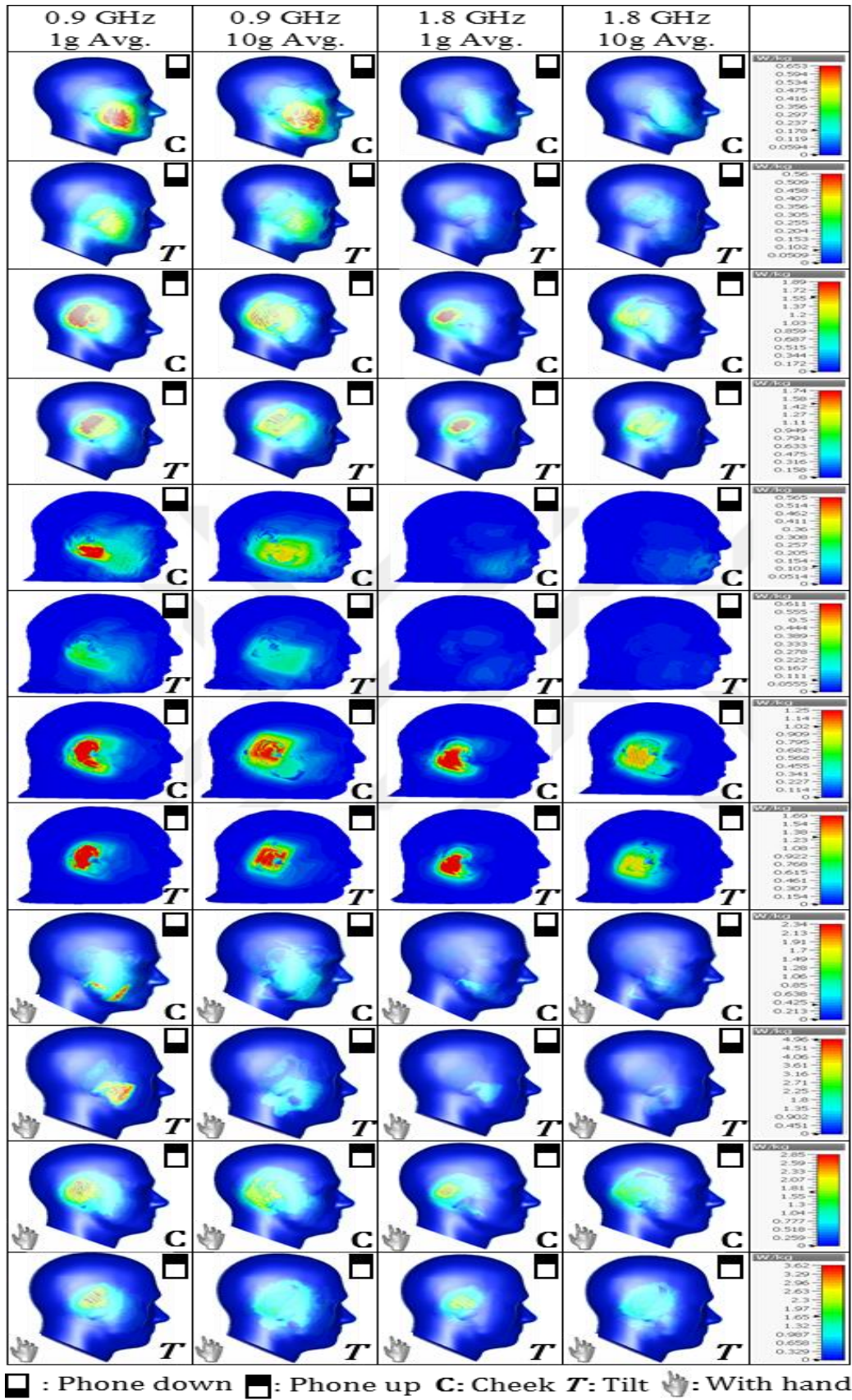


Figure 5.5. SAR distributions in all configurations considered

5.4. Antenna Characteristics in the Presence of Hand and Head Models

The terminal impedance characteristics of the mobile phone in the presence of the head and hand models are investigated from the following plots (Fig 5.6, Fig 5.7 and Fig. 5.8) of the return loss of the antenna for all configurations considered in simulations.

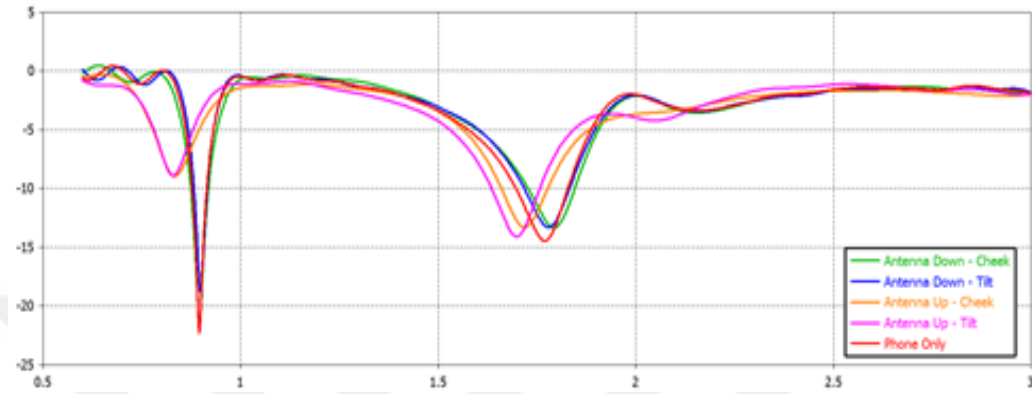


Figure 5.6. $|S_{11}|$ (dB) from using SAM in four configurations

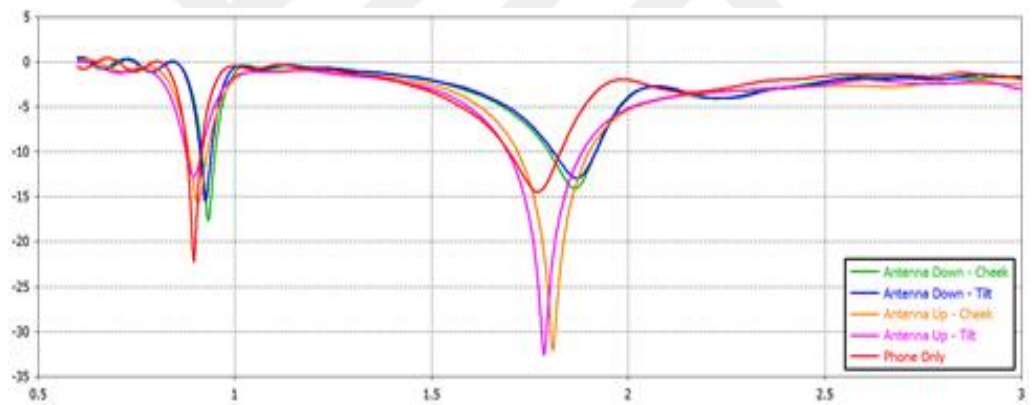


Figure 5.7 $|S_{11}|$ (dB) from using HUGO head in four configurations

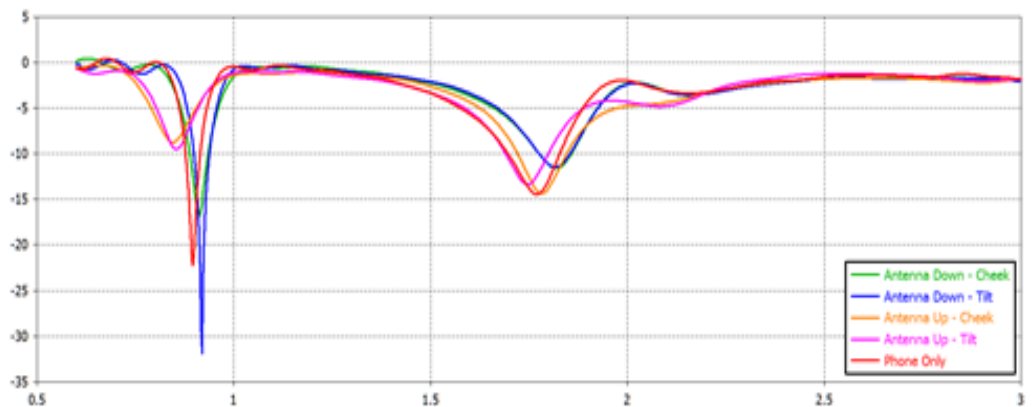


Figure 5.8 $|S_{11}|$ (dB) from using SAM with homogeneous hand in four configurations

With reference to Figures 5.6 and 5.8, even though the cheek and tilt positioning does not have a significant effect, the placement of the antenna at the pinna side by the rotation of the handset by 180 around its center axis, decreases frequency of resonance due to the reactive loading to the antenna by the head placed in the near field of the antenna. For the case of HUGO model, the trend of decreased frequency of resonance occurs for the case of antenna placed at the upper side of the phone. For other configurations, resonance characteristics is said to stay relatively invariant.

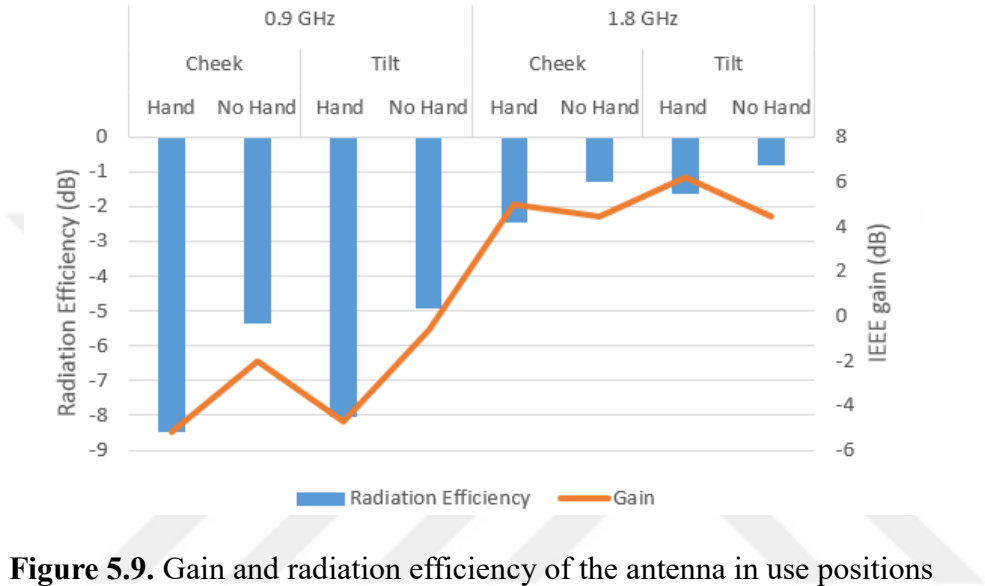


Figure 5.9. Gain and radiation efficiency of the antenna in use positions

In Figure 5.9, the gain and radiation characteristics of the configurations utilizing SAM phantom are shown. The inclusion of the hand model is seen to decrease the radiation efficiency for all configurations. For the gain, the trend is towards a decrease with the inclusion of hand at 900 MHz, whereas, it shows a slight increase at 1800 MHz. Under the same set of configurations, higher gains by up to 6 dB are noted at 1800 MHz when compared with the gain at 900 MHz (Okuyucu, 2017).

CHAPTER 6

CONCLUSION

In the first part of this study as described in chapter two, a compact low-profile frequency reconfigurable mobile phone main antenna is introduced along with a receive diversity antenna that is suitable for use in LTE 1/3/7/8/20 bands. The antennas have been designed and performance characteristics were measured in terms of terminal radiational characteristics by both simulations and measurements. For the main antenna element, multiband characteristic was achieved without the use of a matching circuit by use reactive loading to the grounding pin of the PIFA as to shift the available antenna bandwidth to various bands of interest. For the diversity antenna, the upper metallic part of the phone with a high volume is employed as a simple folded monopole antenna operated for a receive diversity. Both antennas have been fine-tuned by use of stub elements for resonance at their respective frequency of operation, which in an actual physical model, can be constructed by LDS technology on the plastic cover of the phone.

For the GPS and 2.4 GHz WIFI antennas where the top two corners of the mobile phone were used as the radiators, the resonance at the respective frequency of operation have been achieved by use of stub elements and matching circuits. The 5.2 GHz WIFI antenna on the other hand, has been constructed as a single PIFA element constructed solely by and LDS pattern on the back cover of the phone. By the proper adjustment of design parameters of the PIFA, wideband resonance at the frequency of operation has been obtained without the use of an additional matching circuit.

In measuring the terminal impedance characteristics of antennas, two configurations have been considered. In the first configuration where a semirigid cable is connected at the feedline on the PCB of the phone, the measurement result was seen to depend on the positioning of the cable and was observed to show significant changes for various bending of the cable especially at the higher frequency of operation. In the second configuration, the coaxial test cable is connected to the antenna through a

switch connector and this scheme provided more reliable characteristics and good agreement with results obtained from simulations.

In the final part of the study, SAR analysis of a the PIFA based main antenna element has been performed by numerical simulations. The change in spatial average SAR with respect to head type, talk positions, antenna location, averaging method used and the presence of a homogeneous hand has been investigated. In overall, relatively low peak spatial SAR values were obtained at higher frequency of operation due to a reduced peak output power available from the antenna at this frequency. The 10g averaging method was found to provide lower SAR values when compared to that obtained from 1g average. The most influential parameter on SAR was found as the position of the antenna element which produced SAR values even higher than standardized maximum limits when placed near the pinna, at the upper part of the phone. The presence of a homogeneous hand holding the mobile handset was noted to degrade the radiation efficiency of the antenna and had an increasing effect on SAR when compared with the one utilizing no hand model. Additionally, the use of homogeneous head and hand models next to the mobile handset resulted in a down-shift in the frequency of resonance of the antenna. Due to the complex structure of the heterogeneous head model, this characteristic was shown to dependent on use positions and position of the main antenna.

By the completion of this of work, a cumulative knowledge in theoretical design and techniques of practical implementation and measurement of mobile phone antennas have been obtained which will in turn lay down the required groundwork for possible future work emanating from this study.

REFERENCES

- Adibzadeh, Fatemeh, et al. (2015). "Impact of head morphology on local brain specific absorption rate from exposure to mobile phone radiation." *Bioelectromagnetics*, 36.1: 66-76.
- Agrawal, J., et al. (2015). "Evolution of mobile communication network: From 1G to 4G." *International Journal of Multidisciplinary and Current Research* 3: 1100-1103.
- Beard, Brian B., et al. (2006). "Comparisons of computed mobile phone induced SAR in the SAM phantom to that in anatomically correct models of the human head." *IEEE Transactions on Electromagnetic Compatibility* 48.2 (2006): 397-407
- Christ, Andreas, et al. (2006). "The dependence of electromagnetic far-field absorption on body tissue composition in the frequency range from 300 MHz to 6 GHz." *IEEE transactions on microwave theory and techniques* 54.5: 2188-2195
- Ciais, Pascal, et al. (2004). "Design of an internal quad-band antenna for mobile phones." *IEEE Microwave and wireless components letters* 14.4: 148-150.
- Fujimoto, Kyōhei, and James R. James., (2001). *Mobile antenna systems handbook*. Artech House, 2001.
- Ghanmi, Amal, Nadège Varsier, Abdelhamid Hadjem, Emmanuelle Conil, Odile Picon, and Joe Wiart. (2013). "Electromagnetic fields: from dosimetry to human health: Study of the influence of the laterality of mobile phone use on the SAR induced in two head models." *Comptes Rendus - Physique* 14, 418-424.
- Godara, Lal Chand, ed. (2001). *Handbook of antennas in wireless communications*. Vol. 4. CRC press.
- Guo, Yong-Xin, Michael Yan Wah Chia, and Zhi Ning Chen. (2004). "Miniature built-in multiband antennas for mobile handsets." *IEEE Transactions on Antennas and Propagation* 52.8: 1936-1944
- Hossain, M. I., Mohammad Rashed Iqbal Faruque, and Mohammad Tariqul Islam. (2015). "Analysis on the effect of the distances and inclination angles between human head and mobile phone on SAR." *Progress in biophysics and molecular biology* 119.2: 103-110.
- Hossain, Md Iqbal, MR Iqbal Faruque, and M. Tariqul Islam. (2015). "Investigation of hand impact on PIFA performances and SAR in human head." *Journal of applied research and technology* 13.4: 447-453

LKPF - http://www.lpkf.com/_mediafiles/1797-lpkf-laser-direct-structuring-en.pdf,
last access: 22.12.2017.

IEEE, (2013) Recommended Practice for Determining the Peak Spatial-Average Specific Absorption Rate (SAR) in the Human Head from Wireless Communications Devices: Measurement Techniques - Redline' 2013, *IEEE Std 1528-2013* (Revision of IEEE Std 1528-2003).

Keshvari, Jafar, and Teemu Heikkilä. (2011). "Volume-averaged SAR in adult and child head models when using mobile phones: A computational study with detailed CAD-based models of commercial mobile phones." *Progress in biophysics and molecular biology* 107.3: 439-442.

Kivekäs, Outi, et al. "Effect of the chassis length on the bandwidth, SAR, and efficiency of internal mobile phone antennas." *Microwave and Optical Technology Letters* 36.6 (2003): 457-462.

Lee, Ae-Kyoung, and Jaehoon Yun. (2011). "A comparison of specific absorption rates in sam phantom and child head models at 835 and 1900 MHz." *IEEE Transactions on Electromagnetic Compatibility* 53.3: 619-627.

Lee, Ae-Kyoung, et al. (2015). "SAR comparison of SAM phantom and anatomical head models for a typical bar-type phone model." *IEEE Transactions on Electromagnetic Compatibility* 57.5: 1281-1284

Li, Chung-Huan, et al. (2012). "Influence of the hand on the specific absorption rate in the head." *IEEE transactions on antennas and propagation* 60.2: 1066-1074

Monebhurrun, Vikass. (2010). "Conservativeness of the SAM phantom for the SAR evaluation in the child's head." *IEEE Transactions on Magnetics* 46.8: 3477-3480.

Okuyucu, S., et al. (2017). "A numerical parametric study of SAR From a Dual-Band Pifa Based Antenna for Mobile Phone Communication" *ELECO - International Conference on Electrical and Electronics*, 2017.

Özbakış, B. et al. (2017). " Multi-band Frequency Tunable LTE Antenna for Mobile Phone Applications" *Progress in Electromagnetic Research Symposium (PIERS)*, 2017.

Panagamuwa, Chinthana J., Ian Howells, and Amir Kotb. (2013). "Use of a block hand phantom for mobile phone Specific Absorption Rate measurements." *Antennas and Propagation (EuCAP)*, 7th European Conference on. IEEE, 2013

Park, Hoon, and Jaehoon Choi. (2005). "Design of broad quad - band planar inverted - F antenna for cellular/PCS/UMTS/DMB applications." *Microwave and Optical Technology Letters* 47.5: 418-421.

Rowell, Corbett, and Edmund Y. Lam. (2012). "Mobile-phone antenna design." *IEEE*

Antennas and Propagation Magazine 54.4: 14-34.

Satriya, Alfredo Bayu, and Eko Setijadi. (2013). "An analysis method of effect of linear polarized electromagnetic exposure from mobile phone to human head with various incident angles." *Information Technology and Electrical Engineering (ICITEE)*, 2013 International Conference on. IEEE.

Siegbahn, Martin, et al. (2010). "An international interlaboratory comparison of mobile phone SAR calculation with CAD-based models." *IEEE Transactions on Electromagnetic Compatibility* 52.4: 804-811

Singh, Rakesh Kumar, and Ranjan Singh. (2016) "4G LTE Cellular Technology: Network Architecture and Mobile Standards".

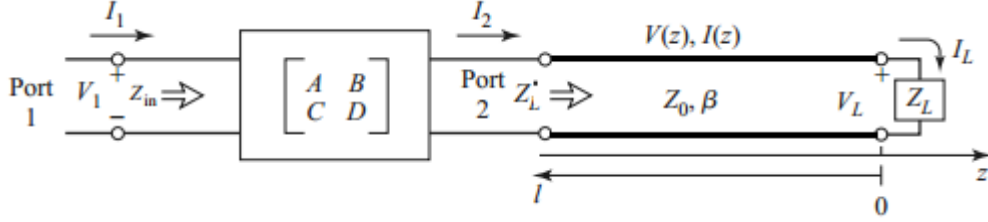
Valkonen, R., et al. (2013). "Inherently non-resonant multi-band mobile terminal antenna." *Electronics Letters* 49.1: 11-13.

Vuchkovikj, M., I. Munteanu, and T. Weiland. (2013). "Application of postured human model for SAR measurements." *Advances in Radio Science* 11.K. 1: 347-352.

Zhang, Zhijun. (2017). *Antenna design for mobile devices*. John Wiley & Sons.

APPENDIX

The procedure outlined here describes the calculation of return loss at the feed terminal of a PIFA from the knowledge of S-parameters at its feed terminal, when a reactive load is connected at the end of a transmission line of length l and characteristic impedance Z_0 connected to its grounding pin.



For the configuration shown above, the transmission (ABCD) matrix elements defining the two-port network is obtained from the knowledge of S-parameters by use following conversion formulas.

$$A = \frac{(1 + S_{11})(1 - S_{22}) + S_{12}S_{21}}{2S_{21}}$$

$$B = Z_0 \frac{(1 + S_{11})(1 + S_{22}) - S_{12}S_{21}}{2S_{21}}$$

$$C = \frac{1}{Z_0} \frac{(1 - S_{11})(1 - S_{22}) - S_{12}S_{21}}{2S_{21}}$$

$$D = \frac{(1 - S_{11})(1 + S_{22}) - S_{12}S_{21}}{2S_{21}}$$

The equivalent load impedance Z_L' at the port 2 of the network is found by referring the load impedance Z_L to the port input over a transmission length l .

$$Z_L' = Z_0 \frac{Z_L + jZ_0 \tan \beta l}{Z_0 + jZ_L \tan \beta l}$$

Finally, the input impedance Z_{in} and the corresponding return loss S_{11} is found as

$$Z_{in} = \frac{A \cdot Z_L' + B}{C \cdot Z_L' + D}$$

$$S_{11} = \frac{Z_{in} - Z_0}{Z_{in} + Z_0}$$